

Corrections

(modified: 21 Feb 2022)

The submitted version of the dissertation contains some typesetting errors. The present PDF file is the corrected version. Corrections are listed below.

Location:	Page 8, first sentence in Section 1.3.1
Original:	formulas
Corrected:	formulae

Location:	Page 11
Original:	$\frac{\partial (\text{tr}(\mathbf{A}^k))}{\partial \mathbf{A}} = \sum_{i=0}^{k-1} (\mathbf{A}^i \mathbf{A}^{k-1-i})^T$
Corrected:	$\frac{\partial (\text{tr}(\mathbf{A}^k))}{\partial \mathbf{A}} = k (\mathbf{A}^{k-1})^T$

Location:	Page 19, eq. (3.1)
Original:	$\boldsymbol{\sigma}^3 - I_1 \boldsymbol{\sigma} + I_2 \boldsymbol{\sigma} - I_3 = 0$
Corrected:	$\boldsymbol{\sigma}^3 - I_1 \boldsymbol{\sigma}^2 + I_2 \boldsymbol{\sigma} - I_3 \boldsymbol{\delta} = \mathbf{0}$

Location:	Page 20, eq. (3.6)
Original:	$\mathbf{s}^3 - J_2 \mathbf{s} - J_3 = 0$
Corrected:	$\mathbf{s}^3 - J_2 \mathbf{s} - J_3 \boldsymbol{\delta} = \mathbf{0}$

Location:	Page 39, eq. (4.34)
Original:	$\frac{9K\alpha \ \mathbf{s}\ \dot{\epsilon}}{\sqrt{2}G}$
Corrected:	$\frac{9K\alpha S \dot{\epsilon}}{\sqrt{2}G}$

Location:	Page 39, eq. (4.34)
Original:	$\frac{9K\alpha \ \mathbf{s}\ \dot{\epsilon}}{\sqrt{2}G}$
Corrected:	$\frac{9K\alpha S \dot{\epsilon}}{\sqrt{2}G}$

Location:	Page 52, eq. (4.115)
Original:	$\frac{A}{\tan \omega_n}$
Corrected:	$\frac{A_e}{\tan \omega_n}$

Location:	Page 120, last row
Original:	(??)
Corrected:	(4.113)



M Ű E G Y E T E M 1 7 8 2

Budapest University of Technology and Economics
Department of Applied Mechanics



Attila Kossa

Exact stress integration schemes for elastoplasticity

PhD dissertation

2011

Supervisor: Professor László Szabó, D.Sc.

Contents

1	Introduction	7
1.1	Aim of the work	7
1.2	Structure of the dissertation	8
1.3	Summary of notations	8
1.3.1	General convention and characters	8
1.3.2	Mathematical notations	11
2	Literature overview of exact integration schemes in elastoplasticity	13
3	Theory of small strain elastoplasticity	19
3.1	Analysis of stress and strain	19
3.1.1	Stress invariants	19
3.1.2	Haigh–Westergaard stress space	20
3.1.3	Linear elastic stress-strain relation	21
3.1.4	Decomposition of the strain	22
3.2	Yield criteria	23
3.2.1	The von Mises yield criterion	23
3.2.2	The Drucker–Prager yield criterion	24
3.3	Plastic flow rules	25
3.4	Hardening laws	25
3.4.1	Isotropic hardening	25
3.4.1.1	Linear isotropic hardening	25
3.4.1.2	Nonlinear isotropic hardening	26
3.4.2	Kinematic hardening	26
3.4.2.1	Linear kinematic hardening	26
3.4.2.2	Nonlinear kinematic hardening	27
3.4.3	Combined linear hardening	27
3.5	Elastic-plastic constitutive models	27
3.5.1	Introduction	27
3.5.2	Associative von Mises elastoplasticity model	27
3.5.3	Non-associative Drucker–Prager elastoplasticity model	30
4	Exact time integration of constitutive models	33
4.1	Introduction	33
4.2	Strain-driven problems with constant strain rate assumption	33
4.2.1	Associative von Mises elastoplasticity model	34
4.2.1.1	Solution in general case	34
4.2.1.2	Solution in radial loading case	37
4.2.1.3	Discussion on the angle ψ	37
4.2.2	Non-associative Drucker–Prager elastoplasticity model	38

4.2.2.1	Solution in general case	38
4.2.2.2	Solution in deviatoric radial loading	43
4.2.2.3	Strain input required to reach the apex	44
4.2.2.4	Solution at the apex	44
4.2.2.5	Discussion on the angle ψ	47
4.3	Stress-driven problems with constant stress rate assumption	48
4.3.1	Associative von Mises elastoplasticity model	48
4.3.1.1	Solution in general case	48
4.3.1.2	Solution in radial loading case	50
4.3.2	Non-associative Drucker–Prager elastoplasticity model	51
4.3.2.1	Solution in general case	51
4.3.2.2	Solution in deviatoric radial loading	52
4.3.2.3	Stress input required to reach the apex	53
4.3.2.4	Solution at the apex	53
5	Stress update procedures	55
5.1	Introduction	55
5.2	Associative von Mises elastoplasticity model	56
5.2.1	Case A: Elastic loading	56
5.2.2	Case B: Plastic loading	56
5.2.3	Case C: Elastic-plastic transition	57
5.2.4	Case D: Elastic-plastic transition due to unloading	58
5.2.5	Case E: Unloading	58
5.3	Non-associative Drucker–Prager elastoplasticity model	59
5.3.1	Case A: Elastic loading	59
5.3.2	Case B: Plastic loading	59
5.3.3	Case C: Elastic-plastic transition	61
5.3.4	Case D: Elastic-plastic transition due to unloading	62
5.3.5	Case E: Unloading	62
6	Consistent tangent tensors	63
6.1	Introduction	63
6.2	Associative von Mises elastoplasticity model	64
6.2.1	General loading case	64
6.2.2	Radial loading case	65
6.3	Non-associative Drucker–Prager elastoplasticity model	65
6.3.1	General loading case	65
6.3.1.1	Stress update without reaching the apex	66
6.3.1.2	Stress update through the apex	66
6.3.2	Deviatoric radial loading case	68
6.3.2.1	Stress update without reaching the apex	68
6.3.2.2	Stress update through the apex	69
6.3.3	n th state located at the apex	69
7	Numerical examples	71
7.1	Introduction	71
7.2	Associative von Mises elastoplasticity model	72
7.2.1	Example 1: Prescribed nonlinear strain input	72
7.2.1.1	The problem description and the reference solution	72

7.2.1.2	Numerical calculations	73
7.2.2	Example 2: Prescribed rectilinear stress loading	74
7.2.2.1	The problem description and the exact solution	74
7.2.2.2	Numerical calculations	76
7.2.3	Example 3: Uniaxial extension of a perforated strip	81
7.2.4	Example 4: Prescribed rectilinear stress path	83
7.2.5	Example 5: Fixed plate under surface pressure loading	85
7.3	Non-associative Drucker–Prager elastoplasticity model	88
7.3.1	Example 6: Strain increment needed to reach the apex	88
7.3.2	Example 7: A non-proportional non-linear strain path	94
8	Conclusions and Theses	97
	Appendices	100
A	The incomplete beta function	101
A.1	Definition	101
A.2	Differentiation rules	102
A.3	Recursion formulae	103
B	Solution of linear non-homogeneous differential equations	105
C	Detailed derivation steps for the von Mises model	107
C.1	Solution for $\boldsymbol{\xi}(t)$ in strain-driven case	107
C.2	Solution for $\boldsymbol{s}(t)$ in strain-driven case	108
C.3	Solution for $\boldsymbol{\xi}(t)$ in stress-driven case	111
C.4	Solution for $\boldsymbol{e}(t)$ in stress-driven case	112
C.5	Consistent elastoplastic tangent tensor	114
C.5.1	General loading case	114
C.5.2	Radial loading	117
D	Detailed derivation steps for the Drucker–Prager model	119
D.1	Solution for $\boldsymbol{s}(t)$ in strain-driven case	119
D.2	Solution for $\boldsymbol{e}(t)$ in stress-driven case	120
D.3	Solution for $\text{tr}\boldsymbol{\varepsilon}(t)$ in stress-driven case	121
D.4	Consistent elastoplastic tangent tensor	121
D.4.1	General case	121
D.4.2	Deviatoric radial loading	128
D.4.3	Special cases when the apex can be reached	130
D.4.3.1	General loading case	130
D.4.3.2	Deviatoric radial loading case	131
D.4.3.3	n th state is located at the apex	131
E	Nested derivatives	133
E.1	Definition	133
E.2	Application of nested derivatives in the stress update algorithm proposed for the von Mises model	134
	References	135

Acknowledgements

First of all, I would like to express my highest appreciation to my Supervisor, Professor László Szabó (Department of Applied Mechanics, Budapest University of Technology and Economics). His constant support and invaluable insights helped me considerably in my research. I would like to thank Professor Gábor Stépán (Head of the Department of Applied Mechanics) the comfortable working environment he provided at the Department.

This research has been supported by the Hungarian Scientific Research Fund, Hungary (under Contract: OTKA, K72572). This support is gratefully acknowledged.

This work is connected to the scientific program of the "Development of quality-oriented and harmonized R+D+I strategy and functional model at BME" project. This project is supported by the New Széchenyi Plan (Project ID: TÁMOP-4.2.1/B-09/1/KMR-2010-0002).

1

Introduction

1.1 Aim of the work

Developing stress integration schemes for elastoplastic constitutive equations is still the part of recent researches worldwide, and the new results are continuously published in scientific journals. The importance of using numerically efficient stress integration schemes is obvious in engineering calculations involving plastic deformation.

The author of this dissertation was motivated to begin his research in this subject, because it was recognized that it may be possible to obtain exact stress solutions for elastoplastic models for which these solutions have been not derived earlier by others.

The main goal of this work is to derive exact stress and strain solutions for two widely used elastoplastic models: a) the associative von Mises elastoplastic model with combined linear hardening; b) the non-associative Drucker–Prager elastoplastic model governed by linear isotropic hardening. The von Mises yield criterion is usually suggested for metals, where the hydrostatic pressure does not exhibit influence on the plastic behavior of the material. By including the effects of the hydrostatic pressure into the definition of the yield criterion, we can arrive at the Drucker–Prager yield criterion, which is applied for pressure-dependent materials such as soils, concrete and some polymers.

Besides obtaining exact stress and strain solutions for the elastoplastic models under consideration, this document is devoted to present the corresponding discretized stress update formulae. In addition, the derivations of the algorithmically consistent tangent tensors are also purpose of this work.

1.2 Structure of the dissertation

The first chapter starts with the presentation of the aim of the work. Then, the structure of the dissertation is briefly reviewed. Finally, it ends with the summary of the mathematical conventions and notations used through the dissertation.

Chapter 2 provides an overview of the literature related to the subject of the dissertation. The relevant papers are summarized and the most important contributions are discussed.

In Chapter 3, the necessary background of the theory of small strain elastoplasticity is provided. After a brief analysis of the stress and strain tensors, two yield criteria are introduced, which are investigated substantially in this work. The summary of the most widely used hardening laws is also an important part of this chapter. Finally, the chapter ends with a section in which, the two elastoplastic models considered in this dissertation are formulated.

Chapter 4 presents the exact time integrations of the constitutive models under consideration. Besides the strain-driven formulation, the solutions for the stress-driven case are also derived.

Chapter 5 is concerned with the numerical implementation of the exact schemes derived in Chapter 4. The complete stress update procedures are presented including the special loading cases as well.

In Chapter 6, the algorithmically consistent tangent tensors are constructed. For the simplicity of the presentation, this chapter summarizes the final formulas without providing the detailed derivation steps. These details are given in Appendices C and D.

A series of numerical examples for both material models is presented in Chapter 7.

Chapter 8 gives a brief summary of the main results of the dissertation and presents the theses.

The dissertation includes Appendices as well. Appendix A is concerned with the definition and analysis of the incomplete beta function. Appendix B gives a brief summary of the solution for linear non-homogeneous differential equations. For simplicity reason, the main chapters of the dissertation exclude the detailed derivation steps of the new solutions. These details can be found in Appendix C and Appendix D. Finally, Appendix E briefly reviews the definition of the nested derivatives and it presents an efficient approach to invert an incomplete beta function introduced in the solution obtained for the von Mises model.

1.3 Summary of notations

1.3.1 General convention and characters

In order to simplify the presentation of formulae, specific font styles are used to represent different mathematical quantities. The convention employed for this reason is the following:

- Scalar-valued functions: italic light-face letters (e.g. p , E , ζ).
- Vectors and second-order tensors: italic bold-face letters (e.g. \mathbf{s} , $\boldsymbol{\sigma}$, $\boldsymbol{\varepsilon}$).
- Fourth-order tensors: italic bold-face calligraphic letters (e.g. \mathcal{T} , \mathcal{D}^e).

Exceptions are indicated in the surrounding text.

Important characters are summarized below.

Latin letters

a, b	Parameters introduced for both elastoplastic models
A_ξ, B_ξ	Parameters introduced for the von Mises model
A_s, B_s	Parameters introduced both for the von Mises model and the Drucker–Prager model
A_e, B_e	Parameters introduced both for the von Mises model and the Drucker–Prager model
B	Material parameter used in the Armstrong–Frederick hardening rule
c	Parameter measuring the strain increment part required to reach the yield surface
c_a	Parameter measuring the strain increment part required to reach the apex of the Drucker–Prager yield surface
\mathbf{C}^e	Fourth-order elastic compliance tensor
\mathbf{C}^{ep}	Fourth-order elastoplastic compliance tangent tensor
\mathbf{D}^e	Fourth-order elasticity tensor
\mathbf{D}^{ep}	Fourth-order elastoplastic tangent tensor
\mathbf{D}^{cons}	Fourth-order consistent tangent tensor
e	Deviatoric strain tensor
E	Young’s modulus
F	Yield function
g	Plastic potential function used for non-associative flow rules
G	Shear modulus
h	Hardening parameter related to the plastic hardening modulus
\tilde{h}	Material parameter introduced for the Drucker–Prager model
H	Plastic hardening modulus
H_1	Material parameter used in the power law hardening rule
I_1, I_2, I_3	Scalar invariants of the Cauchy stress tensor
\mathcal{I}	Fourth-order identity tensor, $\mathcal{I}_{ijkl} = \frac{1}{2}(\delta_{ik}\delta_{jl} + \delta_{il}\delta_{jk})$
j	Material parameter introduced for the Drucker–Prager model
J_1, J_2, J_3	Scalar invariants of the deviatoric stress tensor
k	Material parameter related to the yield stress
K	Bulk modulus
m	Material parameter used in the power law and the exponential law rules
M	Combined hardening parameter
\mathbf{N}	Outward normal of the yield surface
p	Hydrostatic stress (or pressure)
\mathbf{p}	Hydrostatic (or spherical) stress tensor
q, \tilde{q}	Parameters introduced for the deviatoric radial loading case of the Drucker–Prager model

Q	Gradient of the plastic potential function
R	Scalar parameter related to the yield stress as $R = \sqrt{\frac{2}{3}}\sigma_Y$
s_1, s_2, s_3	Principal stresses of the deviatoric stress tensor
\mathbf{s}	Deviatoric stress tensor
S	Norm of the deviatoric relative stress tensor in the von Mises model; norm of the deviatoric stress tensor in the Drucker–Prager model,
t	Time
\mathcal{T}	Fourth-order deviatoric tensor, $\mathcal{T} = \mathcal{I} - \frac{1}{3}\delta \otimes \delta$
V	Parameter related to the material parameters and the strain rate in the Drucker–Prager model

Greek letters

α, β	Material parameters for the Drucker–Prager model
$\boldsymbol{\alpha}$	Back-stress tensor
γ	Parameter related to the accumulated plastic strain
$\boldsymbol{\delta}$	Second-order identity tensor
$\boldsymbol{\varepsilon}$	Small (or infinitesimal) strain tensor
$\boldsymbol{\varepsilon}^e$	Elastic part of the strain tensor
$\boldsymbol{\varepsilon}^p$	Plastic part of the strain tensor
$\bar{\varepsilon}^p$	Accumulated plastic strain
ϵ	Volumetric strain
$\boldsymbol{\epsilon}$	Volumetric strain tensor
θ	Lode angle
ϑ	The angle defined between the outward normal of the yield surface and the trial stress increment
κ	Half-angle of the Drucker–Prager yield surface cone
λ	Plastic multiplier (or consistency parameter)
ν	Poisson’s ratio
$\boldsymbol{\xi}$	Deviatoric reduced (or relative) stress tensor
$\sigma_1, \sigma_2, \sigma_3$	Principal stresses of the Cauchy stress tensor
$\boldsymbol{\sigma}$	Cauchy stress tensor
$\bar{\sigma}$	Effective (or equivalent) stress
σ_Y	Yield stress
$\sigma_{Y\infty}$	Material parameter used in the exponential law hardening
ψ	The angle introduced between $\boldsymbol{\xi}$ and $\dot{\boldsymbol{\epsilon}}$ in the von Mises model; The angle introduced between \mathbf{s} and $\dot{\boldsymbol{\epsilon}}$ in the Drucker–Prager model
ω	The angle introduced between $\boldsymbol{\xi}$ and $\dot{\mathbf{s}}$ in the von Mises model; The angle introduced between \mathbf{s} and $\dot{\mathbf{s}}$ in the Drucker–Prager model

1.3.2 Mathematical notations

Operations:

$\text{tr} \mathbf{A}$	Trace of \mathbf{A}
$\det \mathbf{A}$	Determinant of \mathbf{A}
$\text{dev} \mathbf{A}$	Deviatoric part of \mathbf{A}
\mathbf{A}^T	Transpose of \mathbf{A}
$\dot{\mathbf{A}}$	Material time derivative of \mathbf{A}
\mathbf{A}^{-1}	Inverse of \mathbf{A}
$\ \mathbf{A}\ $	Euclidean norm of \mathbf{A} ; $\ \mathbf{A}\ = \sqrt{\mathbf{A} : \mathbf{A}}$ for second-order tensor, while $\ \mathbf{A}\ = \sqrt{\mathbf{A}^2}$ for vectors
$\mathbf{A} \otimes \mathbf{B}$	Dyadic (or tensor) product of \mathbf{A} and \mathbf{B}
$\mathbf{A} : \mathbf{B}$	Double dot product (or double contraction) between \mathbf{A} and \mathbf{B} , ($\mathbf{A} : \mathbf{B} = A_{ij}B_{ij}$)

Subscripts n and $n + 1$ refer to the values of the particular variables at the beginning and the end of the increment, whereas the sign Δ is used to denote the increment.

Some important derivative rules for second order tensor \mathbf{A} are (Itskov, 2009):

$$\frac{\partial \|\mathbf{A}\|}{\partial \mathbf{A}} = \frac{\mathbf{A}}{\|\mathbf{A}\|},$$

$$\frac{\partial (\text{tr} \mathbf{A}^k)}{\partial \mathbf{A}} = k (\mathbf{A}^{k-1})^T,$$

$$\frac{\partial (\text{tr} \mathbf{A})}{\partial \mathbf{A}} = \boldsymbol{\delta},$$

$$\frac{\partial (\text{tr} (\mathbf{A}^k \mathbf{L}))}{\partial \mathbf{A}} = \sum_{i=0}^{k-1} (\mathbf{A}^i \mathbf{L} \mathbf{A}^{k-1-i})^T,$$

$$\frac{\partial (\text{tr} (\mathbf{A}^k))}{\partial \mathbf{A}} = k (\mathbf{A}^{k-1})^T,$$

$$\frac{\partial (\det \mathbf{A})}{\partial \mathbf{A}} = \det \mathbf{A} \mathbf{A}^{-T}.$$

2

Literature overview of exact integration schemes in elastoplasticity

Elastoplasticity theory can be regarded as an essential part of solid mechanics. It combines the theory of elasticity and the theory of plasticity. Thus, this theory has been developed to understand and to describe the deformation of materials, where beyond the elastic limit permanent deformation occurs. In the last few centuries, a great number of attempts have been made to propose theories which are applicable to describe the deformation of ductile materials. A brief historical survey can be found in the book of Westergaard (1952).

From practical point of view, the classical continuum approach is a well suitable theory to analyze elastic-plastic problems. In this case, the stresses, strains and internal variables are considered as averaged quantities in the Representative Volume Element (RVE). Thus, this assumption neglects the local heterogeneity in the material. As plenty of textbooks, papers and commercial softwares prove, the continuum approach is well applicable for most of the structural calculations. However, it should be noted, that many higher-order approaches have been developed to describe more precisely the underlying physical phenomena in real materials. For instance, crystal plasticity (see Nemat-Nasser (2004) or Gambin (2001) for details), Cosserat theory (based on the work of Cosserat and Cosserat (1909)¹), microcontinuum field theories (introduced by Eringen (1999)) are a few examples of these higher-order theories.

Depending on the kinematic description, the classical continuum approach can be divided into *small* (or *infinitesimal*) strain theory and *finite* (or *large*) strain theory. In the former case the

¹An English version translated by D. H. Delphenich of this book is also available.

CHAPTER 2. LITERATURE OVERVIEW OF EXACT INTEGRATION SCHEMES IN ELASTOPLASTICITY

displacement gradient is infinitesimal at every material point in the body, thus, the small strain theory is a simplification of the finite strain theory using kinematic linearization. Finite strain theory has to be involved only in calculations, where the material deforms so much that the application of small strain theory would predict inaccurate solution. In elastoplastic problems, these are mostly metal-forming processes such as forging, extrusion, drawing, rolling etc., which produce very large deformation. On the other end, many elastoplastic engineering problems can be solved accurately enough using the small strain formulation. In addition, the computational cost is much less than using finite strain theory, consequently, the small strain theory is a widely accepted approach in elastoplastic engineering calculations for structural and machine designers.

Two approaches exist to describe mathematically the plastic deformations of materials. Namely, the *deformation theory* of plasticity and the *incremental form* (or rate form) theory of plasticity. In the first case, the theory provides relations between the current components of the stress and strain, whereas in the latter case, the plastic deformation is assumed to be depended on the loading path. Thus, the incremental formulation defines relation between the stress and the strain increments. For simplicity of the presentation, many authors prefer to use stress rate and strain rate instead of stress increment and strain increment. However, it should be noted, that in case of *rate-independent* theories, the deformation does not depend on time and the rate of deformation. The introduction of rate form quantities instead of incremental forms is applied only for convenience. Obviously, *rate-independent* problems require the use of rate form quantities. Since measurements indicated that plastic deformation in general is path dependent, the application of the deformation theory is limited. However, it is still a part of recent developments, see Jones (2009), for example.

A particular elastoplastic material model strongly depends on the selection of the *yield criteria*, the *elastic law*, the *flow rule* and the *hardening rule*. Numerous yield criteria have been proposed for the yielding of solids, which can be categorized as *pressure-independent* (von Mises criterion, Tresca criterion for example) and *pressure-dependent* ones (Drucker–Prager criterion, Mohr–Coulomb criterion, for instance). Usually, elastoplastic material models employs the *Hooke's law* to describe the elastic response of the material. However, there are models for which the elastic strains are neglected compared to the plastic ones. The flow rule is used to determine the direction of the plastic strain rate tensor. Experimental results indicated that in many cases, the associative flow rule is violated. Consequently, in order to predict more accurately the material response the non-associative flow rule has been suggested for some material. One possible categorization of the hardening rules is to separate them into perfect plasticity, kinematic hardening, isotropic hardening and into combined hardening rules. Furthermore, there exist linear and non-linear hardening rules both for isotropic and kinematic hardenings.

One of the most widely known elastoplastic material models is the so-called *Prandtl–Reuss equations* (see Chen and Han (2007); Khan and Huang (1995); Mendelson (1968); Prandtl (1925); Reuss (1930) for example). This material model applies the von Mises yield criterion with associative flow rule and without hardening. The Prandtl–Reuss equations served origin for the

development of more complicated elastoplastic models. In general, authors prefer to use the terms "von Mises model" or "J2 theory of flow" to refer to elastoplastic material models which based on the von Mises yield criterion. The Prandtl–Reuss equations can be extended by incorporating a particular hardening law, therefore, several new model can be formulated. Elastoplastic models based on the Drucker–Prager yield criterion are usually called as "Drucker–Prager material" for convenience. These models can be considered as an extension of the von Mises model by incorporating the pressure dependence of the plastic deformation.

Closed-form solutions of elastoplastic problems exist only for a limited class of regular geometries with simple loading. In general, elastoplastic problems are usually modeled as boundary-value problems (BVP) and typically solved using the Finite Element Method (FEM). This strategy requires the integration of the rate-form constitutive equation at every integration point of all the elements. The global accuracy of the solution strongly depends on the integration technique adopted in the calculations. One of the possible categorization of these integration schemes is to separate them into numerical techniques and into exact schemes.

The relevant contributions related to the exact schemes proposed for the von Mises model are discussed in the following paragraphs.

For the simplest case (perfect plasticity), an analytical solution was presented by Krieg and Krieg (1977) using constant strain rate assumption in strain-driven case. It should be noted that another form of the analytical solution was derived by Reuss (1930), where the author solved a system of differential equations of the stress components. Hong and Liu (1997) treated the problem as a two-phase linear system with an on-off switch, and presented an integration method solution. By exact linearization of the stress update procedure, Wei et al. (1996) derived the consistent modulus corresponding to the exact integration formula.

For the purely linear kinematic hardening model, Wang and Chang (1985, 1987) proposed an exact formula for the integration of the constitutive equations. Numerical implementation of their method can be found in the work of Szabó and Kovács (1987). The integration scheme presented by Auricchio and Beirão da Veiga (2003) is also an exact solution for purely linear kinematic hardening. A closed-form solution of purely linear kinematic hardening and softening is also given in the paper of Yoder and Whirley (1984) in strain space description.

In case of purely linear isotropic hardening, Ristinmaa and Tryding (1993) extended the method proposed by Krieg and Krieg (1977) and presented a solution technique involving an integral expression, which cannot be integrated explicitly. Thus, the authors combined their method with numerical techniques. Szabó (2009) proposed a solution to overcome this problem by using the incomplete beta function in solving the governing equation. This yields a semi-analytical solution for the von Mises elastoplasticity model with linear isotropic hardening.

For combined hardening, a truncated series solution was presented by Chan (1996). Romashchenko et al. (1999) proposed an analytical solution when the loading is given in the form of multisection polygonal lines in the deviatoric stress space. The solution obtained by Ristinmaa and Tryding (1993) requires numerical integration during the stress update procedure. An ap-

proach for this numerical integration can be found in the work of Krieg and Xu (1997). Another exact scheme is presented in the work of Liu (2004a), where the author has proposed two numerical schemes to solve the constitutive equation reformulated into an integral formulation. Therefore, the latter schemes also involve numerical solutions in the final derivation. The exact stress solution for combined linear hardening case using constant strain rate assumption was presented by Kossa and Szabó (2009b). In that paper, the authors extended the exact solution proposed for linear isotropic hardening by Szabó (2009). In addition, Kossa and Szabó (2009b) presented the exact strain solution for the stress-driven case, assuming constant stress rate input. The numerical efficiency of the exact stress solution was demonstrated by Kossa and Szabó (2010b).

Many papers have been published analyzing numerical integration methods for constitutive equations of elastoplastic solids. Although this dissertation is mainly concerned with the analytical solution of the governing equations, some relevant numerical studies are summarized in the following. Two of the most widely used schemes are the generalized trapezoidal (GTR) and the generalized midpoint rule (GMR). For the von Mises material model with combined isotropic-kinematic hardening, Ristinmaa and Tryding (1993) derived the consistent tangent modulus of the GTR and GMR in case of general loading, where the integration path starts from an elastic state and ends in an elastoplastic state. A detailed discussion, and the construction of the consistent tangent modulus of GMR in case of isotropic hardening, is given by Gratacos et al. (1992). Caddemi (1994) has presented an unified treatment of the backward-difference, midpoint, and trapezoidal algorithm for combined hardening. The error involved in backward-difference time integrations of elastoplastic models has been discussed in the paper of Cocchetti and Perego (2003). Auricchio and Beirão da Veiga (2003) proposed a new integration scheme based on the computation of an integration factor for von Mises elastoplasticity model with combined linear hardening. A new exponential based integration algorithm for associative von Mises elastoplasticity model with combined linear isotropic-kinematic hardening has been presented by Artioli et al. (2006). A comprehensive study of four integration methods based on the GMR is given by Artioli et al. (2007). The numerical performance of the GTR is investigated by Yang et al. (2008) by using an advanced soil model. Application of the return map algorithm and the corresponding consistent tangent tensor to nonlinear combined hardening is given by Auricchio and Taylor (1995), where authors have discussed also the generalized plasticity model. Khoei and Jamali (2005) developed a solution method based on the return map algorithm for a multi-surface plasticity model with both isotropic and kinematic hardening. In the work of Wallin and Ristinmaa (2001), a Runge–Kutta integration scheme is investigated for von Mises materials with isotropic hardening and for von Mises materials with damage evolution coupled to nonlinear mixed hardening. Application of explicit Runge–Kutta methods with error control to general class of elastoplastic models are under consideration in the paper of Hiley and Rouainia (2008). When the problem is considered in finite strain framework, Ponthot (2002) proposed an unified integration algorithm based on the classical radial return method for von Mises materials. Detailed study of the integration of inelastic constitutive models is given in the textbooks of Simo and Hughes (1998), Dunne and Petrinic

(2005), Stein et al. (2004), de Souza Neto et al. (2008) and Anandarajah (2010), for instance.

The following paragraph summarizes the relevant papers related to exact integration of the constitutive equation of the Drucker–Prager elastoplastic model.

Loret and Prevost (1986) presented a stress solution for the Drucker–Prager elastoplastic model governed by linear isotropic hardening assuming constant strain rate input. They adopted the analytical solution technique proposed by Krieg and Krieg (1977) for the von Mises elastoplastic model without hardening. Since the solution scheme derived by Loret and Prevost (1986) requires a Runge–Kutta procedure, it cannot be regarded as a complete exact solution. Liu (2004b) developed an integration scheme based on exponential mapping for the Drucker–Prager elastoplastic model, which can be regarded as another way of obtaining an exact scheme. This method had already been proposed earlier for the von Mises elastoplasticity model (Auricchio and Beirão da Veiga, 2003; Liu, 2004a). The method obtained by Liu (2004b) also utilizes a Runge–Kutta scheme, therefore, this exponential-based solution method cannot be regarded as complete exact solution. For the linear isotropic hardening case, Szabó and Kossa (2012) presented the exact solution. The authors extended the solution scheme proposed by Loret and Prevost (1986), by solving the differential equation, which describes the evolution of an internal variable. In addition, Szabó and Kossa (2012) proposed an exact solution for the case, when the stress state is located at the apex of the yield surface.

Besides analytical treatment of the solution, there are papers treating the problem numerically. In the paper of Loret and Prevost (1986), the authors derived two approximate methods, namely the incremental tangent prediction with radial projection and the one-step Euler integration techniques. Based on the work of Liu (2004a), Rezaiee-Pajand and Nasirai (2008) and Rezaiee-Pajand et al. (2011) proposed two numerical integration techniques involving the exponential maps for the solution of the associative Drucker–Prager elastoplastic constitutive law. Genna and Pandolfi (1994) demonstrated the application of a general two-step integration method assuming linear mixed hardening and associative flow rule. Based on the introduction of a bi-potential function, Hjjaj et al. (2003) derived an implicit scheme and also discussed the treatment of the apex in the non-associated case for non-hardening material. In the paper of Rezaiee-Pajand and Sharifian (2012), the authors reformulated the constitutive models governed by non-linear kinematic and linear hardening using the method proposed by Krieg and Krieg (1977). Finally, they utilized numerical schemes to obtain the corresponding stress solution.

This dissertation presents the derivations of the exact stress and strain solutions, the formulations of the discretized stress update formulae and the constructions of the algorithmically consistent tangent tensors for the associative von Mises elastoplastic model with combined linear hardening, and for the non-associative Drucker–Prager elastoplastic model governed by linear isotropic hardening. These results were presented in the papers of Kossa and Szabó (2009b) and Szabó and Kossa (2012).

3

Theory of small strain elastoplasticity

3.1 Analysis of stress and strain

3.1.1 Stress invariants

Consider the Cauchy stress tensor $\boldsymbol{\sigma}$. The characteristic equation of $\boldsymbol{\sigma}$ is

$$\boldsymbol{\sigma}^3 - I_1 \boldsymbol{\sigma}^2 + I_2 \boldsymbol{\sigma} - I_3 \boldsymbol{\delta} = \mathbf{0}, \quad (3.1)$$

where the *scalar stress invariants* I_1 , I_2 and I_3 are computed according to the formulas (de Souza Neto et al., 2008):

$$I_1 = \text{tr} \boldsymbol{\sigma}, \quad I_2 = \frac{1}{2} ((\text{tr} \boldsymbol{\sigma})^2 - \text{tr} (\boldsymbol{\sigma}^2)), \quad I_3 = \det \boldsymbol{\sigma}. \quad (3.2)$$

These stress invariants can be written in a simpler form using Cauchy principal stresses:

$$I_1 = \sigma_1 + \sigma_2 + \sigma_3, \quad I_2 = \sigma_1 \sigma_2 + \sigma_2 \sigma_3 + \sigma_3 \sigma_1, \quad I_3 = \sigma_1 \sigma_2 \sigma_3. \quad (3.3)$$

The *deviatoric stress tensor* is obtained by subtracting the *hydrostatic* (or *spherical*) *stress tensor* \mathbf{p} from the Cauchy stress tensor:

$$\mathbf{s} = \boldsymbol{\sigma} - \mathbf{p} = \boldsymbol{\sigma} - p \boldsymbol{\delta}, \quad \text{where} \quad p = \frac{1}{3} \text{tr} \boldsymbol{\sigma}. \quad (3.4)$$

Its scalar invariants are

$$J_1 = \text{tr} \mathbf{s} = 0, \quad J_2 = \frac{1}{2} \text{tr} (\mathbf{s}^2), \quad J_3 = \det \mathbf{s} = \frac{1}{3} \text{tr} (\mathbf{s}^3). \quad (3.5)$$

The characteristic equation of the deviatoric stress \mathbf{s} is

$$\mathbf{s}^3 - J_2\mathbf{s} - J_3\boldsymbol{\delta} = \mathbf{0}, \tag{3.6}$$

where the stress invariants J_2 and J_3 can be expressed using the principal stress of \mathbf{s} :

$$J_1 = s_1 + s_2 + s_3 = 0, \quad J_2 = \frac{1}{2}(s_1^2 + s_2^2 + s_3^2), \quad J_3 = s_1s_2s_3 = \frac{1}{3}(s_1^3 + s_2^3 + s_3^3). \tag{3.7}$$

The relations between the invariants J_1, J_2, J_3 and I_1, I_2, I_3 are

$$J_2 = \frac{1}{3}(I_1^2 - 3I_2), \quad J_3 = \frac{1}{27}(2I_1^3 - 9I_1I_2 + 27I_3). \tag{3.8}$$

3.1.2 Haigh–Westergaard stress space

In the study of elastoplasticity theory, it is usually convenient if we can somehow illustrate the meaning of expressions using geometrical representation. The basis of such illustrations is the introduction of the so-called *Haigh–Westergaard stress space* (Chen and Han, 2007; Haigh, 1920; Westergaard, 1920), where principal stresses are taken as coordinate axes. In this principal stress space, it is possible to illustrate a certain stress state¹ as a geometrical point with coordinates σ_1, σ_2 and σ_3 , as shown in Figure 3.1.

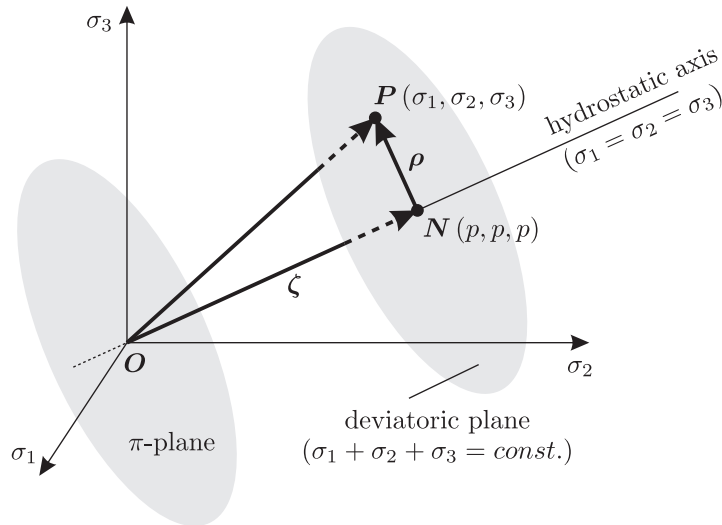


Figure 3.1: Haigh–Westergaard stress space.

The straight line for which $\sigma_1 = \sigma_2 = \sigma_3$ defines the *hydrostatic axis*, while the planes perpendicular to this axis are the *deviatoric planes*. The particular deviatoric plane containing the origin O is called as *π -plane*. The distance of a deviatoric plane from the origin is measured with the parameter ζ as

$$\zeta = \|\boldsymbol{\zeta}\| = \sqrt{3}p. \tag{3.9}$$

¹It should be noted that two stress matrices with the same eigenvalues but with different eigenvector orientations are mapped to the same geometrical point in the principal stress space. Consequently, this type of illustration does not provide information about the stress orientation with respect to the material body.

The deviatoric part $\boldsymbol{\rho}$ is defined as

$$\boldsymbol{\rho} = \mathbf{OP} - \mathbf{ON}, \quad (3.10)$$

which can be represented by the vector components

$$[\boldsymbol{\rho}] = \begin{bmatrix} \sigma_1 \\ \sigma_2 \\ \sigma_3 \end{bmatrix} - \begin{bmatrix} p \\ p \\ p \end{bmatrix} = \begin{bmatrix} s_1 \\ s_2 \\ s_3 \end{bmatrix} \quad (3.11)$$

with length

$$\rho = \|\boldsymbol{\rho}\| = \sqrt{2J_2} = \|\mathbf{s}\|. \quad (3.12a)$$

The *Lode angle* measures the angle between the deviatoric projection of the σ_1 axis and the radius vector of the current stress point (Jirásek and Bažant, 2002). It is defined by the relation

$$\cos 3\theta = \frac{3\sqrt{3}}{2} \frac{J_3}{\sqrt{J_2^3}}. \quad (3.13)$$

Consequently, the principal stresses can be expressed as

$$\sigma_1 = \frac{\zeta}{\sqrt{3}} + \sqrt{\frac{2}{3}}\rho \cos\theta, \quad (3.14)$$

$$\sigma_2 = \frac{\zeta}{\sqrt{3}} + \sqrt{\frac{2}{3}}\rho \cos\left(\theta - \frac{2\pi}{3}\right), \quad (3.15)$$

$$\sigma_3 = \frac{\zeta}{\sqrt{3}} + \sqrt{\frac{2}{3}}\rho \cos\left(\theta + \frac{2\pi}{3}\right). \quad (3.16)$$

Here, $\sigma_1 \geq \sigma_2 \geq \sigma_3$.

3.1.3 Linear elastic stress-strain relation

The general form of the linear elastic stress-strain relation for isotropic material can be written as

$$\boldsymbol{\sigma} = \mathcal{D}^e : \boldsymbol{\varepsilon}, \quad (3.17)$$

where $\boldsymbol{\varepsilon}$ is the *small strain tensor*, whereas \mathcal{D}^e denotes the *fourth-order elasticity tensor*, which can be formulated in general form as (Doghri, 2000)

$$\mathcal{D}^e = 2G\mathcal{T} + K\boldsymbol{\delta} \otimes \boldsymbol{\delta}. \quad (3.18)$$

Expression (3.17) represents the *Hooke's law*. In (3.18), G stands for the *shear modulus*, while K denotes the *bulk modulus*. Their connections to the *Young's modulus* E and to the *Poisson's ratio* ν are (Chen and Saleeb, 1982; Sadd, 2009)

$$G = \frac{E}{2(1+\nu)}, \quad K = \frac{E}{3(1-2\nu)}. \quad (3.19)$$

The inverse relation of (3.17) has the form

$$\boldsymbol{\varepsilon} = \boldsymbol{\mathcal{C}}^e : \boldsymbol{\sigma}, \tag{3.20}$$

where $\boldsymbol{\mathcal{C}}^e$ denotes the fourth-order elastic compliance tensor, the inverse of $\boldsymbol{\mathcal{D}}^e$ (Doghri, 2000):

$$\boldsymbol{\mathcal{C}}^e = \frac{1}{2G} \boldsymbol{\mathcal{I}} - \frac{\nu}{E} \boldsymbol{\delta} \otimes \boldsymbol{\delta} = \frac{1}{2G} \boldsymbol{\mathcal{T}} + \frac{1}{9K} \boldsymbol{\delta} \otimes \boldsymbol{\delta}. \tag{3.21}$$

3.1.4 Decomposition of the strain

The additive decomposition of the total strain into elastic and plastic parts is a fundamental assumption in the small strain elastoplasticity theory. It means the relation

$$\boldsymbol{\varepsilon} = \boldsymbol{\varepsilon}^e + \boldsymbol{\varepsilon}^p, \tag{3.22}$$

where $\boldsymbol{\varepsilon}$ denotes the total strain, whereas $\boldsymbol{\varepsilon}^e$ and $\boldsymbol{\varepsilon}^p$ stand for the elastic and for the plastic parts. The additive decomposition is also adopted for the strain rates. For one-dimensional case, Figure 3.2 illustrates the strain decomposition.

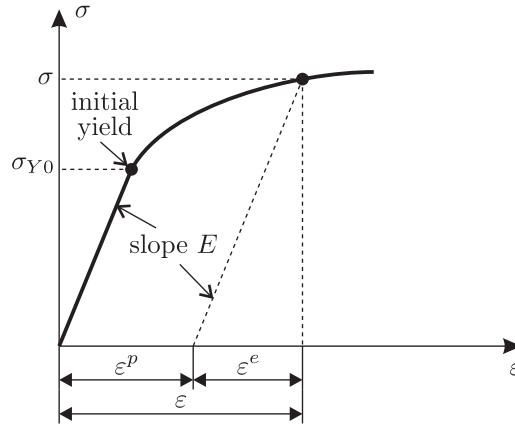


Figure 3.2: Strain decomposition in uniaxial case.

Furthermore, the strain tensor can be decomposed additively as

$$\boldsymbol{\varepsilon} = \boldsymbol{e} + \boldsymbol{\epsilon}, \tag{3.23}$$

where \boldsymbol{e} denotes the *deviatoric strain tensor*, whereas the *volumetric strain tensor*, $\boldsymbol{\epsilon}$, is given by

$$\boldsymbol{\epsilon} = \boldsymbol{\epsilon} \boldsymbol{\delta}, \quad \boldsymbol{\epsilon} = \frac{1}{3} \text{tr} \boldsymbol{\varepsilon}. \tag{3.24}$$

The decomposition into elastic and plastic parts is valid for the deviatoric and the volumetric strain, and for the strain rate quantities, as well.

3.2 Yield criteria

The law defining the elastic limit under an arbitrary combination of stresses is called *yield criterion*. In general three-dimensional case, where the stress state is described by six independent stress components, the yield criterion can be imagined as a *yield surface* in the six-dimensional stress space. This yield surface divides the whole stress space into elastic and plastic domains. Therefore, the yield criterion can be represented as a yield surface. In the Haigh–Westergaard stress space, the yield surface constitutes a three-dimensional surface with the definition

$$F(\boldsymbol{\sigma}, \sigma_Y) = 0, \quad (3.25)$$

where $F(\boldsymbol{\sigma}, \sigma_Y)$ denotes the *yield function*, whereas σ_Y represents the *yield stress*. $F = 0$ means yielding or plastic deformation, while for elastic deformation we have $F < 0$. Thus, the yield criterion is expressible in the form

$$F(\boldsymbol{\sigma}, \sigma_Y) \leq 0. \quad (3.26)$$

A particular yield function depends on the definition of the equivalent stress and the characteristic of the yield stress. For isotropic materials the yield criterion can be written in terms of the scalar invariants of the total stress (Chen and Han, 2007):

$$F(I_1, I_2, I_3, \sigma_Y) \leq 0. \quad (3.27)$$

3.2.1 The von Mises yield criterion

The von Mises yield criterion states that plastic yielding occurs, when the octahedral shearing stress reaches a critical value $k = \sigma_Y/\sqrt{3}$ (von Mises, 1913). This behavior can be written using the yield function

$$F(\boldsymbol{\sigma}, \sigma_Y) = \sqrt{\frac{3}{2} \mathbf{s} : \mathbf{s}} - \sigma_Y \quad (3.28)$$

or in an alternative way:

$$F(\boldsymbol{\sigma}, \sigma_Y) = \sqrt{J_2} - k \equiv \frac{1}{\sqrt{2}} \|\mathbf{s}\| - k. \quad (3.29)$$

The yield function (3.28) can be reformulated in a simpler, but equivalent form as

$$F(\mathbf{s}, R) = \|\mathbf{s}\| - R, \quad (3.30)$$

where $R = \sqrt{\frac{2}{3}}\sigma_Y$ (Simo and Hughes, 1998). The yield surface corresponding to this yield criterion is a cylinder parallel to the hydrostatic axis (see Figure 3.3). Consequently, its locus on a particular deviatoric plane (including the π -plane) is a circle with radius R .

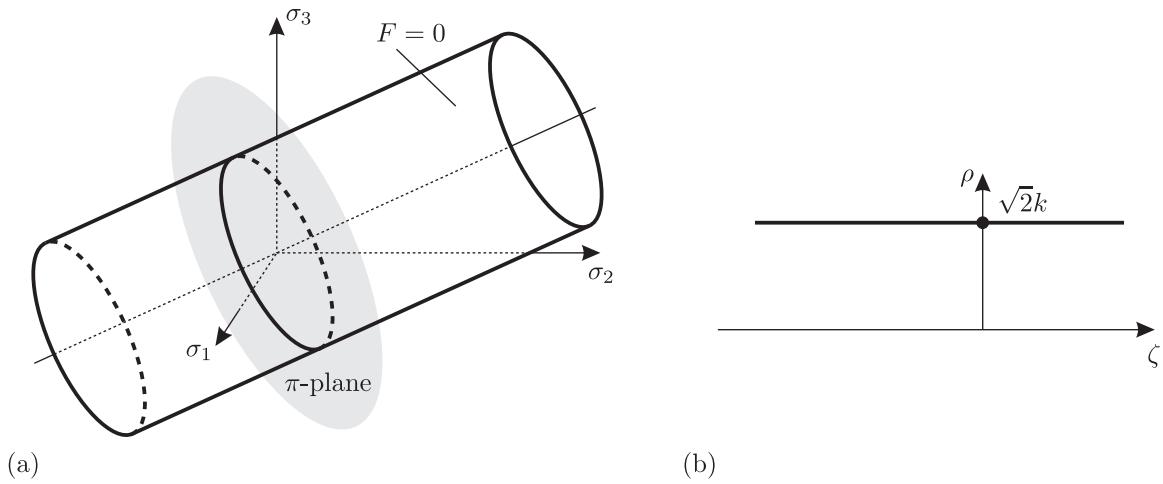


Figure 3.3: (a) The von Mises yield surface. (b) Meridian plane of the von Mises yield surface.

3.2.2 The Drucker–Prager yield criterion

The Drucker–Prager yield criterion is a simple modification of the von Mises criterion, in which the hydrostatic stress component is also included to introduce pressure-sensitivity (Drucker and Prager, 1952). The yield function for this case can be written as (Chen, 2007; de Souza Neto et al., 2008; Jirásek and Bažant, 2002)

$$F(\boldsymbol{\sigma}, \sigma_Y, \alpha) = \frac{1}{\sqrt{2}} \|\mathbf{s}\| + 3\alpha p - k, \tag{3.31}$$

where α is an additional material parameter. The yield surface in the principal stress space is represented by a circular cone around the hydrostatic axis (see Figure 3.4).

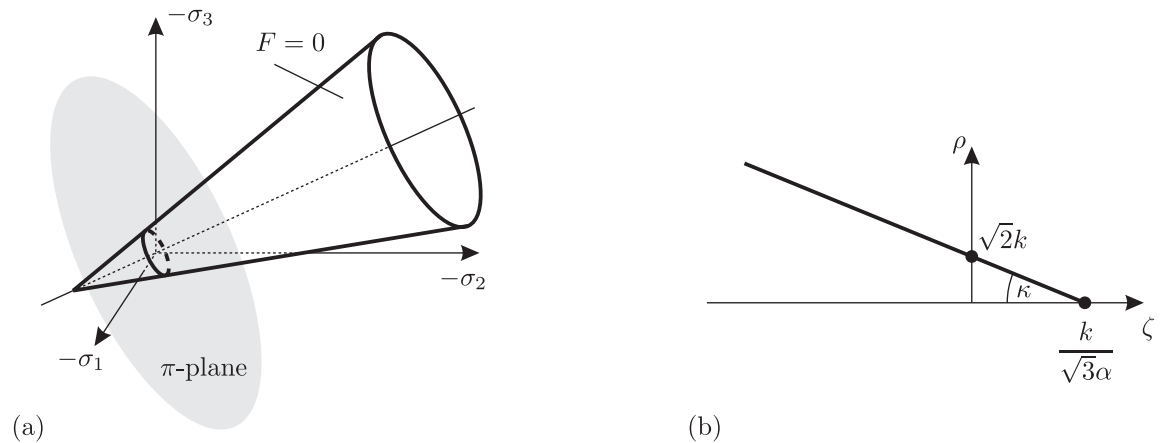


Figure 3.4: (a) Drucker–Prager yield surface. (b) Meridian plane of the Drucker-Prager yield surface.

The angle κ in the meridian plane is defined as

$$\tan \kappa = \sqrt{6}\alpha. \tag{3.32}$$

3.3 Plastic flow rules

The material starts to deform plastically, when the yield surface is reached. Upon further loading, the deformation produces plastic flow. The direction of the plastic strain rate is defined according to the *plastic flow rule*

$$\dot{\boldsymbol{\varepsilon}}^p = \dot{\lambda} \frac{\partial g}{\partial \boldsymbol{\sigma}}, \quad (3.33)$$

where the scalar function $\dot{\lambda}$ denotes the *plastic multiplier* (or *consistency parameter*), whereas g is the *plastic potential function*, which itself is a function of the stresses. The plastic flow rule is called *associative* if the plastic potential function in (3.33) equals to the yield function. Otherwise, the flow rule is termed *non-associative*. For the associative case, the direction of the strain rate is the outward normal of the yield surface, whereas for non-associative flow rule it is the gradient of the plastic potential surface.

3.4 Hardening laws

In uniaxial experiment, it is observed that the yield stress associated to a material can vary upon plastic loading. Furthermore, for some class of materials the yield stress in the reverse load direction (compression) is different than for tension. These phenomena can be modelled using various *hardening laws*. The simplest case is the *perfectly plastic material*, for which, the yield stress remains unchanged under loading. In this case the yield function becomes

$$F(\boldsymbol{\sigma}, \sigma_{Y0}) = \bar{\sigma}(\boldsymbol{\sigma}) - \sigma_{Y0}, \quad (3.34)$$

where σ_{Y0} indicates the *initial yield stress*, whereas $\bar{\sigma}(\boldsymbol{\sigma})$ stands for the *effective (or equivalent) stress*.

3.4.1 Isotropic hardening

The hardening behavior is termed *isotropic* if the shape of the yield surface remains fixed, whereas the size of the yield surface changes under plastic deformation. In other words, the yield surface expands without translation under plastic loading.

3.4.1.1 Linear isotropic hardening

If the material behavior, in the plastic region of the uniaxial stress-strain curve, is modelled with linear schematization, then we arrive at the linear isotropic hardening rule:

$$\sigma_Y(\bar{\boldsymbol{\varepsilon}}^p) = \sigma_{Y0} + H\bar{\boldsymbol{\varepsilon}}^p, \quad (3.35)$$

where the slope of the curve is given by the constant *plastic hardening modulus* H , whereas $\bar{\varepsilon}^p$ denotes the *accumulated* (or *cumulative*) *plastic strain*, which defined by (Chen and Han, 2007)

$$\bar{\varepsilon}^p = \sqrt{\frac{2}{3}} \int_0^t \|\dot{\varepsilon}^p\| \, d\tau. \quad (3.36)$$

An alternative, but equivalent, way to define the linear isotropic hardening is (Simo and Hughes, 1998)

$$R(\gamma) = R_0 + h\gamma, \quad (3.37)$$

where

$$R_0 = \sqrt{\frac{2}{3}} \sigma_{Y0}, \quad h = \frac{2}{3} H, \quad \gamma = \int_0^t \|\dot{\varepsilon}^p\| \, d\tau. \quad (3.38)$$

3.4.1.2 Nonlinear isotropic hardening

Nonlinear empirical idealization of the plastic hardening, in most cases, provides more accurate prediction of the material behavior. The most commonly used forms for the nonlinear isotropic hardening rule are the *power law* and the *exponential law* hardening (Doghri, 2000):

$$\sigma_Y(\bar{\varepsilon}^p) = \sigma_{Y0} + H_1 (\bar{\varepsilon}^p)^m, \quad \text{and} \quad \sigma_Y(\bar{\varepsilon}^p) = \sigma_{Y0} + \sigma_{Y\infty} (1 - e^{-m\bar{\varepsilon}^p}), \quad (3.39)$$

where H_1 , m and $\sigma_{Y\infty}$ are material parameters. There exist some other nonlinear schematizations, which can be found in the textbook of Skrzypek (1993), for instance.

3.4.2 Kinematic hardening

The *kinematic hardening* rule assumes that during plastic flow, the yield surface translates in the stress space and its shape and size remains unchanged. This hardening model based on the *Bauschinger effect* observed in uniaxial tension-compression test for some material (Bauschinger, 1881; Lemaitre and Chaboche, 1990). The use of kinematic hardening rules involves the modification (shifting) the stress tensor $\boldsymbol{\sigma}$ with the so-called *back-stress* (or *translation*) *tensor* $\boldsymbol{\alpha}$, in the yield function. Thus, the yield function becomes $F(\boldsymbol{\sigma} - \boldsymbol{\alpha}, \sigma_Y)$. Depending of the evolution of the back-stress tensor, a few kinematic hardening models exist. Two widely used rules are presented in the following.

3.4.2.1 Linear kinematic hardening

The simplest evolutionary equation for the back-stress tensor $\boldsymbol{\alpha}$ is the *Prager's linear hardening rule* (Chen and Han, 2007; de Souza Neto et al., 2008; Prager, 1955, 1956):

$$\dot{\boldsymbol{\alpha}} = \frac{2}{3} H \dot{\varepsilon}^p = h \dot{\varepsilon}^p. \quad (3.40)$$

3.4.2.2 Nonlinear kinematic hardening

Among different type of nonlinear kinematic hardening rules, the *Armstrong–Frederick’s* type is the most widely used and adopted one (Armstrong and Frederick, 1966; Frederick and Armstrong, 2007; Jirásek and Bažant, 2002). This rule introduces a fading memory effect of the strain path as

$$\dot{\alpha} = \frac{2}{3}H\dot{\epsilon}^p - B\dot{\epsilon}^p\alpha, \quad (3.41)$$

where B is a material constant.

3.4.3 Combined linear hardening

By combining the isotropic and kinematic hardening rules we arrive at the *combined hardening* (or *mixed hardening*) rule, by which the characteristics of real materials can be predicted more accurately. The combined linear hardening rules involves both the linear isotropic hardening rule (3.35) and the linear evolutionary equation (3.40) for the back-stress.

The plastic hardening modulus corresponding to the isotropic and to the kinematic hardening can be defined as

$$H_{iso} = MH, \quad H_{kin} = (1 - M)H, \quad h_{iso} = \frac{2}{3}H_{iso}, \quad h_{kin} = \frac{2}{3}H_{kin}, \quad (3.42)$$

where the *combined hardening parameter* $M \in [0, 1]$ defines the share of the isotropic part in the total amount of hardening (Axelsson and Samuelsson, 1979; Chen and Han, 2007; Simo and Hughes, 1998). In this case, H_{iso} has to be used in (3.35), whereas H_{kin} replaces H in (3.40). Consequently, $M = 1$ means purely isotropic hardening, while $M = 0$ denotes purely kinematic hardening.

3.5 Elastic-plastic constitutive models

3.5.1 Introduction

This section presents the constitutive equations of the two elastic-plastic constitutive models under consideration in this dissertation. Besides the formulation of the corresponding elastoplastic tangent tensors, the inverse forms of the constitutive equations are also presented.

3.5.2 Associative von Mises elastoplasticity model with combined linear hardening

Based on (3.30), the yield function of the von Mises elastoplasticity model with combined linear hardening is given by

$$F = \|\xi\| - R, \quad (3.43)$$

where $\boldsymbol{\xi} = \boldsymbol{s} - \boldsymbol{\alpha}$ denotes the *deviatoric relative* (or *reduced*) *stress*. The plastic flow direction, according to (3.33), is defined by the associative flow rule

$$\dot{\boldsymbol{\epsilon}}^p = \dot{\lambda} \boldsymbol{N}, \quad \boldsymbol{N} = \frac{\partial F}{\partial \boldsymbol{\sigma}} = \frac{\boldsymbol{\xi}}{\|\boldsymbol{\xi}\|}, \quad \|\dot{\boldsymbol{\epsilon}}^p\| = \dot{\lambda} = \dot{\gamma}, \quad (3.44)$$

where \boldsymbol{N} represents the outward normal of the yield surface. The linear isotropic hardening rule (3.37) takes the form

$$R(\gamma) = R_0 + h_{iso}\gamma. \quad (3.45)$$

The evolutionary law for the back-stress according to the Prager's linear hardening rule (3.40) is defined as

$$\dot{\boldsymbol{\alpha}} = h_{kin}\dot{\boldsymbol{\epsilon}}^p = \dot{\lambda}h_{kin}\boldsymbol{N} = \dot{\lambda}h_{kin}\frac{\boldsymbol{\xi}}{\|\boldsymbol{\xi}\|}. \quad (3.46)$$

The loading/unloading conditions can be expressed in the *Kuhn-Tucker form* as (de Souza Neto et al., 2008; Luenberger and Ye, 2008; Simo and Hughes, 1998)

$$\dot{\lambda} \geq 0, \quad F \leq 0, \quad \dot{\lambda}F = 0. \quad (3.47)$$

The plastic multiplier can be derived from the *consistency condition* $\dot{F} = 0$ using with combination of (3.17) and (3.22):

$$\dot{F} = \frac{\partial F}{\partial \boldsymbol{\sigma}} : \dot{\boldsymbol{\sigma}} + \frac{\partial F}{\partial \boldsymbol{\alpha}} : \dot{\boldsymbol{\alpha}} - \dot{R} = \boldsymbol{N} : \mathcal{D}^e : \dot{\boldsymbol{\epsilon}} - (2G + h)\dot{\lambda}, \quad (3.48)$$

$$\dot{\lambda} = \frac{\boldsymbol{N} : \mathcal{D}^e : \dot{\boldsymbol{\epsilon}}}{2G + h} = \frac{2G\boldsymbol{\xi} : \dot{\boldsymbol{\epsilon}}}{(2G + h)\|\boldsymbol{\xi}\|}. \quad (3.49)$$

The *fourth-order elastoplastic tangent tensor* \mathcal{D}^{ep} , which relates the strain rate $\dot{\boldsymbol{\epsilon}}$ to the stress rate $\dot{\boldsymbol{\sigma}}$ is computed from

$$\dot{\boldsymbol{\sigma}} = \mathcal{D}^e : \dot{\boldsymbol{\epsilon}}^e = \mathcal{D}^e : \dot{\boldsymbol{\epsilon}} - \mathcal{D}^e : \dot{\boldsymbol{\epsilon}}^p = \mathcal{D}^e : \dot{\boldsymbol{\epsilon}} - \frac{\boldsymbol{N} : \mathcal{D}^e : \dot{\boldsymbol{\epsilon}}}{2G + h} \mathcal{D}^e : \boldsymbol{N} \quad (3.50)$$

$$= \left(\mathcal{D}^e - \frac{\mathcal{D}^e : \boldsymbol{N} \otimes \boldsymbol{N} : \mathcal{D}^e}{2G + h} \right) : \dot{\boldsymbol{\epsilon}}. \quad (3.51)$$

Therefore the rate-form elastic-plastic constitutive equation has the following form:

$$\boxed{\dot{\boldsymbol{\sigma}} = \mathcal{D}^{ep} : \dot{\boldsymbol{\epsilon}}}, \quad (3.52)$$

where

$$\mathcal{D}^{ep} = \mathcal{D}^e - \frac{\mathcal{D}^e : \boldsymbol{N} \otimes \boldsymbol{N} : \mathcal{D}^e}{2G + h} = \mathcal{D}^e - \frac{4G^2}{(2G + h)\|\boldsymbol{\xi}\|^2} \boldsymbol{\xi} \otimes \boldsymbol{\xi}. \quad (3.53)$$

The constitutive equation (3.52) can be separated into deviatoric and hydrostatic (spherical) parts as follows

$$\boxed{\dot{\mathbf{s}} = 2G\dot{\boldsymbol{\epsilon}} - \frac{4G^2}{(2G+h)\|\boldsymbol{\xi}\|^2} (\boldsymbol{\xi} : \dot{\boldsymbol{\epsilon}}) \boldsymbol{\xi}} \quad (3.54)$$

and

$$\boxed{\dot{p} = 3K\dot{\epsilon}}. \quad (3.55)$$

It can be clearly concluded, that in this model, the hydrostatic part of the total stress is governed by pure elastic law. Therefore, the plastic deformation affects only the deviatoric stress components.

The evolutionary equation for the back-stress can be expressed by combining (3.46) and (3.49):

$$\dot{\boldsymbol{\alpha}} = \frac{2Gh(1-M)}{(2G+h)\|\boldsymbol{\xi}\|^2} (\boldsymbol{\xi} : \dot{\boldsymbol{\epsilon}}) \boldsymbol{\xi}. \quad (3.56)$$

The evolution law of the parameter R related to the yield stress is obtained by taking the time derivative of (3.45):

$$\dot{R} = \frac{2GMh}{(2G+h)\|\boldsymbol{\xi}\|} (\boldsymbol{\xi} : \dot{\boldsymbol{\epsilon}}). \quad (3.57)$$

In this description, R represents the radius of the yield surface (cylinder). Finally, the definition for the rate of the deviatoric relative stress is given by

$$\dot{\boldsymbol{\xi}} = \dot{\mathbf{s}} - \dot{\boldsymbol{\alpha}} = 2G\dot{\boldsymbol{\epsilon}} - \frac{2G}{\|\boldsymbol{\xi}\|^2} \left(1 - \frac{Mh}{2G+h}\right) (\boldsymbol{\xi} : \dot{\boldsymbol{\epsilon}}) \boldsymbol{\xi}. \quad (3.58)$$

Inverse elastoplastic constitutive equation

The inverse elastic-plastic constitutive equation, which relates the stress rate to the strain rate, is given by the relation

$$\dot{\boldsymbol{\epsilon}} = \mathbf{C}^{\text{ep}} : \dot{\boldsymbol{\sigma}}, \quad (3.59)$$

where the *fourth-order elastoplastic compliance tangent tensor* \mathbf{C}^{ep} can be derived by inverting the elastoplastic tangent tensor \mathbf{D}^{ep} using the *Sherman–Morrison* formula (Sherman and Morrison, 1949; Szabó, 1985):

$$\mathbf{C}^{\text{ep}} = (\mathbf{D}^{\text{ep}})^{-1} = \mathbf{C}^{\text{e}} + \frac{1}{h} \mathbf{N} \otimes \mathbf{N} = \mathbf{C}^{\text{e}} + \frac{1}{h\|\boldsymbol{\xi}\|^2} \boldsymbol{\xi} \otimes \boldsymbol{\xi}. \quad (3.60)$$

The constitutive equation (3.59) can be separated into deviatoric and hydrostatic parts as follows

$$\dot{\boldsymbol{\epsilon}} = \frac{1}{2G} \dot{\mathbf{s}} + \frac{1}{h\|\boldsymbol{\xi}\|^2} (\boldsymbol{\xi} : \dot{\mathbf{s}}) \boldsymbol{\xi}, \quad (3.61)$$

and

$$\dot{\epsilon} = \frac{1}{3K} \dot{p}. \quad (3.62)$$

Combining (3.61) with (3.57), (3.58) and (3.56) we arrive at

$$\dot{R} = \frac{M}{\|\xi\|} (\xi : \dot{s}), \quad \dot{\alpha} = \frac{1-M}{\|\xi\|^2} (\xi : \dot{s}) \xi, \quad \dot{\xi} = \dot{s} - \frac{1-M}{\|\xi\|^2} (\xi : \dot{s}) \xi. \quad (3.63)$$

3.5.3 Non-associative Drucker–Prager elastoplasticity model with linear isotropic hardening

The yield function (3.31) for the Drucker–Prager model with linear isotropic hardening can be formulated as

$$F = \frac{1}{\sqrt{2}} \|\mathbf{s}\| + 3\alpha p - k. \quad (3.64)$$

Since non-associative case is considered, the plastic flow potential function has to be defined. A commonly adopted form is given by (Chen and Han, 2007)

$$g = \frac{1}{\sqrt{2}} \|\mathbf{s}\| + 3\beta p, \quad (3.65)$$

where β is a material parameter. The gradients of the yield function and the plastic potential function, with respect to $\boldsymbol{\sigma}$ are the following:

$$\mathbf{N} = \frac{\partial F}{\partial \boldsymbol{\sigma}} = \frac{\mathbf{s}}{\sqrt{2} \|\mathbf{s}\|} + \alpha \boldsymbol{\delta}, \quad (3.66)$$

$$\mathbf{Q} = \frac{\partial g}{\partial \boldsymbol{\sigma}} = \frac{\mathbf{s}}{\sqrt{2} \|\mathbf{s}\|} + \beta \boldsymbol{\delta}, \quad (3.67)$$

The non-associative flow rule for the plastic strain rate is defined using (3.33) as

$$\dot{\epsilon}^p = \dot{\lambda} \mathbf{Q} = \dot{\lambda} \left(\frac{\mathbf{s}}{\sqrt{2} \|\mathbf{s}\|} + \beta \boldsymbol{\delta} \right). \quad (3.68)$$

The norm of plastic strain rate and the rate of the accumulated plastic strain (3.36) are the following:

$$\|\dot{\epsilon}^p\| = \dot{\lambda} \sqrt{\frac{1}{2} + 3\beta^2}, \quad \dot{\bar{\epsilon}}^p = \dot{\lambda} \sqrt{\frac{1}{3} + 2\beta^2}. \quad (3.69)$$

The linear isotropic hardening rule (3.35) for this model becomes (Chen and Han, 2007)

$$k(\bar{\epsilon}^p) = \left(\alpha + \frac{1}{\sqrt{3}} \right) \sigma_Y(\bar{\epsilon}^p). \quad (3.70)$$

The loading/unloading conditions can be expressed in the Kuhn–Tucker form (3.47). The plastic multiplier can be obtained from the consistency condition $\dot{F} = 0$, using with combination of (3.17) and (3.22):

$$\dot{F} = \frac{\partial F}{\partial \boldsymbol{\sigma}} : \dot{\boldsymbol{\sigma}} - \dot{k} = \mathbf{N} : \mathcal{D}^e : \dot{\boldsymbol{\epsilon}} - \dot{\lambda} \left(\mathbf{N} : \mathcal{D}^e : \mathbf{Q} + H \left(\alpha + \frac{1}{\sqrt{3}} \right) \sqrt{\frac{1}{3} + 2\beta^2} \right), \quad (3.71)$$

$$\dot{\lambda} = \frac{\mathbf{N} : \mathcal{D}^e : \dot{\boldsymbol{\epsilon}}}{\mathbf{N} : \mathcal{D}^e : \mathbf{Q} + H \left(\alpha + \frac{1}{\sqrt{3}} \right) \sqrt{\frac{1}{3} + 2\beta^2}} = \frac{1}{\tilde{h}} \left(\frac{2G}{\sqrt{2}\|\mathbf{s}\|} \mathbf{s} : \dot{\boldsymbol{\epsilon}} + 3K\alpha\text{tr}\dot{\boldsymbol{\epsilon}} \right), \quad (3.72)$$

where the scalar parameter \tilde{h} is defined as

$$\tilde{h} = G + 9K\alpha\beta + H \left(\alpha + \frac{1}{\sqrt{3}} \right) \sqrt{\frac{1}{3} + 2\beta^2}. \quad (3.73)$$

The elastoplastic tangent tensor is derived from

$$\dot{\boldsymbol{\sigma}} = \mathcal{D}^e : \dot{\boldsymbol{\epsilon}}^e = \mathcal{D}^e : \dot{\boldsymbol{\epsilon}} - \mathcal{D}^e : \dot{\boldsymbol{\epsilon}}^p = \mathcal{D}^e : \dot{\boldsymbol{\epsilon}} - \frac{\mathbf{N} : \mathcal{D}^e : \dot{\boldsymbol{\epsilon}}}{\tilde{h}} \mathcal{D}^e : \mathbf{Q} \quad (3.74)$$

$$= \left(\mathcal{D}^e - \frac{\mathcal{D}^e : \mathbf{Q} \otimes \mathbf{N} : \mathcal{D}^e}{\tilde{h}} \right) : \dot{\boldsymbol{\epsilon}}. \quad (3.75)$$

Using the result above, the elastoplastic constitutive law can be written as

$$\dot{\boldsymbol{\sigma}} = \mathcal{D}^{\text{ep}} : \dot{\boldsymbol{\epsilon}}, \quad (3.76)$$

where

$$\mathcal{D}^{\text{ep}} = \mathcal{D}^e - \frac{\mathcal{D}^e : \mathbf{Q} \otimes \mathbf{N} : \mathcal{D}^e}{\tilde{h}} \quad (3.77)$$

$$= \mathcal{D}^e - \frac{1}{\tilde{h}} \left(\frac{2G^2}{\|\mathbf{s}\|^2} \mathbf{s} \otimes \mathbf{s} + \frac{6KG\alpha}{\sqrt{2}\|\mathbf{s}\|} \mathbf{s} \otimes \boldsymbol{\delta} + \frac{6KG\beta}{\sqrt{2}\|\mathbf{s}\|} \boldsymbol{\delta} \otimes \mathbf{s} + 9K^2\alpha\beta \boldsymbol{\delta} \otimes \boldsymbol{\delta} \right). \quad (3.78)$$

The constitutive equation (3.76) can be separated into deviatoric and hydrostatic parts as follows

$$\dot{\mathbf{s}} = 2G\dot{\boldsymbol{\epsilon}} - \frac{2G^2}{\tilde{h}\|\mathbf{s}\|^2} \left(\mathbf{s} : \dot{\boldsymbol{\epsilon}} + \frac{9K\alpha\|\mathbf{s}\|\dot{\boldsymbol{\epsilon}}}{\sqrt{2}G} \right) \mathbf{s} \quad (3.79)$$

and

$$\dot{p} = 3K\dot{\boldsymbol{\epsilon}} - \frac{3\sqrt{2}KG\beta}{\tilde{h}\|\mathbf{s}\|} \left(\mathbf{s} : \dot{\boldsymbol{\epsilon}} + \frac{9K\alpha\|\mathbf{s}\|\dot{\boldsymbol{\epsilon}}}{\sqrt{2}G} \right). \quad (3.80)$$

Inverse elastoplastic constitutive equation

The inverse of the constitutive law (3.76) is defined as

$$\dot{\boldsymbol{\epsilon}} = \mathcal{C}^{\text{ep}} : \dot{\boldsymbol{\sigma}}, \quad (3.81)$$

where the fourth-order elastoplastic compliance tangent tensor \mathcal{C}^{ep} is obtained by the inversion of

(3.77) using the *Sherman–Morrison* formula (Sherman and Morrison, 1949; Szabó, 1985):

$$\mathbf{c}^{\text{ep}} = (\mathcal{D}^{\text{ep}})^{-1} = \mathbf{c}^e + \frac{1}{j} \mathbf{Q} \otimes \mathbf{N} \quad (3.82)$$

$$= \mathbf{c}^e + \frac{1}{j} \left(\frac{1}{2 \|\mathbf{s}\|^2} \mathbf{s} \otimes \mathbf{s} + \frac{\alpha}{\sqrt{2} \|\mathbf{s}\|} \mathbf{s} \otimes \boldsymbol{\delta} + \frac{\beta}{\sqrt{2} \|\mathbf{s}\|} \boldsymbol{\delta} \otimes \mathbf{s} + \alpha\beta \boldsymbol{\delta} \otimes \boldsymbol{\delta} \right), \quad (3.83)$$

where the scalar parameter j is defined as

$$j = \tilde{h} - G - 9K\alpha\beta = H \left(\alpha + \frac{1}{\sqrt{3}} \right) \sqrt{\frac{1}{3} + 2\beta^2}. \quad (3.84)$$

The inverse constitutive law (3.81) can be separated into deviatoric and hydrostatic part as follows:

$$\dot{\mathbf{e}} = \frac{1}{2G} \dot{\mathbf{s}} + \frac{1}{2j \|\mathbf{s}\|^2} \left(\mathbf{s} : \dot{\mathbf{s}} + 3\sqrt{2} \|\mathbf{s}\| \alpha \dot{p} \right) \mathbf{s} \quad (3.85)$$

and

$$\dot{\epsilon} = \left(\frac{1}{3K} + \frac{3\alpha\beta}{j} \right) \dot{p} + \frac{\beta (\mathbf{s} : \dot{\mathbf{s}})}{\sqrt{2} \|\mathbf{s}\| j}. \quad (3.86)$$

4

Exact time integration of constitutive models

4.1 Introduction

This chapter presents the two alternative ways used to obtain stress and strain solutions for the rate-form constitutive equation. In the first description, the problem is defined in *strain-driven* formulation. In this case, the strain field (path) is assumed to be known in the whole loading history and the stress field (path) has to be determined by the integration of the rate-form constitutive equation. Whereas, the *stress-driven* formulation is employed in the case when the stress field (path) is given and we are interested in the solution of the corresponding strain field (path). Thus, for this description the inverse of the rate-form constitutive equation is needed to be formulated and integrated.

The solutions in strain-driven and stress-driven cases, are presented in the following sections for both elastoplastic model under consideration.

4.2 Strain-driven problems with constant strain rate assumption

Under strain-driven formulations it is assumed that the total and plastic strain fields, the stress field and the internal variables appearing in the particular model are known at time instant $t_n \in [0, T]$, where $[0, T] \subset \mathbb{R}$ denotes the time interval under consideration. Furthermore, the total strain field $\boldsymbol{\varepsilon}$ is assumed to be given in the whole interval $[0, T]$, consequently, the loading history is defined by the given strain field $\boldsymbol{\varepsilon}(t)$. Therefore, in strain-driven problems, the stress field, the plastic strain field and the internal variables have to be determined for a given time $t \in [t_n, T]$, $t > t_n$.

In the following, the solution for plastic loading is derived for the case when $\dot{\boldsymbol{\varepsilon}}$ is constant. For simplicity of the presentation, the dependence on the variable t is omitted in the following expressions. Exceptions are indicated in the surrounding text.

4.2.1 Associative von Mises elastoplasticity model with combined linear hardening

4.2.1.1 Solution in general case

Define the following inner product (Kossa and Szabó, 2009b):

$$\boldsymbol{\xi} : \dot{\boldsymbol{\epsilon}} = \|\boldsymbol{\xi}\| \|\dot{\boldsymbol{\epsilon}}\| \cos\psi = S \|\dot{\boldsymbol{\epsilon}}\| \cos\psi, \tag{4.1}$$

where the notation $S = \|\boldsymbol{\xi}\|$ introduced¹, which represents the norm of the deviatoric relative stress $\boldsymbol{\xi}$. By definition the angle ψ is restricted to be $0 \leq \psi \leq \pi$. The schematic illustration of ψ is given in Figure 4.1.

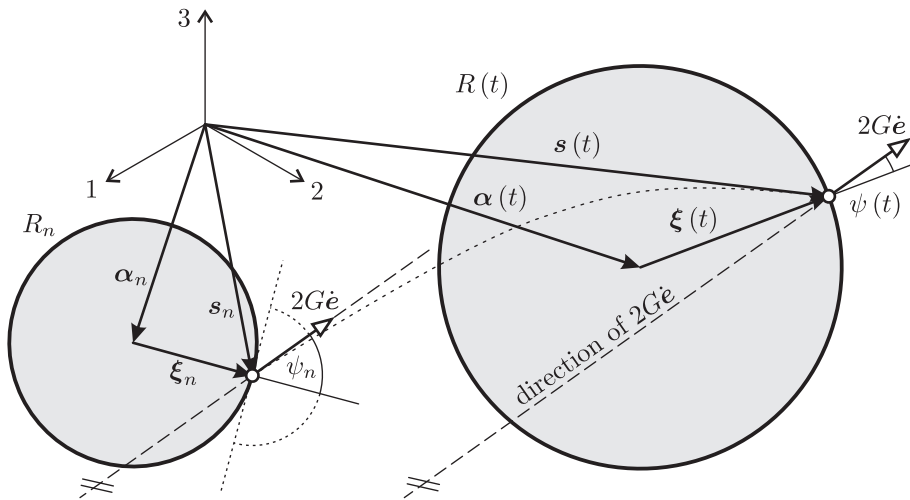


Figure 4.1: Schematic illustration of the stress solution in the deviatoric principal stress plane.

Substituting (4.1) into the expression of the plastic multiplier (3.49), we have

$$\dot{\lambda} = \frac{2G \|\dot{\boldsymbol{\epsilon}}\| \cos\psi}{2G + h}. \tag{4.2}$$

Consequently, the plastic yielding condition $\dot{\lambda} > 0$ implies that in plastic loading case the angle ψ is restricted to be between $0 \leq \psi < \pi/2$.

Substituting (4.1) into (3.57) and using the yield criteria, the evolutionary equation for S can be formulated as

$$\boxed{\dot{S} = -4Gb \|\dot{\boldsymbol{\epsilon}}\| \cos\psi}, \tag{4.3}$$

where the scalar parameter

$$b = -\frac{Mh}{2(2G + h)} \tag{4.4}$$

is introduced for simplicity.

¹According to the yield criterion, $S = R$ in case of plastic loading

The time derivative of (4.1) has the form

$$\dot{\xi} : \dot{e} = \dot{S} \|\dot{e}\| \cos\psi - S \|\dot{e}\| \sin\psi \dot{\psi}. \quad (4.5)$$

Taking the double-dot product of (3.58) and \dot{e} gives

$$\dot{\xi} : \dot{e} = 2G \|\dot{e}\|^2 - 2G \left(1 - \frac{Mh}{2G+h}\right) \|\dot{e}\|^2 \cos^2\psi. \quad (4.6)$$

Combining (4.5), (4.6) and (4.3) allows us to express $\dot{\psi}$:

$$\boxed{\dot{\psi} = -\frac{2G \|\dot{e}\|}{S} \sin\psi}. \quad (4.7)$$

By dividing (4.7) with (4.3), the problem can be reduced to the separable ordinary differential equation

$$\frac{1}{S} dS = 2b \frac{1}{\tan\psi} d\psi, \quad (4.8)$$

with the initial conditions $\psi(t = t_n) = \psi_n$ and $S(t = t_n) = S_n$. Thus, the solution of parameter S in terms of the angle ψ , can be simply obtained as

$$\int_{S_n}^S \frac{1}{\tilde{S}} d\tilde{S} = 2b \int_{\psi_n}^{\psi} \frac{1}{\tan\tilde{\psi}} d\tilde{\psi}, \quad (4.9)$$

$$\boxed{S = S_n \left(\frac{\sin\psi}{\sin\psi_n} \right)^{2b}}. \quad (4.10)$$

This result was published also by Krieg and Xu (1997) and Ristinmaa and Tryding (1993). Substituting (4.10) into (4.7) leads to the separable differential equation

$$(\sin\psi)^{2b-1} d\psi = -\frac{2G \|\dot{e}\|}{S_n} \sin^{2b}\psi_n dt, \quad (4.11)$$

which can be integrated yielding the solution

$$\int_{\psi_n}^{\psi} (\sin\tilde{\psi})^{2b-1} d\tilde{\psi} = -\frac{2G \|\dot{e}\|}{S_n} \sin^{2b}\psi_n \int_{t_n}^t d\tilde{t}, \quad (4.12)$$

$$\frac{1}{2} B\left(\cos^2\psi_n, \frac{1}{2}, b\right) - \frac{1}{2} B\left(\cos^2\psi, \frac{1}{2}, b\right) = -\frac{2G \|\dot{e}\|}{S_n} \sin^{2b}\psi_n (t - t_n), \quad (4.13)$$

$$\boxed{B\left(\cos^2\psi, \frac{1}{2}, b\right) - B\left(\cos^2\psi_n, \frac{1}{2}, b\right) = \frac{4G \|\dot{e}\| (t - t_n)}{S_n} \sin^{2b}\psi_n}, \quad (4.14)$$

where function $B(x, a, b)$ denotes the *incomplete beta function*, which is discussed in detail in

Appendix A. Having these solutions, the solution for ξ can be expressed by the following linear combination (see Appendix C.1 for detailed derivation steps):

$$\boxed{\xi = A_\xi \xi_n + B_\xi \dot{\epsilon}}, \quad (4.15)$$

where

$$A_\xi = \frac{S \sin \psi}{S_n \sin \psi_n}, \quad B_\xi = \frac{S \sin(\psi_n - \psi)}{\|\dot{\epsilon}\| \sin \psi_n}. \quad (4.16)$$

After ξ is obtained, it can be substituted into (3.54):

$$\dot{s} = \dot{A}_s \xi_n + \dot{B}_s \dot{\epsilon}, \quad (4.17)$$

where

$$\dot{A}_s = -\frac{2G^2 \|\dot{\epsilon}\| \sin(2\psi)}{(2G+h) S_n \sin \psi_n}, \quad \dot{B}_s = 2G - \frac{4G^2 \cos \psi \sin(\psi_n - \psi)}{(2G+h) \sin \psi_n}. \quad (4.18)$$

Integrating both sides in (4.17) yields the solution (see Appendix C.2 for detailed derivation steps)

$$\boxed{s = s_n + A_s \xi_n + B_s \dot{\epsilon}}, \quad (4.19)$$

$$A_s = \frac{2G(A_\xi - 1)}{(2G+h)(2b+1)}, \quad (4.20)$$

$$B_s = 2G(t - t_n) + \frac{2G(B_\xi - 2G(t - t_n))}{(2G+h)(2b+1)}. \quad (4.21)$$

The schematic illustration of the stress solution is given in Figure 4.1.

The hydrostatic stress follows the elastic evolutionary law (3.55), thus the solution is

$$\boxed{p = p_n + 3K\dot{\epsilon}(t - t_n)}. \quad (4.22)$$

Remark: The basic assumption is that the plastic hardening modulus H is smaller than the shear modulus G and greater than zero, i.e., $0 < H/G < 1$ and $0 < h/G < 2/3$. Parameter b in (4.4) can be expressed as

$$b = -\frac{M \frac{2}{3} H}{2(2G + \frac{2}{3} H)} = -\frac{MH}{6G + 2H} = -\frac{M \frac{H}{G}}{6 + 2 \frac{H}{G}}. \quad (4.23)$$

The variation of parameter b in terms of parameter M and the ratio H/G is illustrated in Figure 4.2. Thus, it can be clearly concluded that b is restricted to be

$$\boxed{-\frac{1}{8} < b < 0}. \quad (4.24)$$

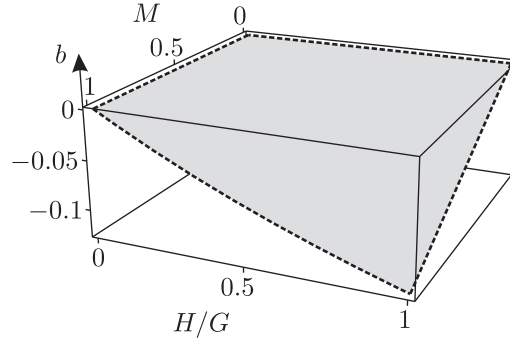


Figure 4.2: Variation of parameter b .

4.2.1.2 Solution in radial loading case

The stress solution derived in the preceding section has singularity if $\psi_n = 0$. This particular case is called as *radial loading* (or *proportional loading*) case. Since $\psi_n = 0$ we can use the identity (Kossa, 2007)

$$\frac{\boldsymbol{\xi}}{\|\boldsymbol{\xi}\|} = \frac{\dot{\mathbf{e}}}{\|\dot{\mathbf{e}}\|}. \quad (4.25)$$

According to (4.3), the solution for S reduces to

$$\boxed{S = S_n - 4Gb \|\dot{\mathbf{e}}\| (t - t_n)}. \quad (4.26)$$

From (4.25) it follows that

$$\boxed{\boldsymbol{\xi} = S \frac{\dot{\mathbf{e}}}{\|\dot{\mathbf{e}}\|}}. \quad (4.27)$$

In view of (4.25), the solution of the deviatoric stress can be simply obtained by integrating (3.54):

$$\boxed{\mathbf{s} = \mathbf{s}_n + \frac{2Gh(t - t_n)}{(2G + h)} \dot{\mathbf{e}}}. \quad (4.28)$$

4.2.1.3 Discussion on the angle ψ

Equation (4.14) defines the solution for the angle ψ in an implicit manner. This expression can be written in the form

$$B\left(\cos^2\psi, \frac{1}{2}, b\right) = x, \quad \text{where} \quad x = B\left(\cos^2\psi_n, \frac{1}{2}, b\right) + \frac{4G \|\dot{\mathbf{e}}\| (t - t_n)}{S_n \sin^{-2b}\psi_n}. \quad (4.29)$$

The angle ψ as a function of the variable x is illustrated in Figure 4.3. Based on the general characteristics of the incomplete beta function, it can be clearly concluded from (4.29) that ψ is a strictly monotonically decreasing function. Consequently, it follows that $\psi < \psi_n$ for $t > t_n$. Furthermore, another important property can be easily observed in (4.29). Namely, the angle ψ cannot reach zero for finite strain input $\|\dot{\mathbf{e}}\| (t - t_n)$.

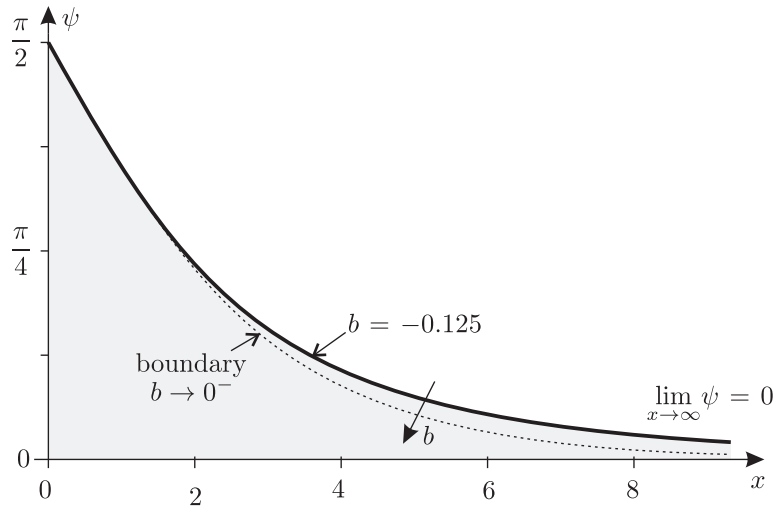


Figure 4.3: Illustration of the angle ψ .

4.2.2 Non-associative Drucker–Prager elastoplasticity model with linear isotropic hardening

4.2.2.1 Solution in general case

Define the following inner product (Szabó and Kossa, 2012):

$$\mathbf{s} : \dot{\boldsymbol{\epsilon}} = \|\mathbf{s}\| \|\dot{\boldsymbol{\epsilon}}\| \cos\psi = S \|\dot{\boldsymbol{\epsilon}}\| \cos\psi, \tag{4.30}$$

where² $S = \|\mathbf{s}\|$. The angle ψ is illustrated in Figure 4.4, where $\dot{\boldsymbol{\sigma}}^e = \mathcal{D}^e : \dot{\boldsymbol{\epsilon}}$ is the elastic stress rate.

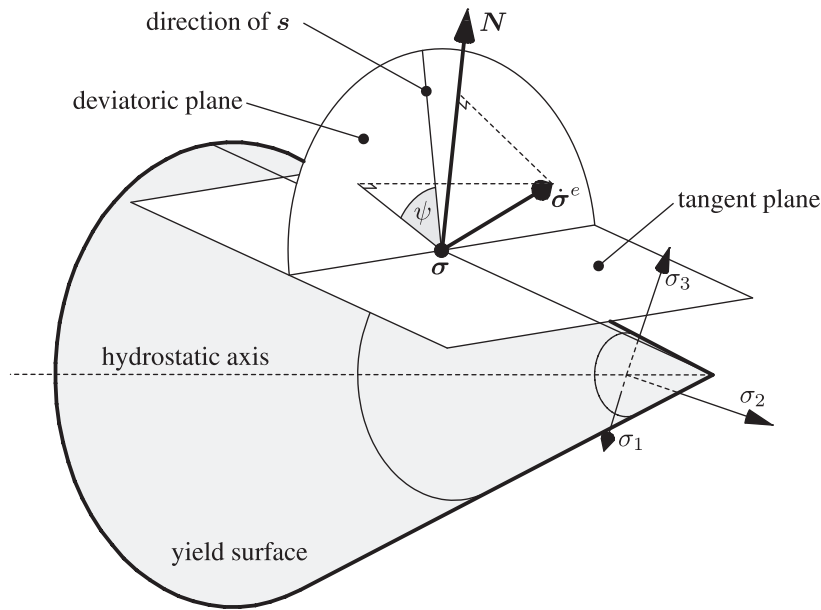


Figure 4.4: Schematic illustration of the angle ψ .

²Here, the parameter S differs from that introduced for the von Mises model.

4.2. STRAIN-DRIVEN PROBLEMS WITH CONSTANT STRAIN RATE ASSUMPTION

Using (4.30), the plastic multiplier (3.72) can be written in the form

$$\dot{\lambda} = \frac{\sqrt{2}G \|\dot{\epsilon}\|}{\tilde{h}} (\cos\psi + V), \quad (4.31)$$

where the parameter V was introduced by Loret and Prevost (1986) as

$$V = \frac{9K\alpha\dot{\epsilon}}{\sqrt{2}G \|\dot{\epsilon}\|}. \quad (4.32)$$

For simplifying the presentation of the solutions it is convenient to introduce two additional scalar parameters, which are (Szabó and Kossa, 2012)

$$a = \frac{G}{2\tilde{h}} (1 - V) - \frac{1}{2}, \quad b = \frac{G}{2\tilde{h}} (1 + V) - \frac{1}{2}. \quad (4.33)$$

The evolutionary equation of S is obtained by

$$\dot{S} = \frac{\mathbf{s}}{\|\mathbf{s}\|} : \dot{\mathbf{s}} = 2G \|\dot{\epsilon}\| \cos\psi - \frac{2G^2}{\tilde{h}S} \left(S \|\dot{\epsilon}\| \cos\psi + \frac{9K\alpha S \dot{\epsilon}}{\sqrt{2}G} \right), \quad (4.34)$$

$$\boxed{\dot{S} = 2G \|\dot{\epsilon}\| (a - b - (a + b) \cos\psi)} \quad (4.35)$$

Combining (4.35) with the time derivative of (4.30) gives

$$\dot{\mathbf{s}} : \dot{\epsilon} = 2G \|\dot{\epsilon}\|^2 (a - b - (a + b) \cos\psi) \cos\psi - S \|\dot{\epsilon}\| \sin\psi \dot{\psi}. \quad (4.36)$$

Taking the double dot product of (3.79) with $\dot{\epsilon}$ gives

$$\dot{\mathbf{s}} : \dot{\epsilon} = 2G \|\dot{\epsilon}\|^2 \sin^2\psi + 2G \|\dot{\epsilon}\|^2 \cos\psi (a - b - (a + b) \cos\psi). \quad (4.37)$$

The evolutionary equation for the angle ψ is obtained by equating (4.36) and (4.37):

$$\boxed{\dot{\psi} = -\frac{2G \|\dot{\epsilon}\|}{S} \sin\psi}. \quad (4.38)$$

Combining expression (4.35) with (4.38) leads to the separable differential equation

$$\frac{1}{S} dS = \left((a + b) \frac{1}{\tan\psi} - (a - b) \frac{1}{\sin\psi} \right) d\psi. \quad (4.39)$$

with the initial conditions $\psi(t = t_n) = \psi_n$ and $S(t = t_n) = S_n$. Using the identity $\sin\psi = 2\sin\left(\frac{\psi}{2}\right)\cos\left(\frac{\psi}{2}\right)$ (4.39) can be reformulated as

$$\frac{1}{S} dS = \left(b \frac{\cos\left(\frac{\psi}{2}\right)}{\sin\left(\frac{\psi}{2}\right)} - a \frac{\sin\left(\frac{\psi}{2}\right)}{\cos\left(\frac{\psi}{2}\right)} \right) d\psi. \quad (4.40)$$

Integrating both sides yields the solution for S :

$$\int_{S_n}^S \frac{1}{\tilde{S}} d\tilde{S} = \int_{\psi_n}^{\psi} \left(b \frac{\cos\left(\frac{\tilde{\psi}}{2}\right)}{\sin\left(\frac{\tilde{\psi}}{2}\right)} - a \frac{\sin\left(\frac{\tilde{\psi}}{2}\right)}{\cos\left(\frac{\tilde{\psi}}{2}\right)} \right) d\tilde{\psi}, \quad (4.41)$$

$$\boxed{S = S_n \left(\frac{\cos\left(\frac{\psi}{2}\right)}{\cos\left(\frac{\psi_n}{2}\right)} \right)^{2a} \left(\frac{\sin\left(\frac{\psi}{2}\right)}{\sin\left(\frac{\psi_n}{2}\right)} \right)^{2b}}. \quad (4.42)$$

Substituting the solution (4.42) into (4.38) leads to the separable differential equation

$$\cos^{2a-1}\left(\frac{\psi}{2}\right) \sin^{2b-1}\left(\frac{\psi}{2}\right) d\psi = -\frac{4G \|\dot{\mathbf{e}}\|}{S_n} \cos^{2a}\left(\frac{\psi_n}{2}\right) \sin^{2b}\left(\frac{\psi_n}{2}\right) dt. \quad (4.43)$$

The solution for the angle ψ can be obtained by solving (4.43) (Szabó and Kossa, 2012):

$$\int_{\psi_n}^{\psi} \cos^{2a-1}\left(\frac{\tilde{\psi}}{2}\right) \sin^{2b-1}\left(\frac{\tilde{\psi}}{2}\right) d\tilde{\psi} = -\int_{t_n}^t \frac{4G \|\dot{\mathbf{e}}\|}{S_n} \cos^{2a}\left(\frac{\psi_n}{2}\right) \sin^{2b}\left(\frac{\psi_n}{2}\right) d\tilde{t}, \quad (4.44)$$

$$\boxed{B\left(\cos^2\frac{\psi}{2}, a, b\right) - B\left(\cos^2\frac{\psi_n}{2}, a, b\right) = \frac{4G \|\dot{\mathbf{e}}\| (t - t_n)}{S_n} \cos^{2a}\left(\frac{\psi_n}{2}\right) \sin^{2b}\left(\frac{\psi_n}{2}\right)}. \quad (4.45)$$

Having this solution (4.45) in hand, the solution of the deviatoric stress \mathbf{s} can be expressed as a linear combination (Appendix D.1 contains the detailed derivation steps)

$$\boxed{\mathbf{s} = A_s \mathbf{s}_n + B_s \dot{\mathbf{e}}}, \quad (4.46)$$

where

$$A_s = \frac{S \sin\psi}{S_n \sin\psi_n}, \quad B_s = \frac{S \sin(\psi_n - \psi)}{\|\dot{\mathbf{e}}\| \sin\psi_n}. \quad (4.47)$$

Combining (3.80), (4.30) and (4.35) allows us to reformulate the evolutionary equation for the hydrostatic stress in the form

$$\dot{p} = 3K\dot{\epsilon} - \frac{3\sqrt{2}KG\beta}{(\tilde{h} - G)} \left(\frac{1}{2G} \dot{S} + \|\dot{\mathbf{e}}\| V \right). \quad (4.48)$$

Integrating this expression yields the solution for p :

$$p = p_n + 3K\dot{\epsilon}(t - t_n) - \frac{3\sqrt{2}KG\beta \|\dot{\mathbf{e}}\|}{\tilde{h} - G} \left(\frac{S - S_n}{2G \|\dot{\mathbf{e}}\|} + V(t - t_n) \right), \quad (4.49)$$

$$p = p_n + \dot{\epsilon}(t - t_n) K \left(3 - \frac{27K\alpha\beta}{\tilde{h} - G} \right) - \frac{3\sqrt{2}K\beta}{2(\tilde{h} - G)} (S - S_n). \quad (4.50)$$

The schematic illustration of the stress solution in the Haigh–Westergaard stress space is given in Figure 4.5.

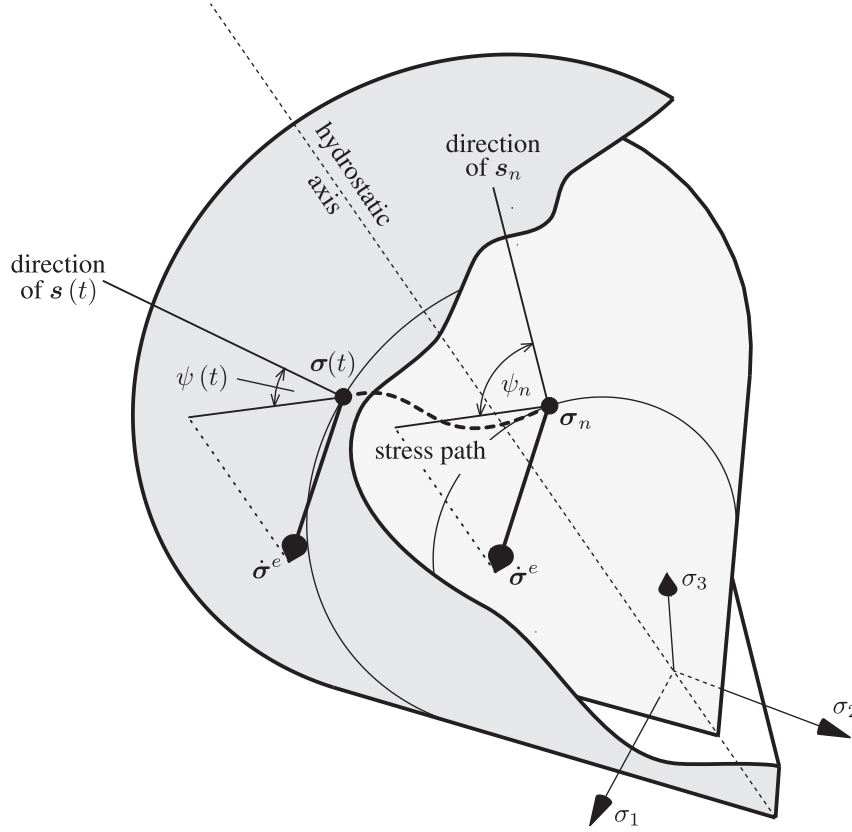


Figure 4.5: Schematic illustration of the stress solution.

Remark: Since the basic assumption is that the plastic hardening modulus H is smaller than the shear modulus G , it follows from (3.73) that $0 < G/\tilde{h} < 1$. According to the expression of the plastic multiplier (3.72), the plastic loading condition $\dot{\lambda} > 0$ for purely hydrostatic loading, i.e., $\dot{\epsilon} = \mathbf{0}$, reduces to $\text{tr} \dot{\epsilon} > 0$. Whereas for general case, i.e., $\dot{\epsilon} \neq \mathbf{0}$, it is simplified, via (4.31), to

$$\frac{G}{\tilde{h}} (V + \cos\psi) > 0, \quad (4.51)$$

(Loret and Prevost, 1986). Because the angle ψ is in the interval $[0, \pi]$, the condition (4.51) implies that $V > -1$. Thus, according to (4.33), the parameters a and b are restricted to be $a < 1/2$ and $b > -1/2$ during plastic process. Using the expressions (4.33), the variation of parameters a and b with respect to the ratio G/\tilde{h} and parameter V are shown in Figure 4.6.

Furthermore, from (4.51) it is clearly follows that the condition when $a > 0$ and $b > 0$ cannot be satisfied. Therefore, only the following three regions are available during plastic flow: $a \geq 0$ and $b < 0$; $a < 0$ and $b \leq 0$; $a < 0$ and $b > 0$. These domains, with condition (4.51) are illustrated in Figure 4.7.d. Figure 4.7.a and Figure 4.7.c show the regions of parameters G/\tilde{h} and V where $\dot{\lambda} > 0$.

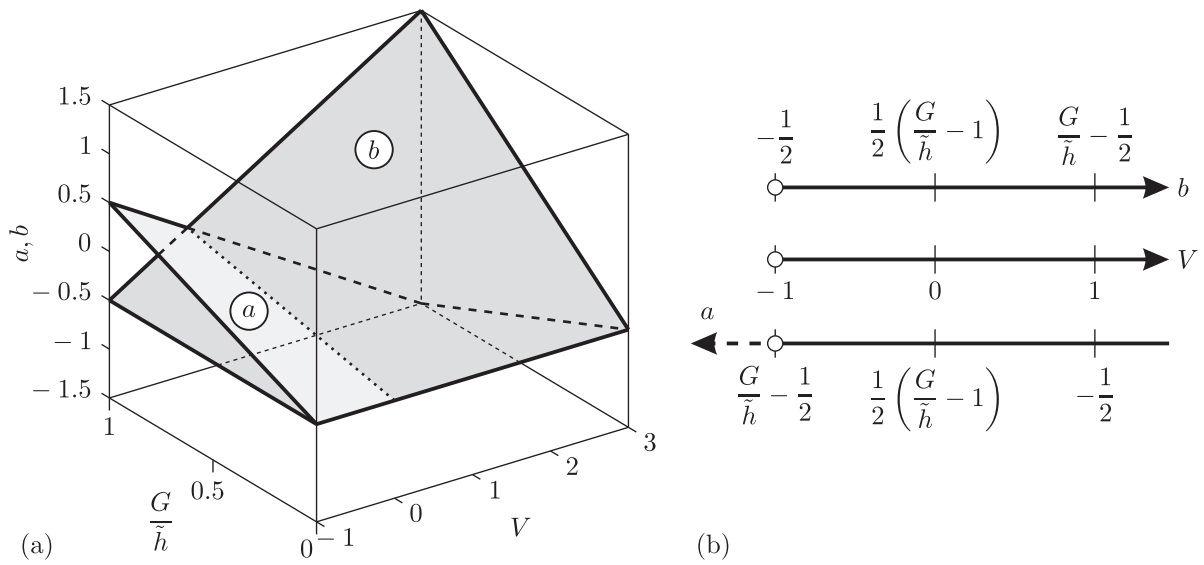


Figure 4.6: Variation of parameters a , b and V .

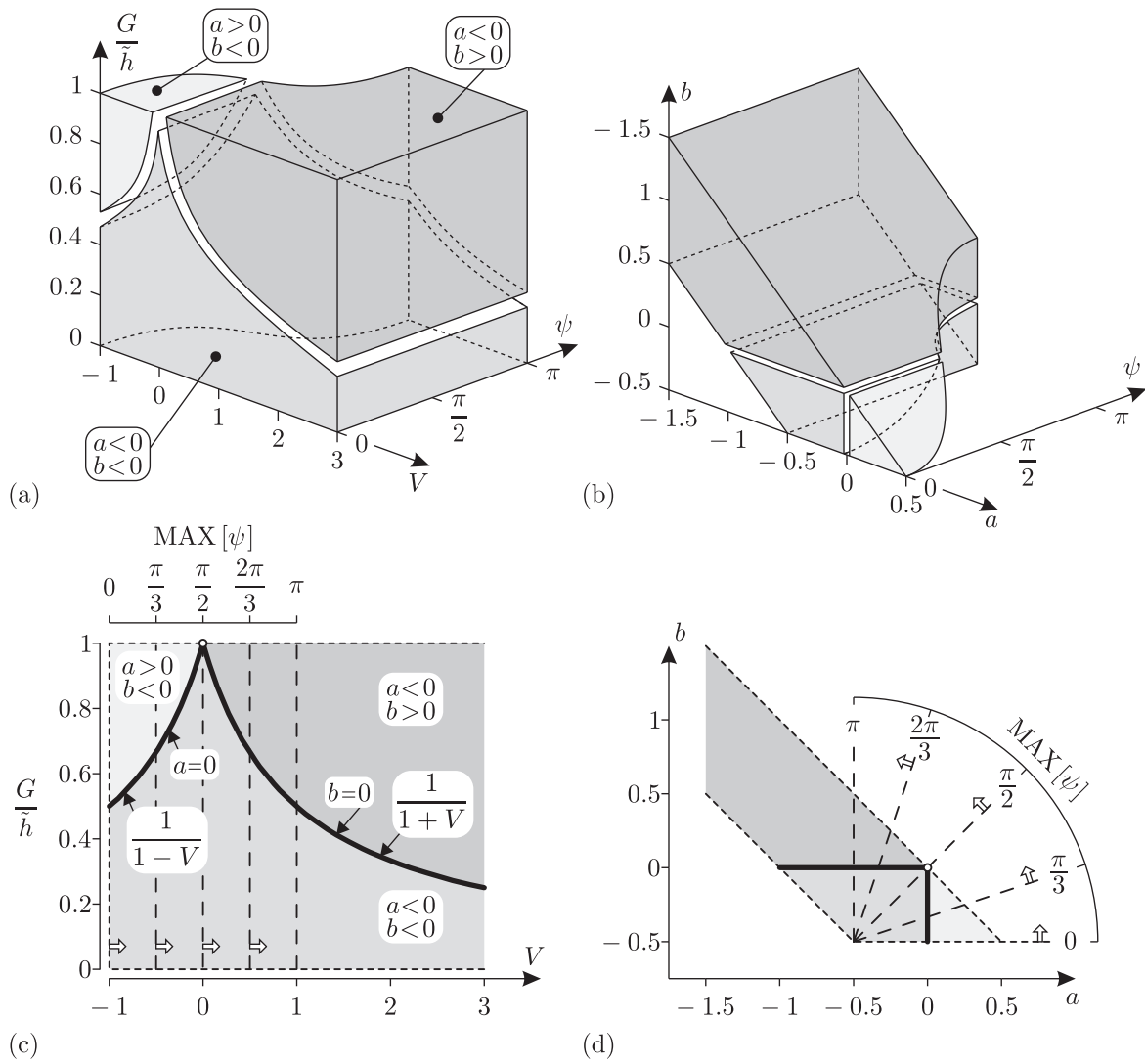


Figure 4.7: Illustration of the regions, where $\lambda > 0$.

4.2. STRAIN-DRIVEN PROBLEMS WITH CONSTANT STRAIN RATE ASSUMPTION

Using the expressions (4.33), the parameters G/\tilde{h} and V can be eliminated from (4.51). Consequently the condition $\dot{\lambda} > 0$ can be written in terms of the initial angle ψ and the parameters a and b . Figure 4.7.b and Figure 4.7.d illustrate the domains where $\dot{\lambda} > 0$ is satisfied.

4.2.2.2 Solution in deviatoric radial loading

The particular loading scenario when $\dot{\epsilon} = \mathbf{0}$, or $\psi = 0$ or $\psi = \pi$ is termed as *deviatoric radial loading* case. In this case the solution for the deviatoric stress is proportional (see Figure 4.8). The stress solutions derived for the general case has singularity in this simple case. The rate-form equation (4.35) can be reformulated for this loading case as

$$\dot{S} = q \cdot 2G \|\dot{\epsilon}\| \left(1 - \frac{G}{\tilde{h}}\right) - \frac{9\sqrt{2}K\alpha G}{\tilde{h}} \dot{\epsilon}, \quad (4.52)$$

where

$$q = \begin{cases} 1 & \text{if } \psi_n = 0, \\ -1 & \text{if } \psi_n = \pi, \\ 0 & \text{if } \|\dot{\epsilon}\| = 0. \end{cases} \quad (4.53)$$

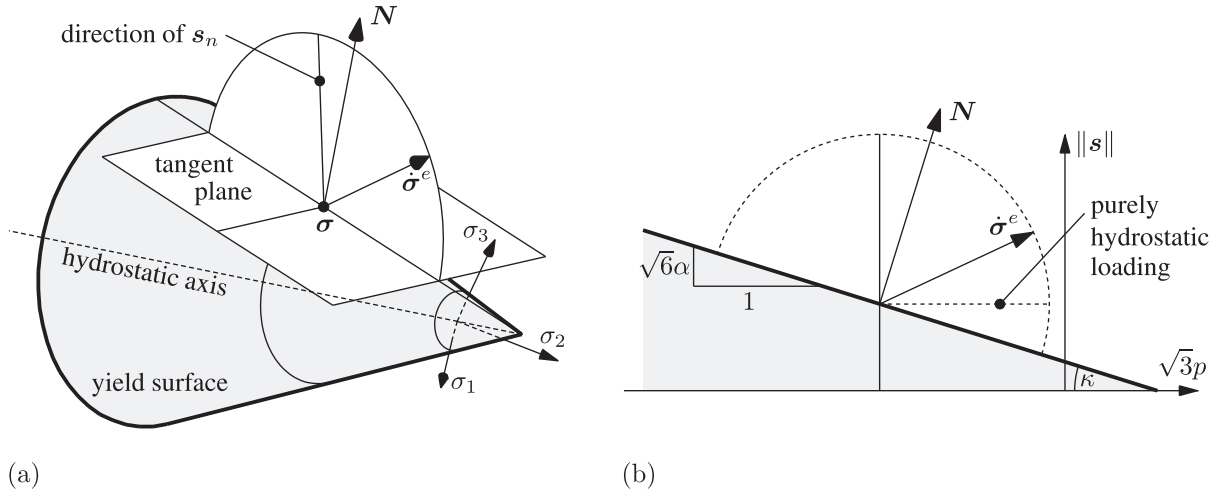


Figure 4.8: Illustration of the deviatoric radial loading case.

Thus, the solution of the norm of the deviatoric stress reduces to the simple form

$$S = S_n - \frac{9\sqrt{2}K\alpha G}{\tilde{h}} \dot{\epsilon} (t - t_n) + q \cdot 2G \|\dot{\epsilon}\| \left(1 - \frac{G}{\tilde{h}}\right) (t - t_n). \quad (4.54)$$

Since the solution for the deviatoric stress is proportional, we have

$$\mathbf{s} = \frac{S}{S_n} \mathbf{s}_n. \quad (4.55)$$

The evolutionary equation (3.80) with combination of (4.52) can be reformulated as

$$\dot{p} = 3K\dot{\epsilon} \left(1 - \frac{9K\alpha\beta}{\tilde{h} - G} \right) - \frac{3K\beta}{\sqrt{2}(\tilde{h} - G)} \dot{S}. \quad (4.56)$$

Therefore, the solution of the hydrostatic stress becomes

$$\boxed{p = p_n + 3K\dot{\epsilon} \left(1 - \frac{9K\alpha\beta}{\tilde{h} - G} \right) (t - t_n) - \frac{3K\beta}{\sqrt{2}(\tilde{h} - G)} (S - S_n)}. \quad (4.57)$$

4.2.2.3 Strain input required to reach the apex

In this subsection the special case is considered, when the strain input implies that the stress arrives to the apex of the yield surface. Both the general loading case and the deviatoric radial loading case can produce this type of loading. Denote $c_a \dot{\epsilon}(t - t_n)$ the strain input required to reach the apex. The particular value of parameter c_a is obtained in the following.

General loading case

When the stress state reaches the apex, then S becomes zero. From (4.42) it follows that this occurs when the angle ψ becomes zero. According to the discussion made in Section 4.2.2.5, this can happen when $a < 0$ and $b > 0$. The parameter c_a can be expressed from (4.45) as

$$c_a = \frac{S_n}{4G \|\dot{\epsilon}\| (t - t_n)} \frac{B(a, b) - B\left(\cos^2 \frac{\psi_n}{2}, a, b\right)}{\cos^{2a} \left(\frac{\psi_n}{2}\right) \sin^{2b} \left(\frac{\psi_n}{2}\right)}, \quad (4.58)$$

where $B(a, b)$ denotes a beta function.

Deviatoric radial loading

From (4.54) it follows that

$$c_a = \frac{S_n}{\frac{9\sqrt{2}K\alpha G}{\tilde{h}} \dot{\epsilon} (t - t_n) - q \cdot 2G \|\dot{\epsilon}\| \left(1 - \frac{G}{\tilde{h}} \right) (t - t_n)}. \quad (4.59)$$

4.2.2.4 Solution at the apex

Neither the general solution nor the solution derived for deviatoric radial loading case can be applied directly for the special case, when the initial stress state at t_n is located at the apex of the yield surface. To overcome this drawback, it is an applicable way to introduce a secondary yield function and a secondary plastic flow potential function as (Hofstetter and Taylor, 1991)

$$F_2 = 3\alpha p - k, \quad g_2 = 3\beta p. \quad (4.60)$$

4.2. STRAIN-DRIVEN PROBLEMS WITH CONSTANT STRAIN RATE ASSUMPTION

This technique was proposed by Koiter (1953) for non-smooth multi-surface plasticity theory. The gradients of F_2 and g_2 , with respect to $\boldsymbol{\sigma}$ are

$$\mathbf{N}_2 = \frac{\partial F_2}{\partial \boldsymbol{\sigma}} = \alpha \boldsymbol{\delta}, \quad \mathbf{Q}_2 = \frac{\partial g_2}{\partial \boldsymbol{\sigma}} = \beta \boldsymbol{\delta}. \quad (4.61)$$

Then the plastic strain rate tensor can be constructed as

$$\dot{\boldsymbol{\epsilon}}^p = \sum_{i=1}^2 \dot{\lambda}_i \mathbf{Q}_i. \quad (4.62)$$

For $i = 1$ we have $F_1 = F$ and $\mathbf{Q}_1 = \mathbf{Q}$ defined by (3.64) and (3.67). Therefore the plastic strain rate is located within the complementary cone of $\frac{\partial g}{\partial \boldsymbol{\sigma}}$. To obtain the direction of this vector in the principal stress space, we have to evaluate (3.67) at the apex. Obviously, expression (3.67) has singularity at this point. To overcome this drawback, it is a possible way to write the identity (Szabó and Kossa, 2012)

$$\frac{\mathbf{s}}{\|\mathbf{s}\|} = \frac{\dot{\boldsymbol{\epsilon}}}{\|\dot{\boldsymbol{\epsilon}}\|}. \quad (4.63)$$

By this substitution, we assume that the plastic strain rate tensor is located in the plane spanned by the hydrostatic and the deviatoric parts of the input strain $\dot{\boldsymbol{\epsilon}}$. Thus

$$\mathbf{N}_1 = \frac{\dot{\boldsymbol{\epsilon}}}{\sqrt{2}\|\dot{\boldsymbol{\epsilon}}\|} + \alpha \boldsymbol{\delta}, \quad \mathbf{Q}_1 = \frac{\dot{\boldsymbol{\epsilon}}}{\sqrt{2}\|\dot{\boldsymbol{\epsilon}}\|} + \beta \boldsymbol{\delta}. \quad (4.64)$$

According to (3.70) it is assumed that the rate of parameter k can be written as

$$\dot{k} = H \left(\alpha + \frac{1}{\sqrt{3}} \right) \sqrt{\frac{1}{3} + 2\beta^2} \sum_{i=1}^2 \dot{\lambda}_i. \quad (4.65)$$

Then, the plastic multipliers $\dot{\lambda}_1$ and $\dot{\lambda}_2$ are obtained by evaluating the consistency conditions $\dot{F}_1 = 0$ and $\dot{F}_2 = 0$:

$$\dot{\lambda}_1 = \sqrt{2}\|\dot{\boldsymbol{\epsilon}}\|, \quad \dot{\lambda}_2 = \frac{9K\alpha\dot{\boldsymbol{\epsilon}}}{\tilde{h} - G} - \sqrt{2}\|\dot{\boldsymbol{\epsilon}}\|. \quad (4.66)$$

Thus, the plastic strain rate (4.62) becomes

$$\dot{\boldsymbol{\epsilon}}^p = \dot{\boldsymbol{\epsilon}} + \frac{9K\alpha\beta\dot{\boldsymbol{\epsilon}}}{\tilde{h} - G} \boldsymbol{\delta} \quad (4.67)$$

Therefore, the constitutive relation reduces to

$$\dot{\boldsymbol{\sigma}} = \mathcal{D}^e : \dot{\boldsymbol{\epsilon}} - \mathcal{D}^e : \dot{\boldsymbol{\epsilon}}^p = 3K\dot{\boldsymbol{\epsilon}}\boldsymbol{\delta} - \frac{27K^2\alpha\beta\dot{\boldsymbol{\epsilon}}}{\tilde{h} - G} \boldsymbol{\delta}. \quad (4.68)$$

It can be clearly observed that the relations for the deviatoric and for the hydrostatic stresses are

$$\dot{\mathbf{s}} = \mathbf{0}, \quad \dot{p} = K\dot{\epsilon} \left(3 - \frac{27K\alpha\beta}{\tilde{h} - G} \right). \quad (4.69)$$

Thus, the stress solutions can be simply obtained as (Szabó and Kossa, 2012)

$$\boxed{\mathbf{s} = \mathbf{0}, \quad p = p_a + K\dot{\epsilon} \left(3 - \frac{27K\alpha\beta}{\tilde{h} - G} \right) (t - t_n)}, \quad (4.70)$$

where p_a denotes the hydrostatic stress corresponding to the apex point. Solutions in (4.70) are valid until the conditions $\lambda_i > 0$ hold. Observing (4.66) it is satisfied when

$$\frac{9K\alpha\dot{\epsilon}}{\tilde{h} - G} > \sqrt{2} \|\dot{\epsilon}\|. \quad (4.71)$$

If (4.71) is violated, then the secondary yield function and the secondary plastic flow potential function are no more active. In this case, the consistency condition $\dot{F}_1 = 0$ yields

$$\dot{\lambda}_1 = \frac{1}{\tilde{h}} \left(\frac{2G}{\sqrt{2}} \|\dot{\epsilon}\| + 9K\alpha\dot{\epsilon} \right). \quad (4.72)$$

Thus, the plastic strain rate becomes

$$\dot{\epsilon}^p = \frac{1}{\tilde{h}} \left(\frac{2G}{\sqrt{2}} \|\dot{\epsilon}\| + 9K\alpha\dot{\epsilon} \right) \left(\frac{\dot{\epsilon}}{\sqrt{2}\|\dot{\epsilon}\|} + \beta\delta \right). \quad (4.73)$$

In this case, the deviatoric and hydrostatic part of the constitutive relation become

$$\dot{\mathbf{s}} = \left(2G \left(1 - \frac{G}{\tilde{h}} \right) - \frac{9\sqrt{2}KG\alpha\dot{\epsilon}}{\tilde{h}\|\dot{\epsilon}\|} \right) \dot{\epsilon}, \quad (4.74)$$

$$\dot{p} = K \left(3 - \frac{27K\alpha\beta}{\tilde{h}} \right) \dot{\epsilon} - \frac{3\sqrt{2}KG\beta}{\tilde{h}} \|\dot{\epsilon}\|. \quad (4.75)$$

Therefore the stress solutions are (Szabó and Kossa, 2012)

$$\boxed{\mathbf{s} = \left(2G \left(1 - \frac{G}{\tilde{h}} \right) - \frac{9\sqrt{2}KG\alpha\dot{\epsilon}}{\tilde{h}\|\dot{\epsilon}\|} \right) (t - t_n) \dot{\epsilon}}, \quad (4.76)$$

$$\boxed{p = p_a + K \left(3 - \frac{27K\alpha\beta}{\tilde{h}} \right) \dot{\epsilon} (t - t_n) - \frac{3\sqrt{2}KG\beta}{\tilde{h}} \|\dot{\epsilon}\| (t - t_n)}. \quad (4.77)$$

4.2.2.5 Discussion on the angle ψ

Equation (4.45) defines the solution for the angle ψ in an implicit manner. This expression can be written in the form

$$B\left(\cos^2\frac{\psi}{2}, a, b\right) = x, \quad \text{where} \quad x = B\left(\cos^2\frac{\psi_n}{2}, a, b\right) + \frac{4G\|\dot{\epsilon}\|(t-t_n)}{S_n\cos^{-2a}\left(\frac{\psi_n}{2}\right)\sin^{-2b}\left(\frac{\psi_n}{2}\right)}. \quad (4.78)$$

Depending on the values of parameters a and b , the incomplete beta function has different property, which is illustrated in Figure 4.9, where the angle ψ is plotted as a function of parameter x .

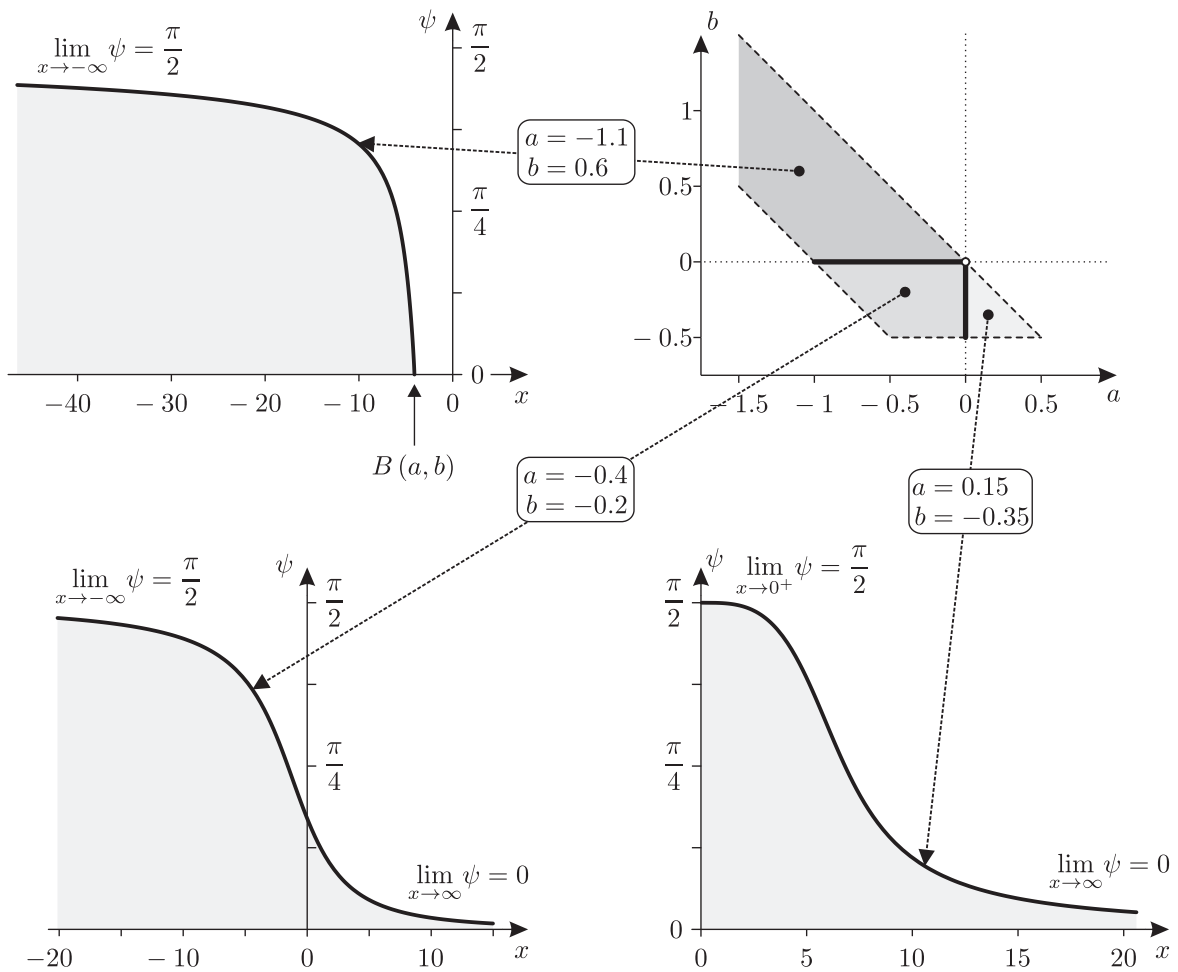


Figure 4.9: Illustration of the angle ψ .

Based on the general characteristics of the incomplete beta function, it can be clearly concluded from (4.78) that ψ is a strictly monotonically decreasing function. Consequently it follows that $\psi < \psi_n$. In addition, one very important feature can be observed: the angle ψ can become zero for the domain where $a < 0$ and $b > 0$. The particular values of parameter x at which ψ will be zero is $x = B(a, b)$, where $B(a, b)$ denotes the beta function (Abramowitz and Stegun, 1968; Spanier and Oldham, 1987).

4.3 Stress-driven problems with constant stress rate assumption

Under stress-driven formulation, it is assumed that the total and plastic strain fields, the stress field and the internal variables appearing in the particular model are known at an instant time $t_n \in [0, T]$, where $[0, T] \subset \mathbb{R}$ denotes the time interval under consideration. Furthermore, the stress field $\boldsymbol{\sigma}$ is given in the whole interval $[0, T]$, consequently, the loading history is defined by the given stress field $\boldsymbol{\sigma}(t)$. Therefore, in stress-driven problems, the strain field, the plastic strain field and the internal variables have to be determined for a given time $t \in [t_n, T]$, $t > t_n$.

In the following, the solution for the plastic solution is derived for the case when $\dot{\boldsymbol{\sigma}}$ is constant, thus

$$\boldsymbol{\sigma} = \boldsymbol{\sigma}_n + \dot{\boldsymbol{\sigma}}(t - t_n), \quad \mathbf{s} = \mathbf{s}_n + \dot{\mathbf{s}}(t - t_n), \quad p = p_n + \dot{p}(t - t_n). \quad (4.79)$$

For simplicity of the presentation the dependence on variable t is omitted in the following expressions.

4.3.1 Associative von Mises elastoplasticity model with combined linear hardening

4.3.1.1 Solution in general case

Define the angle ω through the following inner product (Kossa and Szabó, 2009b):

$$\boldsymbol{\xi} : \dot{\mathbf{s}} = \|\boldsymbol{\xi}\| \|\dot{\mathbf{s}}\| \cos\omega = S \|\dot{\mathbf{s}}\| \cos\omega. \quad (4.80)$$

In this case the plastic multiplier, by inserting (3.61) into (3.49), becomes

$$\dot{\lambda} = \frac{\boldsymbol{\xi} : \dot{\mathbf{s}}}{h \|\boldsymbol{\xi}\|} = \frac{\|\dot{\mathbf{s}}\| \cos\omega}{h}, \quad (4.81)$$

Thus, it follows that during plastic loading the angle ω is restricted to be between $0 \leq \omega < \pi/2$. Substituting (4.80) into (3.63)₁ and using the yield criterion gives

$$\boxed{\dot{S} = M \|\dot{\mathbf{s}}\| \cos\omega}. \quad (4.82)$$

Taking the time derivative of (4.80) yields

$$\dot{\boldsymbol{\xi}} : \dot{\mathbf{s}} = \dot{S} \|\dot{\mathbf{s}}\| \cos\omega - S \|\dot{\mathbf{s}}\| \sin\omega \dot{\omega} = M \|\dot{\mathbf{s}}\|^2 \cos^2\omega - S \|\dot{\mathbf{s}}\| \sin\omega \dot{\omega}. \quad (4.83)$$

Evaluating the double dot product of (3.63)₃ with $\dot{\mathbf{s}}$ gives

$$\dot{\boldsymbol{\xi}} : \dot{\mathbf{s}} = \|\dot{\mathbf{s}}\|^2 - (1 - M) \|\dot{\mathbf{s}}\|^2 \cos^2\omega = \|\dot{\mathbf{s}}\|^2 \sin^2\omega + M \|\dot{\mathbf{s}}\|^2 \cos^2\omega. \quad (4.84)$$

4.3. STRESS-DRIVEN PROBLEMS WITH CONSTANT STRESS RATE ASSUMPTION

Equating (4.83) and (4.84), the rate equation for ω can be obtained as

$$\boxed{\dot{\omega} = -\frac{\|\dot{\mathbf{s}}\| \sin\omega}{S}}. \quad (4.85)$$

Combining (4.82) and (4.85) leads to the separable differential equation

$$\frac{1}{S} dS = -M \frac{1}{\tan\omega} d\omega, \quad (4.86)$$

with initial conditions $\omega(t = t_n) = \omega_n$ and $S(t = t_n) = S_n$. Integrating it gives the solution for S :

$$\int_{S_n}^S \frac{1}{\tilde{S}} d\tilde{S} = -M \int_{\omega_n}^{\omega} \frac{1}{\tan\tilde{\omega}} d\tilde{\omega}, \quad (4.87)$$

$$\boxed{S = S_n \left(\frac{\sin\omega_n}{\sin\omega} \right)^M}. \quad (4.88)$$

Substituting this result into (4.85) yields the separable differential equation

$$(\sin\omega)^{-M-1} d\omega = -\frac{\|\dot{\mathbf{s}}\|}{S_n \sin^M \omega_n} dt. \quad (4.89)$$

Integrating this expression gives

$$\int_{\omega_n}^{\omega} (\sin\tilde{\omega})^{-M-1} d\tilde{\omega} = -\frac{\|\dot{\mathbf{s}}\|}{S_n \sin^M \omega_n} \int_{t_n}^t dt, \quad (4.90)$$

$$\boxed{B \left(\cos^2\omega, \frac{1}{2}, -\frac{M}{2} \right) - B \left(\cos^2\omega_n, \frac{1}{2}, -\frac{M}{2} \right) = \frac{2\|\dot{\mathbf{s}}\|}{S_n \sin^M \omega_n} (t - t_n)}. \quad (4.91)$$

Having the solution for the angle ω , the deviatoric reduced stress can be expressed with the following linear combination (see Appendix C.3 for detailed derivation steps):

$$\boxed{\boldsymbol{\xi} = A_{\xi} \boldsymbol{\xi}_n + B_{\xi} \dot{\mathbf{s}}}, \quad (4.92)$$

where

$$A_{\xi} = \frac{S \sin\omega}{S_n \sin\omega_n}, \quad B_{\xi} = \frac{S \sin(\omega_n - \omega)}{\|\dot{\mathbf{s}}\| \sin\omega_n}. \quad (4.93)$$

After $\boldsymbol{\xi}$ is obtained it can be substituted into (3.61) yielding

$$\dot{\mathbf{e}} = \dot{A}_e \boldsymbol{\xi}_n + \dot{B}_e \dot{\mathbf{s}} \quad (4.94)$$

with

$$\dot{A}_e = \frac{\|\dot{\mathbf{s}}\| \sin 2\omega}{2hS_n \sin \omega_n}, \quad \dot{B}_e = \frac{1}{2G} + \frac{\cos \omega \sin(\omega_n - \omega)}{h \sin \omega_n}. \quad (4.95)$$

Integrating both sides gives (see Appendix C.4 for detailed derivation steps)

$$\boxed{\mathbf{e} = \mathbf{e}_n + A_e \boldsymbol{\xi}_n + B_e \dot{\mathbf{s}}}, \quad (4.96)$$

where

$$A_e = \frac{1 - A_\xi}{h(1 - M)}, \quad B_e = \frac{(t - t_n)}{2G} + \frac{(t - t_n) - B_\xi}{h(1 - M)}. \quad (4.97)$$

The hydrostatic part of the strain is computed using the elastic relation

$$\epsilon = \epsilon_n + \frac{1}{3K} \dot{p}(t - t_n). \quad (4.98)$$

4.3.1.2 Solution in radial loading case

The stress solution derived in the preceding section has singularity if $\omega_n = 0$. In this case we can write the identity (Kossa, 2007)

$$\frac{\boldsymbol{\xi}}{\|\boldsymbol{\xi}\|} = \frac{\dot{\mathbf{s}}}{\|\dot{\mathbf{s}}\|}. \quad (4.99)$$

Integrating (4.82) yields the solution

$$\boxed{S = S_n + M \|\dot{\mathbf{s}}\| (t - t_n)}. \quad (4.100)$$

It follows from (4.99) that

$$\boxed{\boldsymbol{\xi} = S \frac{\dot{\mathbf{s}}}{\|\dot{\mathbf{s}}\|}}. \quad (4.101)$$

Therefore the solution for the deviatoric strain, by combining (3.61) and (4.99), will be

$$\dot{\mathbf{e}} = \frac{1}{2G} \dot{\mathbf{s}} + \frac{1}{h} \dot{\mathbf{s}} = \frac{2G + h}{2Gh} \dot{\mathbf{s}}, \quad (4.102)$$

$$\boxed{\mathbf{e} = \mathbf{e}_n + \frac{2G + h}{2Gh} (t - t_n) \dot{\mathbf{s}}}. \quad (4.103)$$

The hydrostatic part of the strain is computed with (4.98).

4.3.2 Non-associative Drucker–Prager elastoplasticity model with linear isotropic hardening

4.3.2.1 Solution in general case

Define the angle ω through the following inner product:

$$\mathbf{s} : \dot{\mathbf{s}} = \|\mathbf{s}\| \|\dot{\mathbf{s}}\| \cos\omega = S \|\dot{\mathbf{s}}\| \cos\omega. \quad (4.104)$$

The plastic multiplier, by combining (3.72), (3.85) and (3.86) then becomes

$$\dot{\lambda} = \frac{\|\dot{\mathbf{s}}\|}{\sqrt{2}j} \left(\cos\omega + \frac{3\sqrt{2}\alpha\dot{p}}{\|\dot{\mathbf{s}}\|} \right). \quad (4.105)$$

Thus, plastic loading occurs when

$$\dot{p} > -\frac{\|\dot{\mathbf{s}}\|}{3\sqrt{2}\alpha} \cos\omega. \quad (4.106)$$

From (4.104) it follows that

$$\dot{S} = \|\dot{\mathbf{s}}\| \cos\omega. \quad (4.107)$$

Taking the time derivative of (4.104) and then combining it with (4.107) gives

$$\dot{\omega} = -\frac{\|\dot{\mathbf{s}}\| \sin\omega}{S}. \quad (4.108)$$

Dividing (4.107) with (4.108) yields the separable differential equation:

$$\frac{1}{S} dS = -\frac{1}{\tan\omega} d\omega \quad (4.109)$$

with the initial condition $\omega(t = t_n) = \omega_n$ and $S(t = t_n) = S_n$. Thus the parameter S can be written³ as a function of the angle ω :

$$S = S_n \frac{\sin\omega_n}{\sin\omega}. \quad (4.110)$$

By substituting this solution back into expression (4.108) we arrive at the separable differential equation

$$\frac{1}{\sin^2\omega} d\omega = -\frac{\|\dot{\mathbf{s}}\|}{S_n \sin\omega_n} dt, \quad (4.111)$$

³It must be noted that the function $S(t)$ is known because stress-driven problem is considered. The only reason to express it as a function of the angle ω is to simplify the final formulas.

which has the solution⁴

$$\omega = \arctan \left(\frac{S_n \sin \omega_n}{S_n \cos \omega_n + \|\dot{\mathbf{s}}\| (t - t_n)} \right). \quad (4.112)$$

The deviatoric strain can be written as a linear combination (see Appendix D.2 for detailed derivation steps):

$$\mathbf{e} = \mathbf{e}_n + A_e \mathbf{s}_n + B_e \dot{\mathbf{s}}, \quad (4.113)$$

where

$$A_e = \frac{1}{2j} \ln \left(\frac{S}{S_n} \right) + \frac{3\alpha\dot{p}}{\sqrt{2}j \|\dot{\mathbf{s}}\|} \ln \left(\frac{\tan \frac{\omega_n}{2}}{\tan \frac{\omega}{2}} \right), \quad (4.114)$$

$$B_e = \frac{(t - t_n)}{2} \left(\frac{1}{G} + \frac{1}{j} \right) + \frac{3\alpha\dot{p}(S - S_n)}{\sqrt{2}j \|\dot{\mathbf{s}}\|^2} - \frac{S_n \sin \omega_n}{\|\dot{\mathbf{s}}\|} \left(\frac{A_e}{\tan \omega_n} + \frac{\omega_n - \omega}{2j} \right). \quad (4.115)$$

Furthermore, the solution for the hydrostatic part of the strain can be written as (see Appendix D.3 for detailed derivation steps):

$$\epsilon = \epsilon_n + \left(\frac{1}{3K} + \frac{3\alpha\beta}{j} \right) \dot{p} (t - t_n) + \frac{\beta(S - S_n)}{\sqrt{2}j}. \quad (4.116)$$

4.3.2.2 Solution in deviatoric radial loading

The solutions reduce to simpler forms in the case when $\omega_n = 0$ or $\omega_n = \pi$ or $\|\dot{\mathbf{s}}\| = 0$. These scenarios correspond to the deviatoric radial loading case, when we can write that

$$S = S_n + \tilde{q} \|\dot{\mathbf{s}}\| (t - t_n), \quad \mathbf{s} = \frac{S}{S_n} \mathbf{s}_n, \quad (4.117)$$

where \tilde{q} is defined by

$$\tilde{q} = \begin{cases} 1 & \text{if } \omega_n = 0, \\ -1 & \text{if } \omega_n = \pi, \\ 0 & \text{if } \|\dot{\mathbf{s}}\| = 0. \end{cases} \quad (4.118)$$

Inserting (4.117) into (3.85) and (3.86) gives

$$\dot{\mathbf{e}} = \frac{1}{2G} \dot{\mathbf{s}} + \frac{3\alpha\dot{p}}{\sqrt{2}S_n j} \mathbf{s}_n + \tilde{q} \frac{1}{2j} \dot{\mathbf{s}}, \quad (4.119)$$

$$\dot{\epsilon} = \left(\frac{1}{3K} + \frac{3\alpha\beta}{j} \right) \dot{p} + \tilde{q} \frac{\beta \|\dot{\mathbf{s}}\|}{\sqrt{2}j}. \quad (4.120)$$

⁴It must be emphasized that the function $\omega(t)$ can be computed without this formula. Introducing ω as the function of the parameter t and the initial angle ω_n allows us to simplify the final formulas.

Thus, the solutions for the strains will be

$$\boxed{\mathbf{e} = \mathbf{e}_n + \frac{3\alpha\dot{p}(t-t_n)}{\sqrt{2}S_nj}\mathbf{s}_n + \left(\frac{1}{2G} + \tilde{q}\frac{1}{2j}\right)(t-t_n)\dot{\mathbf{s}}}, \quad (4.121)$$

$$\boxed{\epsilon = \epsilon_n + \left(\frac{1}{3K} + \frac{3\alpha\beta}{j}\right)\dot{p}(t-t_n) + \tilde{q}\frac{\beta\|\dot{\mathbf{s}}\|}{\sqrt{2}j}(t-t_n)}. \quad (4.122)$$

4.3.2.3 Stress input required to reach the apex

In this subsection the special case is considered, when the stress input implies that the stress arrives to the apex of the yield surface. In stress-driven case, it is obviously follows that the apex can be reached only due to deviatoric radial loading. Denote $c_a\dot{\boldsymbol{\sigma}}(t-t_n)$ the stress input required to reach the apex. From (4.79) it is clearly follows that

$$c_a = \frac{S_n}{\|\dot{\mathbf{s}}\|(t-t_n)}. \quad (4.123)$$

4.3.2.4 Solution at the apex

When the initial stress state is located at the apex and stress-driven formulation is considered, then it is obvious that the new stress state leaves the apex when $\|\dot{\mathbf{s}}\| > 0$. From (4.105) it follows that plastic loading initiates if

$$\|\dot{\mathbf{s}}\| > -3\sqrt{2}\alpha\dot{p}, \quad (4.124)$$

otherwise elastic unloading occurs. The solutions (4.121) and (4.122) can be used by inserting $\tilde{q} = 1$ into these expressions:

$$\boxed{\mathbf{e} = \mathbf{e}_n + \left(\frac{1}{2G} + \frac{1}{2j}\right)(t-t_n)\dot{\mathbf{s}}}, \quad (4.125)$$

$$\boxed{\epsilon = \epsilon_n + \left(\frac{1}{3K} + \frac{3\alpha\beta}{j}\right)\dot{p}(t-t_n) + \frac{\beta\|\dot{\mathbf{s}}\|}{\sqrt{2}j}(t-t_n)}. \quad (4.126)$$

5

Stress update procedures

5.1 Introduction

Within a time increment $\Delta t = t_{n+1} - t_n$, it is assumed that at time t_n the strain $\boldsymbol{\varepsilon}_n$, the stress $\boldsymbol{\sigma}_n$, and the accumulated plastic strain $\bar{\varepsilon}_n^p$ are known and the material parameters are also given. The main goal of the stress update procedure is to determine the stress at time t_{n+1} for a given strain increment $\Delta\boldsymbol{\varepsilon}$. For this reason, first the trial stress state is introduced by assuming that the strain increment produces purely elastic deformation. Thus we have

$$\boldsymbol{\sigma}_{trial} = \boldsymbol{\sigma}_n + \mathcal{D}^e : \Delta\boldsymbol{\varepsilon} = \boldsymbol{\sigma}_n + \Delta\boldsymbol{\sigma}_{trial} = \mathbf{s}_{trial} + p_{trial}\boldsymbol{\delta}, \quad (5.1)$$

where

$$\Delta\boldsymbol{\sigma}_{trial} = 2G\Delta\mathbf{e} + 3K\Delta\epsilon\boldsymbol{\delta}, \quad \mathbf{s}_{trial} = \mathbf{s}_n + 2G\Delta\mathbf{e}, \quad p_{trial} = p_n + 3K\Delta\epsilon. \quad (5.2)$$

Depending on the n th state and the trial state various scenarios can happen. These are discussed in detail for the particular models under consideration in the following sections.

When the n th state is located on the yield surface, then we can introduce the angle ϑ defined between \mathbf{N}_n , and $\Delta\boldsymbol{\sigma}_{trial}$ as

$$\cos\vartheta = \frac{\mathbf{N}_n : \Delta\boldsymbol{\sigma}_{trial}}{\|\mathbf{N}_n\| \|\Delta\boldsymbol{\sigma}_{trial}\|}, \quad (5.3)$$

where \mathbf{N}_n denotes the yield surface gradient at the n th state.

Since the exact variation of the strain during the increment is not known, it is a commonly adopted approach to assume that the strain varies linearly in the time interval $t_n \leq t \leq t_{n+1}$ (Sloan and Booker, 1992) and thus the strain-rate is constant. Consequently, the exact stress solutions presented in the preceding chapter can be easily implemented in the discretized stress update procedures.

5.2 Associative von Mises elastoplasticity model with combined linear hardening

The various stress update scenarios are summarized in Figure 5.1.

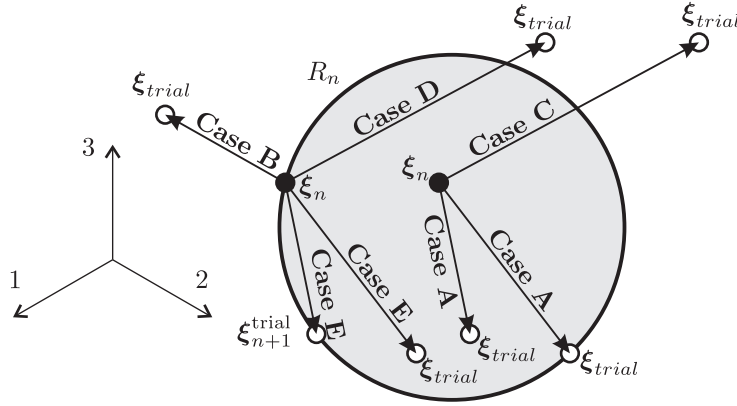


Figure 5.1: Geometrical interpretation of various loading cases in the stress updating procedure.

The yield function at the n th state and at the trial state are obtained using (3.30) as

$$F_n = F(\xi_n, R_n) = \|\xi_n\| - R_n, \quad F_{trial} = F(\xi_{trial}, R_n) = \|\xi_{trial}\| - R_n, \quad (5.4)$$

where

$$\xi_{trial} = s_{trial} - \alpha_{trial} = s_{trial} - \alpha_n = \xi_n + 2G\Delta e. \quad (5.5)$$

In this model, the plastic deformation is pressure-independent, thus the hydrostatic part of the total stress is calculated according to the elastic material law. Therefore $p_{n+1} = p_{trial}$ holds in any case.

5.2.1 Case A: Elastic loading

Both the n th state and the trial state are located in the elastic domain, i.e., $F_n < 0$ and $F_{trial} \leq 0$. Therefore, the stress increment is purely elastic. In this case, the new stress state is simply computed as $\sigma_{n+1} = \sigma_{trial}$.

5.2.2 Case B: Plastic loading

When the stress state at time t_n is plastic, i.e., $F_n = 0$, and the trial stress implies that $F_{trial} > 0$, then, the new stress state becomes also plastic. Plastic process initiates only in the case, when $\vartheta \leq \frac{\pi}{2}$. This condition is satisfied when $\psi_n \leq \frac{\pi}{2}$. According to Section 4.3.1 the stress update formulas are

$$\xi_{n+1} = A_\xi \xi_n + B_\xi \Delta e, \quad (5.6)$$

$$s_{n+1} = s_n + A_s \xi_n + B_s \Delta e, \quad (5.7)$$

where

$$A_\xi = \frac{S_{n+1} \sin \psi_{n+1}}{S_n \sin \psi_n}, \quad B_\xi = \frac{S_{n+1} \sin(\psi_n - \psi_{n+1})}{\|\Delta \mathbf{e}\| \sin \psi_n}, \quad (5.8)$$

$$A_s = \frac{2G(A_\xi - 1)}{(2G + h)(2b + 1)}, \quad B_s = 2G + \frac{2G(B_\xi - 2G)}{(2G + h)(2b + 1)}. \quad (5.9)$$

The initial value of the angle ψ is defined by

$$\psi_n = \arccos \left(\frac{\boldsymbol{\xi}_n : \Delta \mathbf{e}}{S_n \|\Delta \mathbf{e}\|} \right). \quad (5.10)$$

The angle at the end of the increment is computed by solving the equation based on (4.14):

$$B \left(\cos^2 \psi_{n+1}, \frac{1}{2}, b \right) = B \left(\cos^2 \psi_n, \frac{1}{2}, b \right) + \frac{4G \|\Delta \mathbf{e}\|}{S_n} \sin^{2b} \psi_n. \quad (5.11)$$

An efficient method to perform this task is given in Appendix E.2 using the nested derivatives proposed by Dominici (2003). The parameter $S_{n+1} = \|\boldsymbol{\xi}_{n+1}\|$ is computed using (4.10) as

$$S_{n+1} = S_n \left(\frac{\sin \psi_{n+1}}{\sin \psi_n} \right)^{2b}. \quad (5.12)$$

Since the increment is plastic it follows that $R_{n+1} = S_{n+1}$.

If the increment produces radial loading, then the stress update formulas, according to Section 4.2.1.2, reduce to

$$\boldsymbol{\xi}_{n+1} = S_{n+1} \frac{\Delta \mathbf{e}}{\|\Delta \mathbf{e}\|}, \quad \mathbf{s}_{n+1} = \mathbf{s}_n + \frac{2Gh}{(2G + h)} \Delta \mathbf{e}, \quad (5.13)$$

where

$$S_{n+1} = S_n - 4Gb \|\Delta \mathbf{e}\|, \quad R_{n+1} = S_{n+1}. \quad (5.14)$$

5.2.3 Case C: Elastic-plastic transition

The increment starts from the elastic region and ends in a plastic state, i.e., $F_n < 0$ and $F_{trial} > 0$. Therefore, the whole increment is divided into purely elastic and plastic parts. In this case, first the contact stress state, $\boldsymbol{\sigma}_c = \mathbf{s}_c + p_c \boldsymbol{\delta}$, has to be calculated. The contact point at which the stress just reaches the yield surface is obtained from the yield condition

$$F(\boldsymbol{\xi}_c, R_n) = 0, \quad (5.15)$$

where

$$\boldsymbol{\xi}_c = \boldsymbol{\xi}_n + c2G\Delta \mathbf{e}, \quad p_c = p_n + 3cK\Delta \epsilon. \quad (5.16)$$

The parameter c , which describes the share of the elastic part in the total amount of the strain increment, is obtained by solving a quadratic equation based on (5.15)¹:

$$c = \frac{-S_n \cos \psi_n + \sqrt{S_n^2 \cos^2 \psi_n + (R_n^2 - S_n^2)}}{2G \|\Delta \mathbf{e}\|}. \quad (5.17)$$

This expression can be used also for deviatoric loading case. The loading part between the contact point and the trial state is identical to **Case B**. Therefore beyond the contact point, the stress update formulas derived for **Case B** have to be used with the modified strain increment $(1 - c) \Delta \boldsymbol{\varepsilon}$ and with $\boldsymbol{\sigma}_c$ as the n th state. The schematic illustration of this case is presented in Figure 5.2.

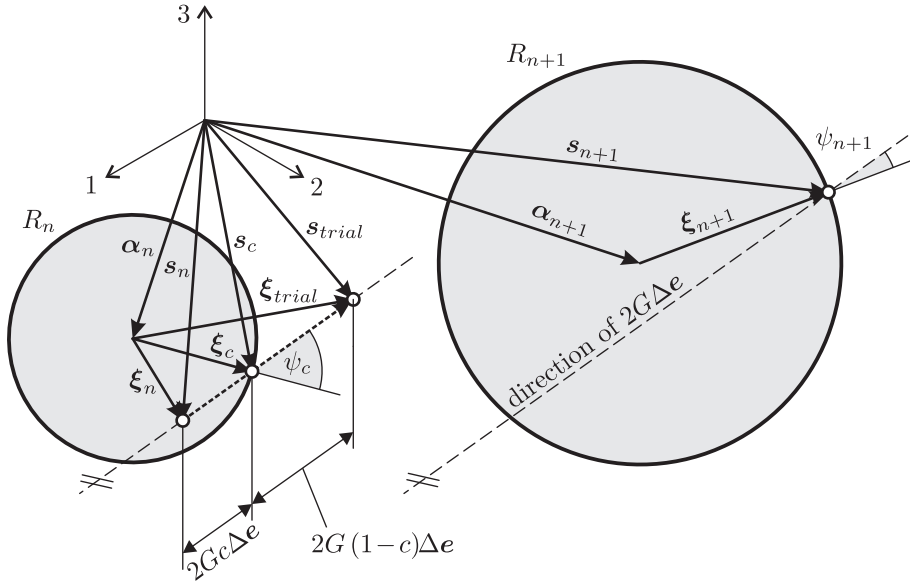


Figure 5.2: Schematics of the stress update for Case C.

5.2.4 Case D: Elastic-plastic transition due to unloading

In this case, the initial stress state at time t_n is located on the yield surface, i.e., $F_n = 0$, as in **Case B**. However, in this case, the trial stress increment intersects the yield surface, i.e., $\vartheta > \pi/2$ (which condition is identical to $\psi_n > \pi/2$), and ends outside of it, i.e., $F_{trial} > 0$. This causes that elastic unloading occurs prior to plastic loading, namely, there is a transition from the plastic to plastic state due to unloading. Consequently, the stress update formulas are identical to those presented for **Case C**. Since in this case $\|\boldsymbol{\xi}_n\| = R_n$, the expression for c , using (5.15), is simplified to:

$$c = -\frac{\boldsymbol{\xi}_n : \Delta \mathbf{e}}{G \|\Delta \mathbf{e}\|^2} = -\frac{R_n}{G \|\Delta \mathbf{e}\|} \cos \psi_n. \quad (5.18)$$

5.2.5 Case E: Unloading

The n th state lies on the yield surface and the trial state is located in the elastic domain, ($F_n = 0$ and $F_{trial} \leq 0$). Therefore the increment produces elastic unloading. In this case, the new stress state can be calculated according to **Case A**.

¹Here $0 \leq \psi_n \leq \pi$. And only the positive value of c is considered.

5.3 Non-associative Drucker–Prager elastoplasticity model with linear isotropic hardening

The yield conditions at the beginning of the increment and at the trial state are defined as

$$F_n = F(\boldsymbol{\sigma}_n, k_n), \quad F_{trial} = F(\boldsymbol{\sigma}_{trial}, k_n). \quad (5.19)$$

The various stress update cases are illustrated in Figure 5.3.

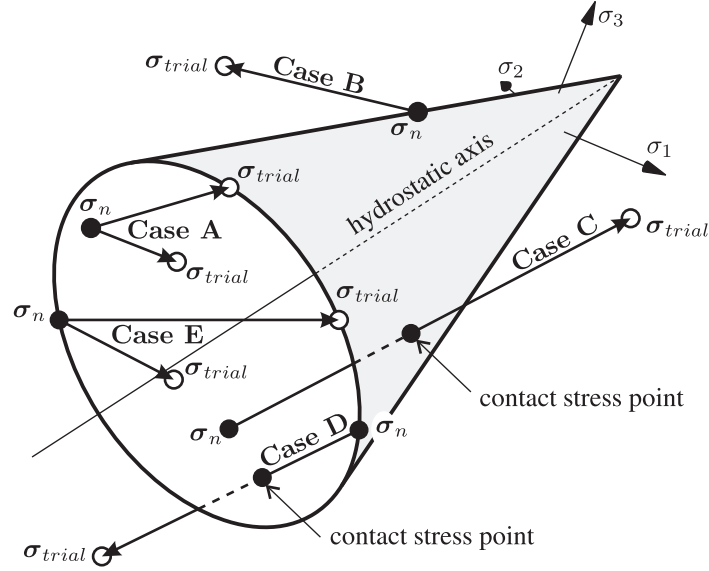


Figure 5.3: Geometrical interpretation of various loading cases in the stress updating procedure.

5.3.1 Case A: Elastic loading

Both the n th state and the trial state are located in the elastic domain, i.e., $F_n < 0$ and $F_{trial} \leq 0$. Therefore, the stress increment is purely elastic. In this case the new stress state is simply computed as $\boldsymbol{\sigma}_{n+1} = \boldsymbol{\sigma}_{trial}$.

5.3.2 Case B: Plastic loading

When, the stress state at time t_n is plastic, i.e., $F_n = 0$, and the trial stress implies that $F_{trial} > 0$, then, the new stress state becomes also plastic. The plastic process initiates only in the case of $\vartheta \leq \pi/2$ excluding the special case when the trial stress path lies on the yield surface and meets the apex. This scenario, when $\vartheta = \pi/2$ and $\psi_n = \pi$, will be discussed in **Case D**.

The initial parameters are calculated as

$$V = \frac{9K\alpha\Delta\epsilon}{\sqrt{2}G\|\Delta\mathbf{e}\|}, \quad \cos\psi_n = \frac{\mathbf{s}_n : \Delta\mathbf{e}}{S_n\|\Delta\mathbf{e}\|}. \quad (5.20)$$

Then, the angle ψ_{n+1} , using (4.45), is determined by solving the equation

$$B\left(\cos^2\frac{\psi_{n+1}}{2}, a, b\right) = B\left(\cos^2\frac{\psi_n}{2}, a, b\right) + \frac{4G\|\Delta\mathbf{e}\|}{S_n}\cos^{2a}\left(\frac{\psi_n}{2}\right)\sin^{2b}\left(\frac{\psi_n}{2}\right). \quad (5.21)$$

With the solution of the final angle ψ_{n+1} in hand, the norm of the deviatoric stress at the new stress state, the pressure and the deviatoric stress can be calculated as

$$S_{n+1} = S_n \left(\frac{\sin \frac{1}{2} \psi_{n+1}}{\sin \frac{1}{2} \psi_n} \right)^{2b} \left(\frac{\cos \frac{1}{2} \psi_{n+1}}{\cos \frac{1}{2} \psi_n} \right)^{2a}, \quad (5.22)$$

$$p_{n+1} = p_n + K \left(3 - \frac{27K\alpha\beta}{\tilde{h} - G} \right) \Delta\epsilon - \frac{3\sqrt{2}\beta K}{2(\tilde{h} - G)} (S_{n+1} - S_n), \quad (5.23)$$

$$\mathbf{s}_{n+1} = \left(\frac{S_{n+1} \sin \psi_{n+1}}{S_n \sin \psi_n} \right) \mathbf{s}_n + \left(\frac{S_{n+1} \sin(\psi_n - \psi_{n+1})}{\|\Delta\mathbf{e}\| \sin \psi_n} \right) \Delta\mathbf{e}. \quad (5.24)$$

Finally, the new total stress is expressed as

$$\boldsymbol{\sigma}_{n+1} = \mathbf{s}_{n+1} + p_{n+1} \boldsymbol{\delta}. \quad (5.25)$$

For the case, when the increment produces deviatoric radial loading, then the stress update formulas, according to (4.54)-(4.57), are simplified to

$$\mathbf{s}_{n+1} = \left(1 - \frac{9\sqrt{2}K\alpha G}{S_n \tilde{h}} \Delta\epsilon + q \frac{2G \|\Delta\mathbf{e}\|}{S_n} \left(1 - \frac{G}{\tilde{h}} \right) \right) \mathbf{s}_n, \quad (5.26)$$

and

$$p_{n+1} = p_n + K \left(3 - \frac{27K\alpha\beta}{\tilde{h} - G} \right) \Delta\epsilon - \frac{3K\beta}{\sqrt{2}(\tilde{h} - G)} (S_{n+1} - S_n). \quad (5.27)$$

Furthermore the stress update formulas when the n th state is located at the apex are

$$\mathbf{s}_{n+1} = \mathbf{0}, \quad (5.28)$$

$$p_{n+1} = p_n + K \Delta\epsilon \left(3 - \frac{27K\alpha\beta}{\tilde{h} - G} \right). \quad (5.29)$$

Rewriting (4.71), these solutions are valid when

$$\frac{9K\alpha\Delta\epsilon}{\tilde{h} - G} > \sqrt{2} \|\Delta\mathbf{e}\|. \quad (5.30)$$

Otherwise

$$\mathbf{s}_{n+1} = \left(2G \left(1 - \frac{G}{\tilde{h}} \right) - \frac{9\sqrt{2}KG\alpha\Delta\epsilon}{\tilde{h} \|\Delta\mathbf{e}\|} \right) \Delta\mathbf{e}, \quad (5.31)$$

$$p_{n+1} = p_n + K \left(3 - \frac{27K\alpha\beta}{\tilde{h}} \right) \Delta\epsilon - \frac{3\sqrt{2}KG\beta}{\tilde{h}} \|\Delta\mathbf{e}\|. \quad (5.32)$$

According to Section 4.2.2.3, the stress solution can reach the apex of the yield surface. The share of the strain increment part needed to reach the apex in the total amount of strain increment

is measured with parameter c_a . For general loading case it is computed using the discretized counterpart of (4.58) as

$$c_a = \frac{S_n}{4G \|\Delta \mathbf{e}\|} \frac{B(a, b) - B\left(\cos^2 \frac{\psi_n}{2}, a, b\right)}{\cos^{2a} \left(\frac{\psi_n}{2}\right) \sin^{2b} \left(\frac{\psi_n}{2}\right)}, \quad (5.33)$$

whereas in case of radial loading it is obtained using (4.59) as

$$c_a = \frac{S_n}{\frac{9\sqrt{2}K\alpha G}{\tilde{h}} \Delta \epsilon - q2G \|\Delta \mathbf{e}\| \left(1 - \frac{G}{\tilde{h}}\right)}. \quad (5.34)$$

5.3.3 Case C: Elastic-plastic transition

The increment starts from the elastic region and ends in a plastic state, i.e., $F_n < 0$ and $F_{trial} > 0$. Therefore, the whole increment is divided into purely elastic and plastic parts. In this case, first the contact stress state, $\boldsymbol{\sigma}_c = \mathbf{s}_c + p_c \boldsymbol{\delta}$ has to be calculated.

The contact point at which the stress just reaches the yield surface is obtained from the yield condition

$$F(\boldsymbol{\sigma}_c, k_n) = 0, \quad (5.35)$$

where

$$\mathbf{s}_c = \mathbf{s}_n + c2G\Delta \mathbf{e}, \quad p_c = p_n + 3cK\Delta \epsilon. \quad (5.36)$$

The parameter c , which describes the share of the elastic part in the total amount of the increment, is obtained by solving a quadratic equation based on (5.35):

$$c = \frac{S_n \cos \psi_n + V\tilde{S} - \sqrt{\left(S_n \cos \psi_n + V\tilde{S}\right)^2 - \left(\tilde{S}^2 - S_n^2\right) (V^2 - 1)}}{2G \|\Delta \mathbf{e}\| (V^2 - 1)}, \quad (5.37)$$

where $\tilde{S} = \sqrt{2}(k_n - 3\alpha p_n)$. After the contact point has been computed, the stress update formulas derived for **Case B** are used with $\boldsymbol{\sigma}_c$ as initial stress state, and with the modified strain increment $(1 - c)\Delta \boldsymbol{\epsilon}$.

In the following, some special cases are clarified. If the strain increment is purely hydrostatic, i.e., $\|\Delta \mathbf{e}\| = 0$, then

$$c = \frac{\tilde{S} - S_n}{9\sqrt{2}\alpha K \Delta \epsilon}. \quad (5.38)$$

In the case, when $V = 1$ and $\|\Delta\mathbf{e}\| \neq 0$, the parameter c can be expressed by

$$c = \frac{\tilde{S}^2 - S_n^2}{4G \|\Delta\mathbf{e}\| (S_n \cos\psi_n + \tilde{S})}. \quad (5.39)$$

When the initial state is stress-free and the strain increment has deviatoric part, i.e., $\boldsymbol{\sigma}_n = \mathbf{0}$ and $\|\Delta\mathbf{e}\| \neq 0$, then

$$c = \frac{\sqrt{2}k_n}{2G \|\Delta\mathbf{e}\| ((1 + V))}, \quad (5.40)$$

whereas for the case, when the increment is purely hydrostatic, i.e., $\|\Delta\mathbf{e}\| = 0$, and starts from the stress-free state ($\boldsymbol{\sigma}_n = \mathbf{0}$), then the contact point is the apex, and (5.40) reduces to

$$c = \frac{k_n}{9\alpha K \Delta\epsilon}. \quad (5.41)$$

5.3.4 Case D: Elastic-plastic transition due to unloading

In this case, the initial stress state at time t_n is plastic as in **Case B**, i.e., $F_n = 0$. However, here, the trial stress increment intersects the yield surface, i.e., $\vartheta > \pi/2$, and ends outside of it ($F_{trial} > 0$). This yields that elastic unloading comes prior to plastic loading, namely, there is a transition from the plastic to plastic state through the elastic region. The stress update formulas are identical to those in **Case C**. The strain increment is divided into a purely elastic part, $c\Delta\boldsymbol{\epsilon}$, and an elastic-plastic part, $(1 - c)\Delta\boldsymbol{\epsilon}$, where the factor c can be calculated according to (5.35):

$$c = \frac{S_n (\cos\psi_n + V)}{G \|\Delta\mathbf{e}\| (V^2 - 1)}. \quad (5.42)$$

It should be noted that the particular scenario when $\|\Delta\mathbf{e}\| = 0$ cannot produce this type of loading case. Furthermore, if $V = 1$, then only the direction corresponding to $\vartheta = \pi/2$ can yield this type of loading case. In this case, the contact point is at the apex and $\psi_n = \pi$. For this particular case, the elastic stress path lies on the yield surface and the parameter c reduces to

$$c = \frac{R_n}{2G \|\Delta\mathbf{e}\|}. \quad (5.43)$$

Beyond the contact point, the stress update formulas derived for the apex case solution in **Case B** are used, where $\boldsymbol{\sigma}_c$ is given as the initial stress state, and the strain increment equals to $(1 - c)\Delta\boldsymbol{\epsilon}$.

5.3.5 Case E: Unloading

The n th state lies on the yield surface and the trial state is located in the elastic domain, i.e., $F_n = 0$ and $F_{trial} \leq 0$. Therefore the increment produces elastic unloading. In this case, the new stress state can be calculated according to **Case A**.

6

Consistent tangent tensors

6.1 Introduction

In general, an elastoplastic finite element analysis involves the stress updating procedure after which the global nonlinear system of algebraic equations is solved. The structure of the tangent tensor has a strong influence on the convergence speed of the calculations. For finite element implementations, where usually the Newton–Raphson method is employed, the construction of the *consistent tangent modulus tensor* (or *consistent tangent operator* or *algorithmic stiffness tensor*) is crucial (Ibrahimbegovic, 2009; Jirásek and Bažant, 2002; Simo and Hughes, 1998). This yields faster convergence of the numerical scheme, compared to the case when continuum tangent modulus is used. The consistent tangent modulus gives a quadratic rate of asymptotic convergence for the iterative solution (Simo and Hughes, 1998). This, so-called algorithmically consistent tangent modulus, can be obtained by exact linearization of the stress update procedure.

The definition for the consistent tangent modulus is based on

$$d\boldsymbol{\sigma}_{n+1} = \frac{\partial \boldsymbol{\sigma}_{n+1}}{\partial \boldsymbol{\varepsilon}_{n+1}} : d\boldsymbol{\varepsilon}_{n+1} = \mathcal{D}^{\text{cons}} : d\boldsymbol{\varepsilon}_{n+1}, \quad (6.1)$$

$$\mathcal{D}^{\text{cons}} = \frac{\partial \boldsymbol{\sigma}_{n+1}}{\partial \boldsymbol{\varepsilon}_{n+1}} = \frac{\partial \boldsymbol{s}_{n+1}}{\partial \boldsymbol{\varepsilon}_{n+1}} + \frac{\partial \boldsymbol{p}_{n+1}}{\partial \boldsymbol{\varepsilon}_{n+1}}. \quad (6.2)$$

Using the additive decomposition of the strain tensor, the expression above can be expressed as

$$\mathcal{D}^{\text{cons}} = \frac{\partial \boldsymbol{\sigma}_{n+1}}{\partial \Delta \boldsymbol{\varepsilon}} : \boldsymbol{\mathcal{T}} + \frac{1}{3} \frac{\partial \boldsymbol{\sigma}_{n+1}}{\partial \Delta \epsilon} \otimes \boldsymbol{\delta}. \quad (6.3)$$

The following two sections present the corresponding algorithmically consistent tangent modulus tensors for stress update procedures presented in Section 5.2 and Section 5.3.

6.2 Associative von Mises elastoplasticity model with combined linear hardening

6.2.1 General loading case

When the initial state is located inside the elastic domain and the trial stress takes place out of the yield surface then the stress update algorithm discussed in Section 5.2.3 has to be used. This case is the most complicated scenario, which can occur during the stress update procedure. Thus, the expression of the consistent tangent tensor will be given for this case. Since the derivation of the consistent tangent tensor is quite lengthy, only the final result is summarized here. Detailed derivation steps are provided in Appendix C.5.1. The structure of the consistent tangent tensor is given as

$$\mathcal{D}^{\text{cons}} = a_1 \boldsymbol{\xi}_c \otimes \boldsymbol{\xi}_c + a_2 \boldsymbol{\xi}_c \otimes \Delta \mathbf{e} + a_3 \Delta \mathbf{e} \otimes \boldsymbol{\xi}_c + a_4 \Delta \mathbf{e} \otimes \Delta \mathbf{e} + a_5 \mathcal{T} + K \boldsymbol{\delta} \otimes \boldsymbol{\delta}, \quad (6.4)$$

where the expressions for the parameters a_1 , a_2 , a_3 , a_4 and a_5 are given in Box 1.

$$\begin{aligned} a_1 &= \frac{2GA_\xi}{2G+h} \left(\frac{D_1}{\tan\psi_{n+1}} - \frac{C_1}{\tan\psi_c} \right), & a_2 &= \frac{2GA_\xi}{2G+h} \left(\frac{D_2}{\tan\psi_{n+1}} - \frac{C_2}{\tan\psi_c} \right), \\ a_3 &= \frac{2GB_\xi}{(2G+h)(2b+1)(1-c)} \times \\ & \left(\frac{2bD_1}{\tan\psi_{n+1}} - \frac{D_1 - C_1}{\tan(\psi_c - \psi_{n+1})} - \frac{(2b+1)C_1}{\tan\psi_c} \right. \\ & \left. - \frac{c}{(1-c)\|\Delta \mathbf{e}\|S_c \cos\psi_c} \right) + c \frac{B_s - 2G(1+A_s)}{S_c \|\Delta \mathbf{e}\| \cos\psi_c}, \\ a_4 &= \frac{2GB_\xi}{(2G+h)(2b+1)(1-c)} \times \\ & \left(\frac{2bC_4}{\tan\psi_{n+1}} - \frac{D_2 - C_2}{\tan(\psi_c - \psi_{n+1})} - \frac{(2b+1)C_2}{\tan\psi_c} - \frac{1}{\|\Delta \mathbf{e}\|^2} \right), \\ a_5 &= B_s(1-c) + 2Gc(1+A_s), \\ C_1 &= \frac{2Gc\|\Delta \mathbf{e}\| - S_c \cos\psi_c}{S_c^2 \|\Delta \mathbf{e}\| \cos\psi_c \sin\psi_c}, & C_2 &= \frac{S_c \cos\psi_c - 2Gc\|\Delta \mathbf{e}\|}{S_c \|\Delta \mathbf{e}\|^2 \sin\psi_c}, \\ D_1 &= \frac{A_\xi}{S_{n+1}^2} (C_1 S_c^2 - 4GbC_1 S_c \|\Delta \mathbf{e}\| (1-c) \cos\psi_c - 2Gc \tan\psi_c), \\ D_2 &= \frac{A_\xi}{S_{n+1}^2} \left(C_2 S_c^2 - 4GbC_2 S_c \|\Delta \mathbf{e}\| (1-c) \cos\psi_c - \frac{2GS_c(1-c)}{\|\Delta \mathbf{e}\|} \sin\psi_c \right). \end{aligned}$$

Box 1: Parameters in the consistent tangent tensor for the von Mises model in case of general loading.

6.2.2 Radial loading case

In the radial loading case, the stress update formulae are much more simpler than in the general loading case. Consequently, the corresponding consistent tangent tensor has a much simpler structure. For this case, it is written in the shorter form

$$\mathcal{D}^{\text{cons}} = a_1 \Delta \mathbf{e} \otimes \boldsymbol{\xi}_c + a_2 \mathcal{T} + a_3 \boldsymbol{\delta} \otimes \boldsymbol{\delta}. \quad (6.5)$$

Box 2 contains the expressions for parameters a_1 , a_2 and a_3 , whereas Appendix C.5.2 provides the detailed derivation steps.

$$a_1 = -\frac{4G^2 c}{S_c \|\Delta \mathbf{e}\| (2G + h) \cos \psi_c}, \quad a_2 = \frac{2G (2Gc + h)}{2G + h}, \quad a_3 = K.$$

Box 2: Parameters in the consistent tangent tensor for the von Mises model in case of radial loading.

6.3 Non-associative Drucker–Prager elastoplasticity model with linear isotropic hardening

6.3.1 General loading case

The consistent tangent tensor is derived for the case when elastic plastic transition occurs. In this case, the stress update formulae presented in Section 5.3.3 have to be applied. Since the calculation is quite lengthy but otherwise straightforward, only the final results are stated in the following. Detailed presentation of the differentiation procedure can be found in Appendix D.4.1.

The corresponding consistent tangent tensor depends on whether the stress path has reached the apex of the yield surface or not. These two situations are illustrated in Figure 6.1.

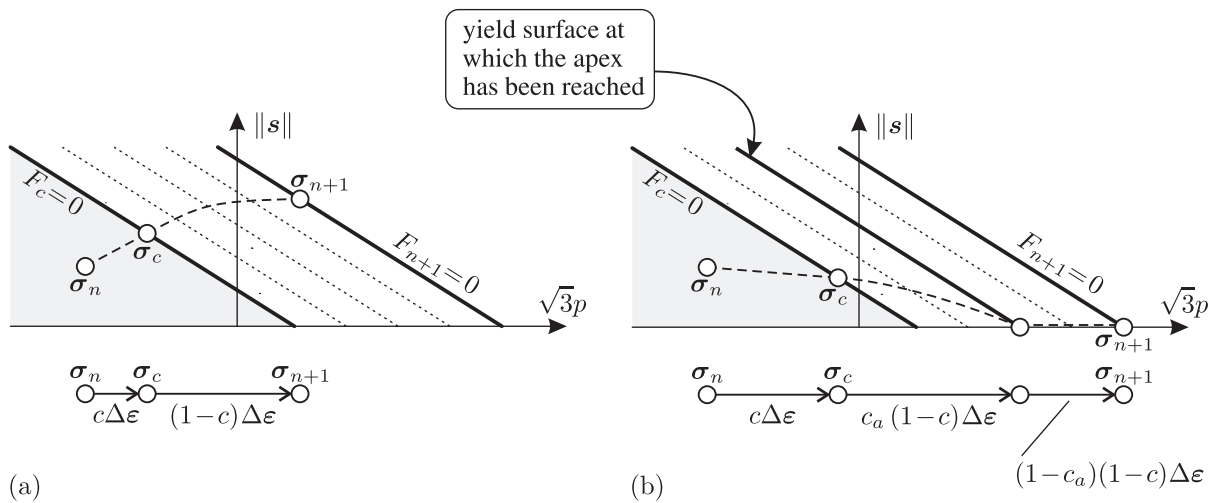


Figure 6.1: Illustration of the stress update procedure, when the n th state is located in the elastic domain. (a) the updated stress state lies on the smooth portion of the updated yield surface; (b) the apex has been reached during the increment.

6.3.1.1 Stress update without reaching the apex

When the n th state is located in the elastic domain and the updated stress state lies on the smooth portion of the yield surface, then the consistent tangent tensor has the form

$$\begin{aligned} \mathcal{D}^{\text{cons}} = & a_1 \mathbf{s}_c \otimes \mathbf{s}_c + a_2 \mathbf{s}_c \otimes \Delta \mathbf{e} + a_3 \mathbf{s}_c \otimes \boldsymbol{\delta} + a_4 \Delta \mathbf{e} \otimes \mathbf{s}_c + a_5 \Delta \mathbf{e} \otimes \Delta \mathbf{e} \\ & + a_6 \Delta \mathbf{e} \otimes \boldsymbol{\delta} + a_7 \boldsymbol{\delta} \otimes \mathbf{s}_c + a_8 \boldsymbol{\delta} \otimes \Delta \mathbf{e} + a_9 \boldsymbol{\delta} \otimes \boldsymbol{\delta} + a_{10} \mathcal{T}, \end{aligned} \quad (6.6)$$

where the expressions of the parameters are collected in Box 3-Box 5. In Box 5, ${}_3F_2(\bullet, \bullet, \bullet; \bullet, \bullet; \bullet)$ denotes the generalized hypergeometric function (Wolfram Research, 2010c), whereas $\Psi(\bullet)$ stands for the digamma function (Wolfram Research, 2010a).

$$\begin{aligned} a_1 &= \frac{R_1}{m_1} - \frac{C_1}{m_2} + \frac{D_1}{m_3} - \frac{m_4}{S_c}, & a_2 &= \frac{R_2}{m_1} - \frac{C_2}{m_2} + \frac{D_2}{m_3}, \\ a_3 &= \frac{R_3}{m_1} - \frac{C_3}{m_2} + \frac{D_3}{m_3} - \frac{m_4 \|\Delta \mathbf{e}\| \cos \psi_c}{\text{tr} \Delta \boldsymbol{\epsilon}}, \\ a_4 &= (1 - c) \left(\frac{R_1}{m_5} + \frac{D_1}{m_6} + \frac{C_1}{m_7} \right) + \frac{c(B_s - 2GA_s)}{S_c \|\Delta \mathbf{e}\| (\cos \psi_c + V)}, \\ a_5 &= (1 - c) \left(\frac{R_2}{m_5} + \frac{D_2}{m_6} + \frac{C_2}{m_7} - \frac{B_s}{\|\Delta \mathbf{e}\|^2} \right), \\ a_6 &= (1 - c) \left(\frac{R_3}{m_5} + \frac{D_3}{m_6} + \frac{C_3}{m_7} \right) + \frac{cV(B_s - 2GA_s)}{\text{tr} \Delta \boldsymbol{\epsilon} (\cos \psi_c + V)}, \\ a_7 &= \frac{R_1}{m_8}, & a_8 &= \frac{R_2}{m_8}, & a_9 &= \frac{R_3}{m_8} + K \left(1 - \frac{9K\alpha\beta}{\tilde{h} - G} \right), \\ a_{10} &= (1 - c) B_s + 2cGA_s, \end{aligned}$$

Box 3: Parameters in the consistent tangent tensor for the Drucker–Prager model in case of general loading.

6.3.1.2 Stress update through the apex

For the special scenario, when the increment starts from an elastic state and the updated stress is located in the apex the consistent tangent tensor is computed simply as

$$\mathcal{D}^{\text{cons}} = K \left(1 - \frac{9K\alpha\beta}{\tilde{h} - G} \right) \boldsymbol{\delta} \otimes \boldsymbol{\delta}. \quad (6.7)$$

The detailed derivation steps are provided in D.4.3.

$$\begin{aligned}
 m_1 &= \frac{S_{n+1}}{A_s}, & m_2 &= \frac{\tan\psi_c}{A_s}, & m_3 &= \frac{S_c \sin\psi_c}{S_{n+1} \cos\psi_{n+1}}, & m_4 &= \frac{2GcVA_s}{S_c(V + \cos\psi_c)}, \\
 m_5 &= \frac{S_{n+1}}{B_s}, & m_6 &= \frac{\tan(\psi_{n+1} - \psi_c)}{B_s}, & m_7 &= \frac{(1-c)\|\Delta\mathbf{e}\| \sin^2\psi_c}{S_{n+1} \sin\psi_{n+1}}, & m_8 &= \frac{\sqrt{2}(G - \tilde{h})}{3K\beta}, \\
 C_1 &= \frac{2Gc(1 + V\cos\psi_c)}{S_c^2 \sin\psi_c (\cos\psi_c + V)} - \frac{1}{S_c \sin\psi_c \|\Delta\mathbf{e}\|}, & C_2 &= \frac{S_c \cos\psi_c - 2Gc\|\Delta\mathbf{e}\|}{S_c \sin\psi_c \|\Delta\mathbf{e}\|^2}, \\
 C_3 &= \frac{2GcV\|\Delta\mathbf{e}\| \sin^2\psi_c}{S_c \operatorname{tr}\Delta\boldsymbol{\varepsilon} \sin\psi_c (\cos\psi_c + V)}, \\
 D_1 &= \frac{C_1}{k_1} + \frac{k_4}{S_c} - \frac{k_5}{S_c}, & D_2 &= \frac{C_2}{k_1} - \frac{k_2}{\|\Delta\mathbf{e}\|} + \frac{k_3}{\|\Delta\mathbf{e}\|} - \frac{2G(1-c)\sin\psi_{n+1}}{S_{n+1}\|\Delta\mathbf{e}\|}, \\
 D_3 &= \frac{C_3}{k_1} + \frac{k_2\|\Delta\mathbf{e}\|}{\operatorname{tr}\Delta\boldsymbol{\varepsilon}} - \frac{k_3\|\Delta\mathbf{e}\|}{\operatorname{tr}\Delta\boldsymbol{\varepsilon}} - \frac{k_4\|\Delta\mathbf{e}\| \cos\psi_c}{\operatorname{tr}\Delta\boldsymbol{\varepsilon}} - \frac{k_5\|\Delta\mathbf{e}\|V}{\operatorname{tr}\Delta\boldsymbol{\varepsilon}}, \\
 k_1 &= \frac{S_{n+1} \sin\psi_c}{\sin\psi_{n+1} (2G\|\Delta\mathbf{e}\| (1-c)(a-b - (a+b)\cos\psi_c) + S_c)}, \\
 k_2 &= \frac{2G(1-c)\sin\psi_{n+1}}{S_{n+1}} (a-b) \ln\left(\tan\frac{\psi_c}{2}\right), \\
 k_3 &= \frac{\sin\psi_{n+1} (b-a) (\tilde{\alpha}_{n+1} - \tilde{\alpha}_c - \tilde{\beta}_{n+1} + \tilde{\beta}_c)}{4\|\Delta\mathbf{e}\| \cos^{2a}\left(\frac{\psi_{n+1}}{2}\right) \sin^{2b}\left(\frac{\psi_{n+1}}{2}\right)}, \\
 k_4 &= \frac{4G^2c(1-c)V\|\Delta\mathbf{e}\| \sin\psi_{n+1}}{S_{n+1}S_c(V + \cos\psi_c)}, & k_5 &= \frac{2Gc \sin\psi_{n+1}}{S_{n+1}(V + \cos\psi_c)}, \\
 R_1 &= D_1n_1 + C_1n_2 + \frac{2GcVS_{n+1}}{S_c^2(V + \cos\psi_c)}, & R_2 &= D_2n_1 + C_2n_2 - \frac{n_3}{\|\Delta\mathbf{e}\|^2}, \\
 R_3 &= D_3n_1 + C_3n_2 + \frac{n_3}{\operatorname{tr}\Delta\boldsymbol{\varepsilon}} - \frac{2G\|\Delta\mathbf{e}\|cVS_{n+1}\cos\psi_c}{S_c \operatorname{tr}\Delta\boldsymbol{\varepsilon} (V + \cos\psi_c)}, \\
 n_1 &= S_{n+1} \frac{b-a + (a+b)\cos\psi_{n+1}}{\sin\psi_{n+1}}, & n_2 &= S_{n+1} \left(a \tan\frac{\psi_c}{2} - \frac{b}{\tan\frac{\psi_c}{2}} \right), \\
 n_3 &= S_{n+1} (a-b) \ln\left(\frac{\tan\frac{\psi_c}{2}}{\tan\frac{\psi_{n+1}}{2}} \right).
 \end{aligned}$$

Box 4: Parameters in the consistent tangent tensor for the Drucker–Prager model in case of general loading.

$$\begin{aligned} \tilde{\alpha}_c &= B \left(\cos^2 \frac{\psi_c}{2}, a, b \right) \ln \left(\cos^2 \frac{\psi_c}{2} \right) - \frac{{}_3F_2 \left(a, a, 1 - b; a + 1, a + 1; \cos^2 \frac{\psi_c}{2} \right)}{a^2 \cos^{-2a} \frac{\psi_c}{2}}, \\ \tilde{\alpha}_{n+1} &= B \left(\cos^2 \frac{\psi_{n+1}}{2}, a, b \right) \ln \left(\cos^2 \frac{\psi_{n+1}}{2} \right) - \frac{{}_3F_2 \left(a, a, 1 - b; a + 1, a + 1; \cos^2 \frac{\psi_{n+1}}{2} \right)}{a^2 \cos^{-2a} \frac{\psi_{n+1}}{2}}, \\ \tilde{\beta}_c &= \frac{{}_3F_2 \left(1 - a, b, b; 1 + b, 1 + b; \sin^2 \frac{\psi_c}{2} \right)}{b^2 \sin^{-2b} \frac{\psi_c}{2}} - B \left(\sin^2 \frac{\psi_c}{2}, b, a \right) \ln \left(\sin^2 \frac{\psi_c}{2} \right) \\ &+ B(a, b) (\Psi(b) - \Psi(a + b)), \\ \tilde{\beta}_{n+1} &= \frac{{}_3F_2 \left(1 - a, b, b; 1 + b, 1 + b; \sin^2 \frac{\psi_{n+1}}{2} \right)}{b^2 \sin^{-2b} \frac{\psi_{n+1}}{2}} - B \left(\sin^2 \frac{\psi_{n+1}}{2}, b, a \right) \ln \left(\sin^2 \frac{\psi_{n+1}}{2} \right) \\ &+ B(a, b) (\Psi(b) - \Psi(a + b)). \end{aligned}$$

Box 5: Parameters in the consistent tangent tensor for the Drucker–Prager model in case of general loading.

6.3.2 Deviatoric radial loading case

When the increment produces deviatoric radial loading, then the corresponding stress update formulae reduce to simpler form as discussed in Section 5.3. Similarly to the general loading case, it is possible that the updated stress lies on the smooth portion of the yield surface or it reaches the apex. The consistent tangent tensors for these two cases are given in the following.

6.3.2.1 Stress update without reaching the apex

If the updated stress lies on the smooth portion of the yield surface, then the consistent tangent tensor can be written as

$$\begin{aligned} \mathcal{D}^{\text{cons}} &= a_1 \mathbf{s}_c \otimes \mathbf{s}_c + a_2 \mathbf{s}_c \otimes \Delta \mathbf{e} + a_3 \mathbf{s}_c \otimes \boldsymbol{\delta} + a_4 \Delta \mathbf{e} \otimes \mathbf{s}_c + a_5 \Delta \mathbf{e} \otimes \boldsymbol{\delta} \\ &+ a_6 \boldsymbol{\delta} \otimes \mathbf{s}_c + a_7 \boldsymbol{\delta} \otimes \Delta \mathbf{e} + a_8 \boldsymbol{\delta} \otimes \boldsymbol{\delta} + a_9 \mathcal{T}, \end{aligned} \tag{6.8}$$

where parameters $a_1 - a_9$ are given in Box 6. The derivation of these parameters is provided in Appendix D.4.2.

$$\begin{aligned}
 a_1 &= \frac{2Gc}{S_c^2} \left(1 - \frac{G}{\tilde{h}} \right) - \frac{2GcS_{n+1}V}{S_c^3(V+q)}, & a_2 &= \frac{2Gq(1-c)}{S_c \|\Delta \mathbf{e}\|} \left(1 - \frac{G}{\tilde{h}} \right), \\
 a_3 &= \frac{3\sqrt{2}K\alpha}{S_c} \left(\frac{cq}{V+q} \frac{S_{n+1}}{S_c} - \frac{G}{\tilde{h}} \right), & a_4 &= -\frac{2GcS_{n+1}}{S_c^2 \|\Delta \mathbf{e}\| (V+q)}, \\
 a_5 &= -\frac{2GcVS_{n+1}}{S_c \text{tr} \Delta \boldsymbol{\varepsilon} (V+q)}, & a_6 &= \frac{-3\sqrt{2}KG\beta c}{\tilde{h}S_c}, \\
 a_7 &= \frac{-3\sqrt{2}GK\beta q(1-c)}{\|\Delta \mathbf{e}\| \tilde{h}}, & a_8 &= K \left(1 - \frac{9K\alpha\beta}{\tilde{h}} \right), & a_9 &= \frac{2GcS_{n+1}}{S_c}.
 \end{aligned}$$

Box 6: Parameters in the consistent tangent tensor for the Drucker–Prager model in case of deviatoric radial loading.

6.3.2.2 Stress update through the apex

In the special case, when the updated stress is located in the apex of the yield surface, then the corresponding consistent tangent tensor is constructed in exactly the same way as for the general loading case. Therefore, it is given by

$$\mathcal{D}^{\text{cons}} = K \left(1 - \frac{9K\alpha\beta}{\tilde{h} - G} \right) \boldsymbol{\delta} \otimes \boldsymbol{\delta}. \quad (6.9)$$

The detailed calculation steps are given in Appendix D.4.3.

6.3.3 n th state located at the apex

When the initial stress is located at the apex, then two situations can happen during the stress update procedure: the stress solution cannot leave the apex; or the updated stress will lie on the smooth portion of the yield surface. Condition (5.30) has to be involved to decide which scenario will occur. Obviously, the consistent tangent tensors are different for these cases.

According to the discussion made in Appendix D.4.3.3, the consistent tangent tensor is

$$\mathcal{D}^{\text{cons}} = K \left(1 - \frac{9K\alpha\beta}{\tilde{h} - G} \right) \boldsymbol{\delta} \otimes \boldsymbol{\delta} \quad (6.10)$$

for the case when the stress solution remains at the apex. Whereas, it is computed as

$$\mathcal{D}^{\text{cons}} = a_1 \Delta \mathbf{e} \otimes \Delta \mathbf{e} + a_2 \Delta \mathbf{e} \otimes \boldsymbol{\delta} + a_3 \boldsymbol{\delta} \otimes \Delta \mathbf{e} + a_4 \boldsymbol{\delta} \otimes \boldsymbol{\delta} + a_5 \mathcal{T}, \quad (6.11)$$

when the updated stress is located on the smooth portion of the yield surface. Box 7 collects the expressions for parameters in (6.11).

$$\begin{aligned}
 a_1 &= \frac{3\sqrt{2}KG\alpha\text{tr}\Delta\boldsymbol{\varepsilon}}{\tilde{h}\|\Delta\boldsymbol{e}\|^3}, & a_2 &= -\frac{3\sqrt{2}KG\alpha}{\tilde{h}\|\Delta\boldsymbol{e}\|}, & a_3 &= -\frac{3\sqrt{2}KG\beta}{\tilde{h}\|\Delta\boldsymbol{e}\|} \\
 a_4 &= K\left(1 - \frac{9K\alpha\beta}{\tilde{h} - G}\right), & a_5 &= 2G\left(1 - \frac{G}{\tilde{h}}\right) - \frac{3\sqrt{2}KG\alpha\text{tr}\Delta\boldsymbol{\varepsilon}}{\tilde{h}\|\Delta\boldsymbol{e}\|}
 \end{aligned}$$

Box 7: Parameters when the n th state located at the apex and the updated stress lies on the smooth portion of the yield surface.

7

Numerical examples

7.1 Introduction

This chapter is devoted to present a number of numerical computations in order to analyze the performance of the new solution methods proposed in this dissertation. The numerical examples are collected in two sections.

In Section 7.2, the associative von Mises elastoplastic model with combined linear hardening is considered. The accuracy of the new stress update scheme presented in Section 5.2 is investigated by presenting five different test examples. In the first example, the aim is to compute the corresponding stress response in the case when a nonlinear strain path is given. The problem is solved by approximating the strain input with rectilinear polygons. The accuracy of the new method is compared to the results obtained using the widely used radial return method (RRM). The second example is performed through a displacement-based finite element analysis. One 3-D hexahedron element is considered under homogenous stress loading defined by combined tension and shear loading. Errors are analyzed at the end of the loading path. Examples 3, 4 and 5 present finite element test examples, where the numerical calculations are performed by the commercial finite element software ABAQUS (ABAQUS, 2007). The new stress update algorithm with the corresponding consistent tangent tensor has been implemented into ABAQUS via the UMAT subroutine interface (Kossa and Szabó, 2010b). The results obtained using the ABAQUS internal scheme and the new UMAT code are compared. In Example 3, a widely adopted test example, a perforated strip subject to uniaxial extension, is analyzed, whereas Example 4 investigates the strain values computed in the case of a prescribed stress path. Finally, Example 5 demonstrates the performance of the two schemes by computing the stress response for a fixed plate under surface pressure loading.

Section 7.3 presents two examples in case of the non-associative Drucker–Prager elastoplastic model governed by linear isotropic hardening. The first example gives a detailed study about the apex problem. Namely, it demonstrates the regions in the stress space where the stress solution

can reach the apex point of the yield surface. Whereas, the second example investigates the accuracy of the stress update formulae in the case when a nonlinear strain input is approximated with strain increment assuming constant strain rate.

7.2 Associative von Mises elastoplasticity model with combined linear hardening

7.2.1 Example 1: Prescribed nonlinear strain input

7.2.1.1 The problem description and the reference solution

In order to apply the stress update formulae presented in Section 5.2 for a problem described with a nonlinear strain path, an approximation of the whole strain path with a multisection polygonal line is needed. Therefore, the proposed technique would yield a solution which can only be considered to be an approximation, where the nonlinear strain input is approximated by superposition of linear segments. The accuracy of the solution depends upon the degree of the approximation. Let the material parameters be the following: $E = 200$ GPa, $\nu = 0.3$, $H = 40$ GPa, $M = 0.5$ and $\sigma_Y = 150$ MPa.

The strain path is given by the prescribed ε_{11} and ε_{12} components of the strain tensor:

$$\varepsilon_{11} = 0.003(1 - \cos t), \quad \varepsilon_{12} = \frac{1}{2}\gamma_{12} = 0.003\sin t, \quad (7.1)$$

whereas the other strain components are kept to be zero. Since the constitutive model is rate-independent, the variable t denotes a dimensionless parameter. The interval $0 \leq t \leq 3\pi/2$ is considered in this calculation. Figure 7.1.a displays the whole strain path in the $(\varepsilon_{11}, \varepsilon_{12})$ plane. At the beginning, pure elastic deformation occurs until the initial yield surface is reached. This point can be calculated from the initial yield condition:

$$\|s(t)\| = \sqrt{\frac{2}{3}}\sigma_Y \implies t_{el} = 0.1884739447. \quad (7.2)$$

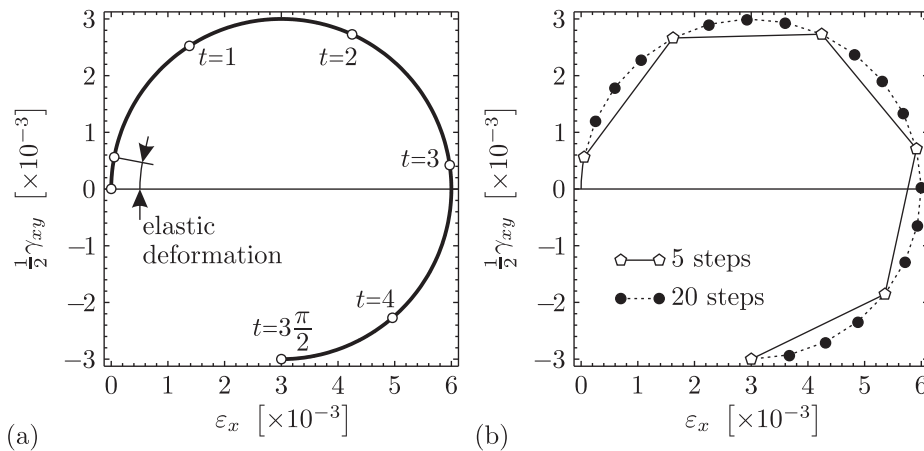


Figure 7.1: (a) Prescribed nonlinear strain path in Example 1. (b) Rectilinear approximations of the prescribed nonlinear strain path.

Elastoplastic loading results in the interval $t_{el} < t \leq 3\pi/2$. The reference solution in the elastoplastic region was obtained by numerically (fourth-order Runge–Kutta method with 1000 steps) solving the corresponding system of nonlinear DEs described by (3.54)–(3.58). These results are collected in Figure 7.2. Figure 7.2.a shows the angle ψ versus the parameter t , Figure 7.2.b illustrates the variation of the radius of the yield surface, while the non-zero components of the back-stress $\boldsymbol{\alpha}$ and the stress $\boldsymbol{\sigma}$ are displayed in Figure 7.2.c and Figure 7.2.d.

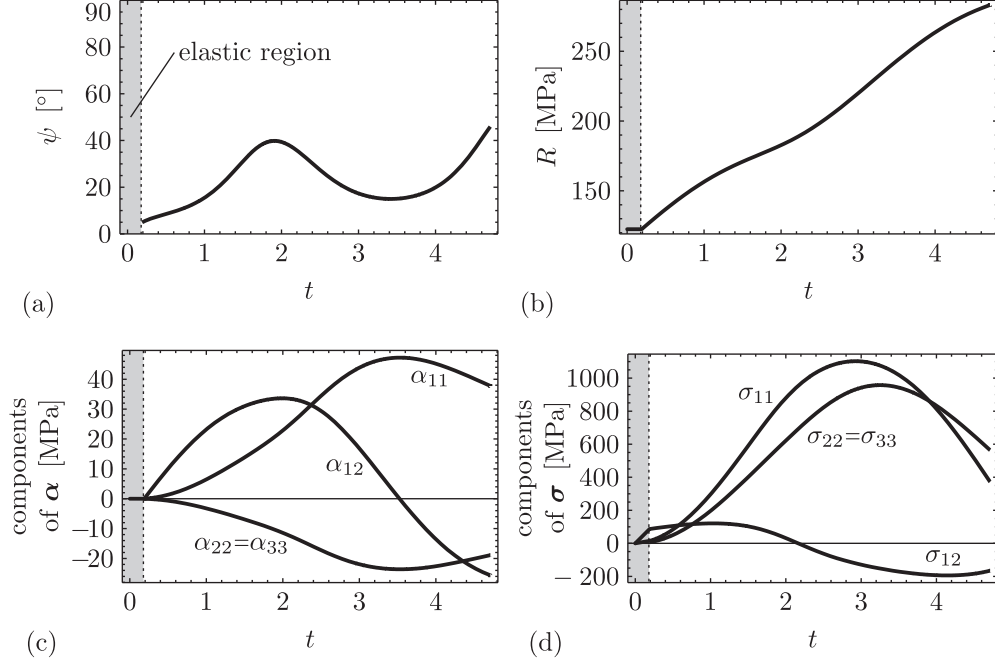


Figure 7.2: Reference solutions in Example 1. (a) Variation of the angle. (b) Radius of the yield surface. (c) Components of the back stress. (d) Components of the stress.

7.2.1.2 Numerical calculations

For calculations using either the new method given in Section 5.2 or the RRM, the strain path given by (7.1) needs to be divided into increments. Figure 7.1.b shows two linear approximations of the originally nonlinear strain path. The errors of both methods at a given time are reported as the relative norm of the error between the reference and the computed solution:

$$\mathcal{E}_{\|R\|} = 100 \frac{|R - R_{\text{ref}}|}{R_{\text{ref}}} [\%], \quad \mathcal{E}_{\|\boldsymbol{\alpha}\|} = 100 \frac{\|\boldsymbol{\alpha} - \boldsymbol{\alpha}_{\text{ref}}\|}{\|\boldsymbol{\alpha}_{\text{ref}}\|} [\%], \quad \mathcal{E}_{\|\boldsymbol{\sigma}\|} = 100 \frac{\|\boldsymbol{\sigma} - \boldsymbol{\sigma}_{\text{ref}}\|}{\|\boldsymbol{\sigma}_{\text{ref}}\|} [\%], \quad (7.3)$$

where R , $\boldsymbol{\alpha}$ and $\boldsymbol{\sigma}$ represent the results obtained by applying the specific algorithm, whereas R_{ref} , $\boldsymbol{\alpha}_{\text{ref}}$ and $\boldsymbol{\sigma}_{\text{ref}}$ denote the exact solutions. Errors resulting in the approximations (5 and 20 steps, respectively) are illustrated in Figure 7.3. Results obtained using the RRM are indicated with squares; whereas, circles denote the solutions computed with the new method. Filled markers correspond to the 20, and empty markers to the 5 step case, respectively. Furthermore, Table 7.1 shows the required computational time (CT), besides the considered errors, for both methods. Here, T_{comp} denotes a dimensionless relative time measure. $T_{\text{comp}} = 1$ represents the required CT for the RRM, when the strain path is approximated with 5 steps. The higher CT of the new solution technique is explained with the more complex structure of the new method. However, in

the calculation of the computational cost, other factors should be considered, besides the CT. For example: how many intermediate steps must be stored in order to obtain a required accuracy? From Table 7.1 it can be clearly concluded that in this simple example, using almost the same amount of CPU time, the new method with 8 steps renders roughly the same accuracy as the RRM can yield with only 30 steps.

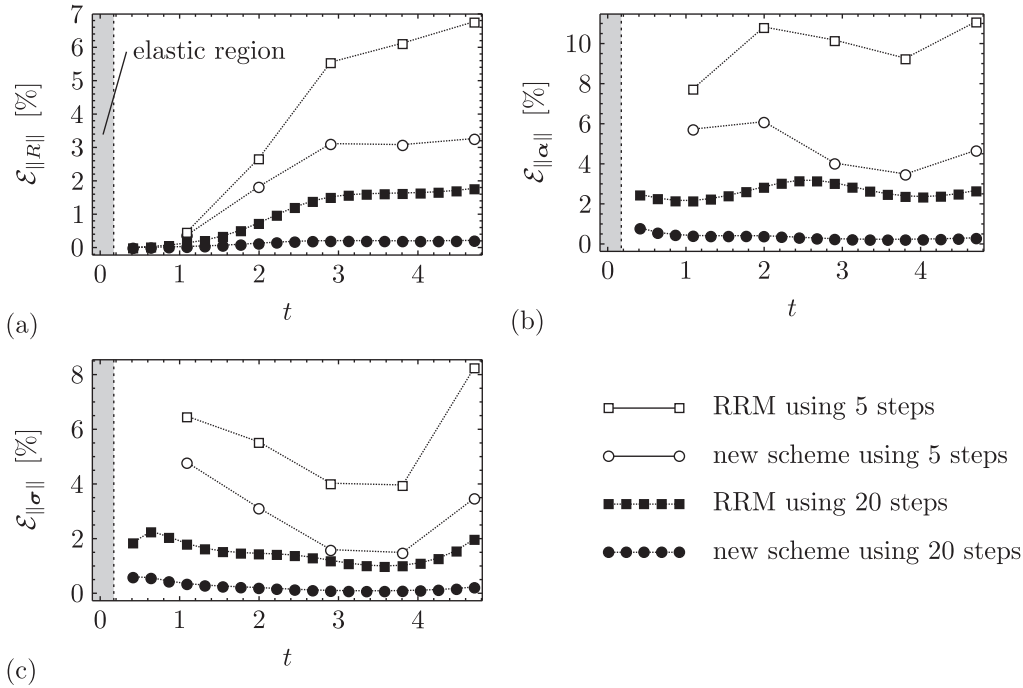


Figure 7.3: Numerical results of the new method and the RRM in Example 1. (a) Comparison of errors in the radius of the yield surface. (b) Comparisons of errors in the back stress. (c) Comparison of errors in the total stress tensor.

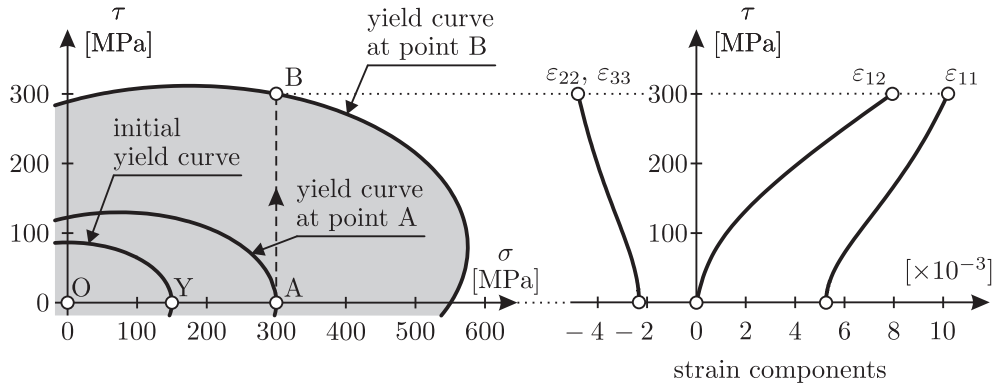
7.2.2 Example 2: Prescribed rectilinear stress loading

7.2.2.1 The problem description and the exact solution

The previous example was a strain-driven problem with a prescribed nonlinear strain path. In this second example, the loading is given in the stress space, or more precisely, in the $(\sigma = \sigma_{11}, \tau = \sigma_{12})$ plane (see Figure 7.4). Since only the σ_{11} and σ_{12} components are controlled, we have a plane stress problem. The whole loading path consists of three different loading sections. Starting from the initial stress-free state (point O), first the initial yield surface is reached (point Y) by uniaxial tension involving only pure elastic deformation. Then, the uniaxial tension is further applied until the point A is reached. This second loading part (Y→A) represents a proportional elastoplastic loading. Beyond the point A, an additional stress component, namely, $\tau = \sigma_{12}$ begins to increase from $\tau_B = 0$ MPa to $\tau_B = 300$ MPa; whereas, $\sigma = \sigma_{11}$ is kept to be constant ($\sigma_B = \sigma_A = 300$ MPa). The last loading section, A→B, is a non-proportional elastoplastic loading. Material parameters are the same as in the first example.

Table 7.1: Comparison of the RRM and the new scheme in Example 1.

Number of segments	RRM				new scheme			
	T_{comp}	Error Values [%]			T_{comp}	Error Values [%]		
		$\mathcal{E}_{\ \sigma\ }$	$\mathcal{E}_{\ \alpha\ }$	\mathcal{E}_R		$\mathcal{E}_{\ \sigma\ }$	$\mathcal{E}_{\ \alpha\ }$	\mathcal{E}_R
5	1.00	8.27	11.10	6.77	3.88	3.48	4.68	3.27
6	1.19	6.87	9.22	5.67	4.57	2.47	3.32	2.31
7	1.38	5.86	7.87	4.91	5.27	1.84	2.47	1.72
8	1.56	5.10	6.86	4.32	6.14	1.42	1.90	1.32
9	1.75	4.52	6.07	3.86	6.89	1.13	1.51	1.05
10	2.00	4.06	5.45	3.49	7.64	0.92	1.23	0.86
15	2.94	2.67	3.59	2.36	11.46	0.41	0.55	0.38
20	3.94	1.99	2.68	1.78	15.45	0.23	0.31	0.22
25	5.00	1.59	2.13	1.43	19.50	0.15	0.20	0.14
30	6.12	1.32	1.77	1.19	23.50	0.10	0.14	0.10
50	10.56	0.79	1.06	0.72	38.83	0.04	0.05	0.04


Figure 7.4: Loading path in Example 2, and the corresponding exact solution of the strain components and yield curve.

The attention is focused on the non-proportional loading part $A \rightarrow B$. Although, the loading path is linear in the stress space (consequently the stress rate is constant), the components of the corresponding strain are nonlinear; therefore, it cannot be characterized by constant strain rate. The main goal during this analysis is to determine the total strain $\boldsymbol{\varepsilon}$, the back-stress $\boldsymbol{\alpha}$ and the radius of the yield surface R at point B. Two solution methods are considered and compared, similar to the previous example. The first one is the new solution technique given in Section 5.2, whereas the second is the RRM. Note that, if the loadings were characterized by constant strain rate (which is equivalent to a linear loading path in the strain space), then the new method would provide the exact solution using only one loading step. However, in this case we do not have constant strain rate. Therefore, the accuracy of each variable is strongly dependent on the number of loading steps applied in section $A \rightarrow B$.

The exact values at point Y are determined according to the elastic Hooke's law. Since the loading $Y \rightarrow A$ is proportional, the exact values at point A can be calculated simply by using the

Table 7.2: Exact values in Example 2 at points Y, A and B, respectively.

	Y	A	B
ε_{11} [$\times 10^{-3}$]	0.75	5.25	10.194
$\varepsilon_{22} = \varepsilon_{33}$ [$\times 10^{-3}$]	-0.225	-2.325	-4.797
$\varepsilon_{12} = \varepsilon_{21}$ [$\times 10^{-3}$]	0	0	7.948
α_{11} [MPa]	0	50	115.924
$\alpha_{22} = \alpha_{33}$ [MPa]	0	-25	-57.962
$\alpha_{12} = \alpha_{21}$ [MPa]	0	0	79.973
R [MPa]	122.474	183.712	327.761

exact solution corresponding to a proportional loading. At the end of the last loading section (A→B), the exact solution is determined by the solution technique presented in Section 4.3.1.1 for stress-driven case using constant stress rate assumption. This can be done, because the loading part A→B is a linear path in the stress space; therefore, we have constant stress rate. The exact values of $\boldsymbol{\varepsilon}$, $\boldsymbol{\alpha}$ and R are summarized in Table 7.2. Furthermore, the shape and the position of the yield curve in the (σ, τ) plane at loading points Y, A and B are illustrated in Figure 7.4, where the contributions of the exact solution of the total strain components in terms of the applied τ stress are also presented.

7.2.2.2 Numerical calculations

In order to obtain information about the performance of the consistent tangent tensor, besides the accuracy of the corresponding stress update algorithm, this example is performed in a standard displacement-based finite element analysis created in MATHEMATICA (Wolfram Research, 2010e). One 3-D linear (8-noded) hexahedron element (with 100 [mm] edge dimension) is considered with 2-point Gaussian quadrature. Because the loading Y→A is proportional, the values computed at point A are unaffected by the number of steps applied in section Y→A. Therefore, even the RRM renders the exact solution using one loading step.

The numerical analysis is focused on the non-proportional loading path A→B, where an iterative solution procedure is involved to obtain the resulting displacement values. Two issues are discussed: (a) The performance of the consistent tangent tensor compared to the continuum tangent tensor, and (b) The accuracies and the computational costs of the RRM and the new method. Issue (a) is demonstrated by presenting the required iterations for various cases of load step number (1, 2, 5 and 10), and presenting the energy and residual norms at the end of each iteration in a selected loading step. Whereas, issue (b) is illustrated by comparing the errors in the computed variables ($\boldsymbol{\varepsilon}$, $\boldsymbol{\alpha}$ and R) at the end of the loading path (point B), and comparing the computational times required for each methods.

The convergence of the iteration in a given load step is measured in terms of the discrete energy norm, which is computed from the incremental nodal displacement vector $\Delta \mathbf{d}_{n+1}$ and the residual vector $\mathbf{R}(\mathbf{d}_{n+1})$ as

$$\Delta E \left(\mathbf{d}_{n+1}^{(i)} \right) := \Delta \mathbf{d}_{n+1}^{(i+1)} \cdot \mathbf{R} \left(\mathbf{d}_{n+1}^{(i)} \right), \quad (7.4)$$

Table 7.3: Iterations for each step using continuum and consistent tangent tensors in Example 2. Four cases are considered: the whole loading path is divided into 1, 2, 5 and 10 steps, respectively.

Step	Number of applied steps							
	1		2		5		10	
	\mathcal{D}^{ep}	$\mathcal{D}^{\text{cons}}$	\mathcal{D}^{ep}	$\mathcal{D}^{\text{cons}}$	\mathcal{D}^{ep}	$\mathcal{D}^{\text{cons}}$	\mathcal{D}^{ep}	$\mathcal{D}^{\text{cons}}$
1	36	5	22	5	10	5	7	4
2			27	4	12	4	7	4
3					15	4	8	4
4					15	4	9	4
5					15	4	10	4
6							10	4
7							10	3
8							10	3
9							10	3
10							10	3

where $\mathbf{d}_{n+1}^{(i)}$ denotes the i th approximation of the nodal displacement corresponding to the actual load step, whereas $\Delta \mathbf{d}_{n+1}^{(i)}$ is the incremental nodal displacement at i th iteration (Simo and Hughes, 1998). The termination criteria is defined by

$$\Delta E \left(\mathbf{d}_{n+1}^{(i)} \right) \leq 10^{-9} \Delta E \left(\mathbf{d}_{n+1}^{(1)} \right). \quad (7.5)$$

The CT is measured with a dimensionless relative time measure T_{comp} . Here, contrary to Example 1, $T_{\text{comp}} = 1$ denotes the CT required for the RRM when the loading in A→B is given in one load step, i.e., path A→B is not divided into steps.

The computed errors are measured in the same manner as in Example 1. Similarly, the error of the computed strain is defined by

$$\mathcal{E}_{\|\varepsilon\|} = 100 \frac{\|\varepsilon - \varepsilon_{\text{exact}}\|}{\|\varepsilon_{\text{exact}}\|} [\%]. \quad (7.6)$$

Table 7.3 contains the number of iterations required for convergence. For illustration purposes, four cases are considered: the loading A→B is divided into 1, 2, 5 and 10 steps, respectively. The obviously better performance of the consistent tangent tensor can be clearly seen in these results. In Table 7.4, the values of the energy and residual norms at the end of each iteration are displayed, corresponding to the last (5th) step of the case when the loading A→B is divided into 5 steps. These results show that, when the iterations are terminated, both the residual and the energy norms have much smaller values if the consistent tangent tensor is used. Table 7.5 is intended to show the numerical accuracies and the CTs of the two methods, in terms of the number of the applied steps. The errors considered are presented in Figure 7.5.a-7.5.c in log-log plots. As can be seen in Table 7.5, the new method requires more CT than the RRM, because of the more

Table 7.4: Energy and residual norm values in Example 2 at the end of each iteration of the last (5th) step in the case when the loading path is divided into 5 steps.

Iteration	Energy norm [Nmm]		Residual norm [N]	
	\mathcal{D}^{ep}	$\mathcal{D}^{\text{cons}}$	\mathcal{D}^{ep}	$\mathcal{D}^{\text{cons}}$
1	5.28 E+3	9.14 E+3	6.19 E+4	5.05 E+3
2	1.01 E+3	3.05 E+1	2.80 E+4	1.22 E+1
3	2.04 E+2	7.29 E−5	1.27 E+4	3.89 E−5
4	4.19 E+1	1.83 E−15	5.80 E+3	1.51 E−9
5	8.67 E+0		2.65 E+3	
6	1.80 E+0		1.21 E+3	
7	3.74 E−1		5.50 E+2	
8	7.78 E−2		2.51 E+2	
9	1.62 E−2		1.14 E+2	
10	3.37 E−3		5.22 E+1	
11	7.00 E−4		2.38 E+1	
12	1.46 E−4		1.08 E+1	
13	3.03 E−5		4.96 E+0	
14	6.30 E−6		2.26 E+0	
15	1.31 E−6		1.03 E+0	

complex structure of the integration scheme. However, substantial information can be extracted from the results if we combine the CTs and the resulting errors. For example, if we consider the error $\mathcal{E}_{\|\varepsilon\|}$ and the corresponding CT of various load step numbers, then we can conclude that the new method can be faster than the RRM when higher accuracy is required (see Figure 7.5.d and Table 7.6). This kind of efficiency of the new method comes from the fact that we need less loading steps in order to achieve the same accuracy.

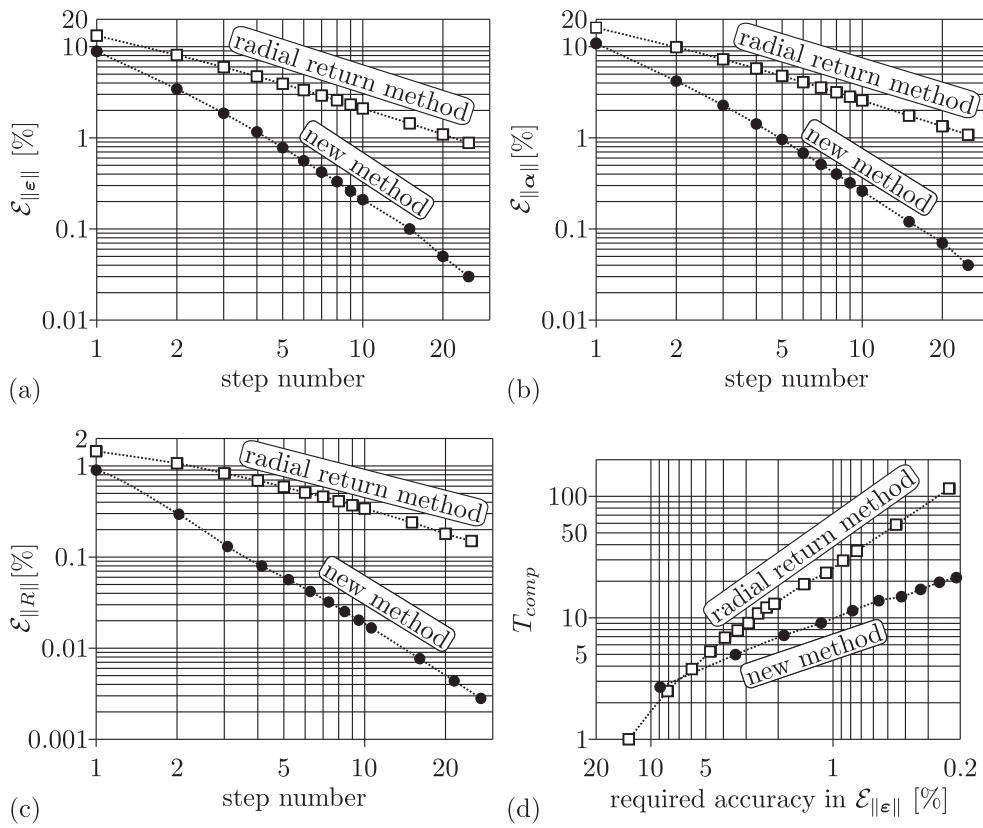


Figure 7.5: Numerical results for the new scheme and the RRM in Example 2 in log-log plots. (a) Comparison of errors in the total strain at point B. (b) Comparison of errors in the back-stress at point B. (c) Comparison of errors in the stress at point B. (d) The CTs of the two methods considered in terms of the required accuracy in the total strain.

Table 7.5: Comparison of the RRM and the new scheme. Σ_{iter} counts the total number of iterations (sum of step \times iterations of step).

Applied Steps	RRM					new scheme				
	T_{comp}	Σ_{iter}	Error values [%]			T_{comp}	Σ_{iter}	Error values [%]		
			$\mathcal{E}_{\ \varepsilon\ }$	$\mathcal{E}_{\ \alpha\ }$	\mathcal{E}_R			$\mathcal{E}_{\ \varepsilon\ }$	$\mathcal{E}_{\ \alpha\ }$	\mathcal{E}_R
1	1.00	3	13.24	16.17	1.45	2.69	5	8.90	10.87	0.94
2	2.49	7	8.11	9.90	1.07	4.97	9	3.43	4.19	0.31
3	3.78	11	5.96	7.27	0.83	7.17	13	1.86	2.27	0.13
4	5.27	15	4.72	5.77	0.69	9.06	17	1.16	1.42	0.08
5	6.87	19	3.92	4.78	0.59	11.45	21	0.78	0.96	0.06
6	7.86	22	3.34	4.08	0.51	13.83	25	0.56	0.68	0.04
7	9.06	25	2.91	3.56	0.46	14.92	27	0.42	0.51	0.03
8	10.85	29	2.58	3.16	0.41	17.11	30	0.33	0.40	0.03
9	12.14	32	2.32	2.83	0.37	19.61	33	0.26	0.32	0.02
10	13.04	35	2.10	2.57	0.34	21.40	36	0.21	0.26	0.02
15	18.90	49	1.44	1.75	0.24	29.96	50	0.10	0.12	0.01
20	23.48	60	1.09	1.34	0.18	37.42	61	0.05	0.07	≈ 0.00
25	29.55	75	0.88	1.08	0.15	46.08	76	0.03	0.04	≈ 0.00
30	35.53	90	0.74	0.90	0.13	54.94	90	0.02	0.03	≈ 0.00
50	58.42	150	0.45	0.55	0.08	90.66	150	0.01	0.01	≈ 0.00
100	115.94	300	0.23	0.28	0.04	182.12	300	≈ 0.00	≈ 0.00	≈ 0.00

Table 7.6: Comparison of the RRM and the new scheme in Example 2, in view of the required accuracy in $\mathcal{E}_{\|\varepsilon\|}$.

Required accuracy in $\mathcal{E}_{\ \varepsilon\ }$ [%]	RRM		new scheme	
	Required steps	T_{comp}	Required steps	T_{comp}
10	2	2.49	1	2.69
5	4	5.27	2	4.97
2	11	13.93	3	7.17
1	22	25.68	5	11.45
0.5	45	54.04	7	14.92
0.1	230	273.29	15	29.96

7.2.3 Example 3: Uniaxial extension of a perforated strip

The present example is a well-known problem in the literature and has been analyzed by many others (Artioli et al., 2006; Auricchio and Beirão da Veiga, 2003; Simo and Hughes, 1998; Szabó, 2009). A perforated strip subject to uniaxial extension is considered under plane strain condition. The strip dimension in [mm] is given in Figure 7.6, where due to symmetry only a quarter of the strip is outlined. The material parameters are taken as $E = 7$ GPa, $\nu = 0.3$, $\sigma_{Y0} = 24.3$ MPa, $H = 275$ MPa and $M = 0.81818$. Loading is performed by controlling the horizontal displacement of the right boundary in two steps as illustrated in Figure 7.7.

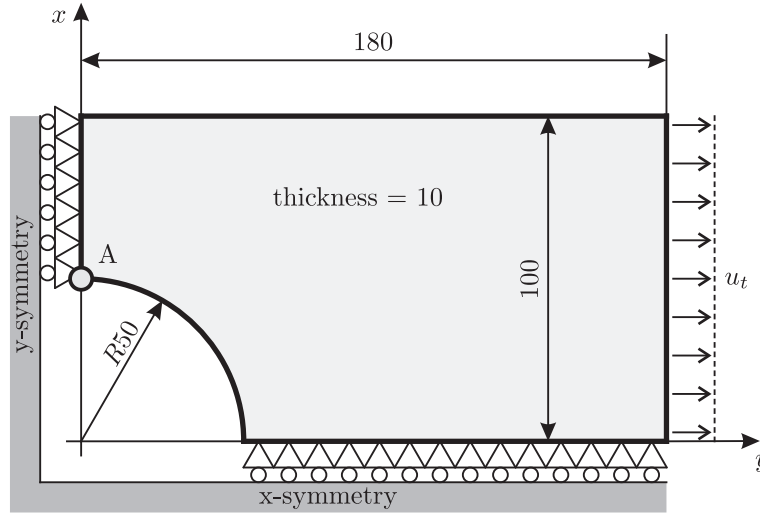


Figure 7.6: Strip dimensions in Example 3.

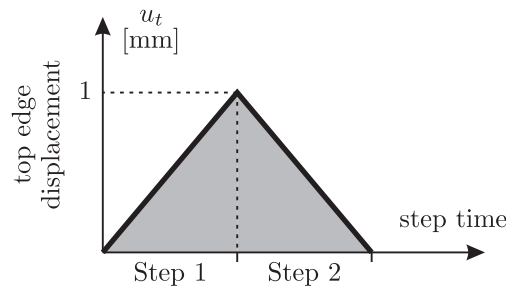


Figure 7.7: Loading history of the right edge in Example 3.

We are interested in the resulting displacement of point A at the end of the step 2. Relative errors obtained for a given mesh are calculated by

$$\mathcal{E}_A = \left| \frac{u_A - u_A^{ref}}{u_A^{ref}} \right| \cdot 100 \quad [\%], \quad (7.7)$$

where u_A^{ref} denotes the reference ("exact") solution and u_A means the computed value. $u_A^{ref} = 0.0146756973$ mm has been calculated with the UMAT code using 2048 equal load increments in each load steps. Two cases of mesh discretization are considered as illustrated in Figure 7.8. The coarse mesh consist of 192 (with 450 nodes), while the fine mesh of 1344 (with 2860 nodes) C3D8 elements with one element along the thickness.

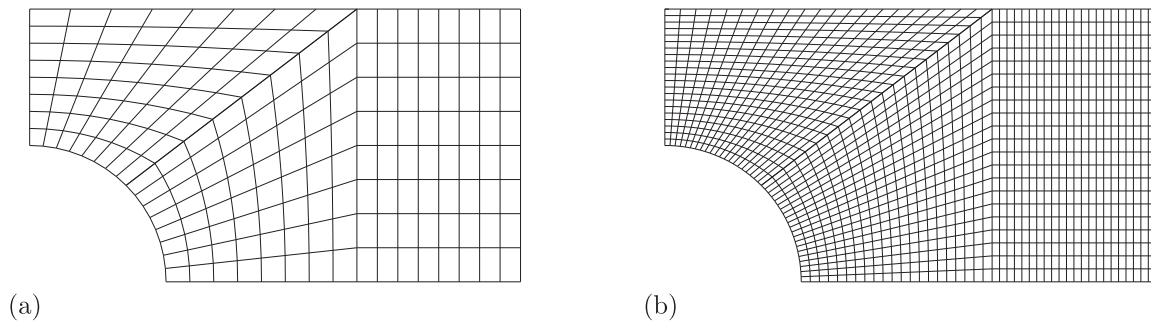


Figure 7.8: Finite element discretizations in Example 3. (a) coarse mesh. (b) fine mesh.

The results are compared in Figure 7.9, where (a) and (c) display the relative errors of ABAQUS internal scheme and the new UMAT code, respectively, in terms of the load increments applied in each step. In Figure 7.9, (b) and (d) demonstrate the CPU time in terms of the required accuracy in \mathcal{E}_A . It is relevant to note that these calculations have been performed on the same computer. The number of iterations for a given load increment are collected in Table 7.7.

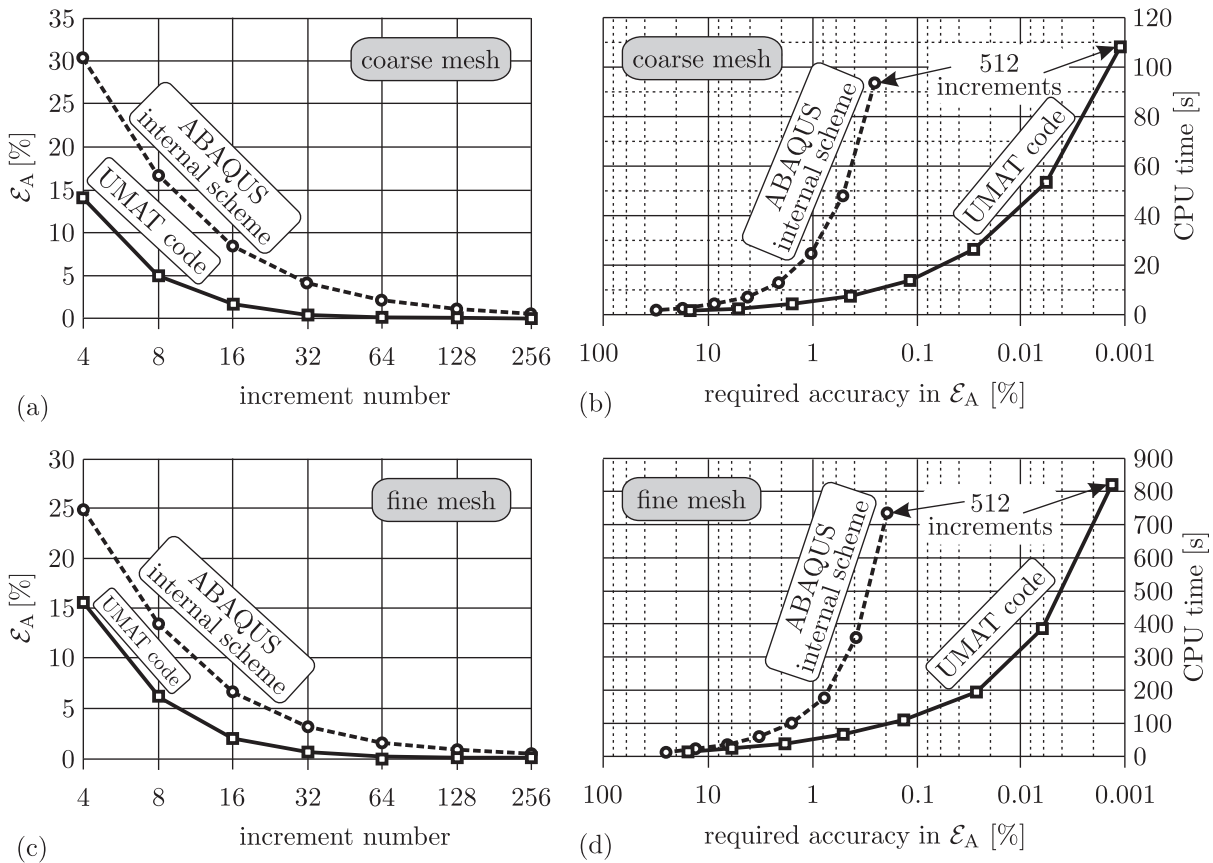


Figure 7.9: Comparisons of the ABAQUS internal scheme and the new method. (a) Relative errors of the residual displacement in point A (coarse mesh.) (b) CPU time in view of resulting accuracy (coarse mesh). (c) Relative errors of the residual displacement in point A (fine mesh). (d) CPU time in view of resulting accuracy (fine mesh).

The superior accuracy of the new UMAT code can be clearly concluded from Figure 7.9. Although, for the same number of applied load increments, the ABAQUS internal scheme needs less CPU time, the UMAT code is more accurate yielding that the new scheme is faster if we

Table 7.7: Total number of iterations in Example 3.

Applied increments in each step	Total number of iterations	
	ABAQUS internal scheme	UMAT code
4	20	20
8	31	30
16	51	51
32	83	78
64	138	138
128	259	259
256	513	513
512	1024	1024

consider the problem globally. For example: in order to achieve 1% accuracy in \mathcal{E}_A using the fine mesh, ABAQUS internal scheme needs about 150 s CPU time, while the new UMAT code requires only about 50 s.

7.2.4 Example 4: Prescribed rectilinear stress path

Here, one 3D hexahedron element is considered with stress loading history illustrated in Figure 7.10. The final step is the unloading from point D to O. Let the material parameters be the following: $E = 200$ GPa, $\nu = 0.3$, $\sigma_{Y0} = 150$ MPa, $H = 40$ GPa and $M = 0.5$. Since the loading path is consist of linear segments in the stress space, the new solution technique derived in Section 4.3.1 for constant stress rate loading can be applied to obtain the exact solution at points A, B, C and D. The first loading point A is reached by proportional loading, therefore the quantities at this stage can be derived with the analytical solution corresponding to the proportional loading. The exact nonzero strain components are given in Table 7.8.

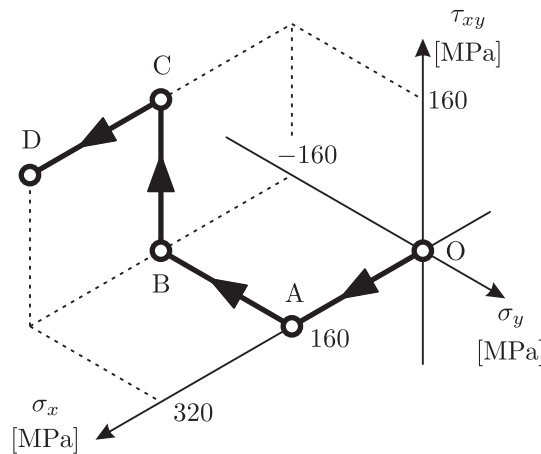


Figure 7.10: Loading path in Example 4.

For comparison purposes the resulting error in the strain tensor is considered with the relative

Table 7.8: Exact solution in Example 4.

Loading point	Strain components [$\times 10^{-3}$]			
	ϵ_x	ϵ_y	ϵ_z	γ_{xy}
A	1.050000	-0.365000	-0.365000	0
B	4.052273	-3.452002	-0.600270	0
C	6.256050	-5.802965	-0.453085	5.822912
D	8.764326	-7.489331	-0.954995	8.942970
E	6.924326	-6.209331	-0.714995	6.862970

error measure

$$\mathcal{E}_{\|\epsilon\|} = \frac{\|\epsilon - \epsilon_{\text{exact}}\|}{\|\epsilon_{\text{exact}}\|} \cdot 100 \quad [\%], \tag{7.8}$$

where ϵ means the strain computed with ABAQUS internal scheme or with the UMAT code, respectively, while ϵ_{exact} denotes the exact values (see Table 7.8). Relative errors at the end of the loading path (point O) are reported in Figure 7.11 in terms of the increment number applied in each loading segments, whereas Figure 7.12 illustrates the evolution of $\mathcal{E}_{\|\epsilon\|}$ during the loading history in two cases: a) one increment is applied in each segment; b) each segments are divided into 8 increments.

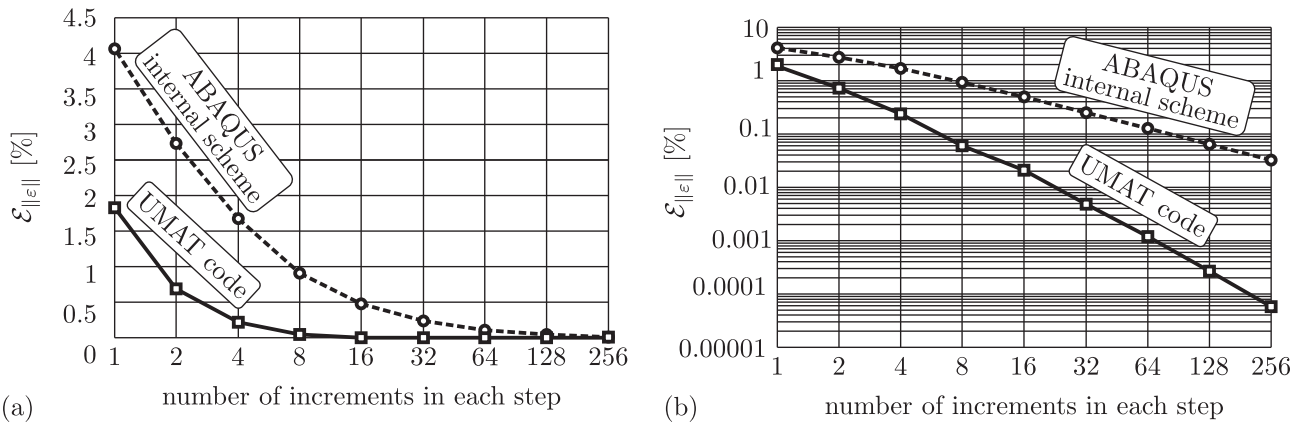


Figure 7.11: Relative errors at the end of loading path (point O) in Example 4 (a) log-normal plot (b) log-log plot.

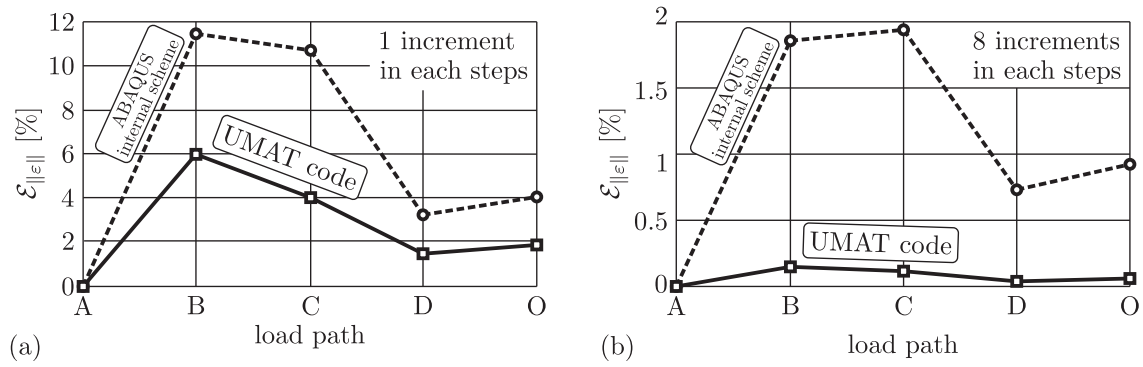


Figure 7.12: Relative errors during the loading path in Example 4 (a) 1 increment in each step (b) 8 increments in each steps.

7.2.5 Example 5: Fixed plate under surface pressure loading

As the fourth example this fifth one presents also an initial boundary value problem. A rectangular plate with fix supported edges is analyzed (see Figure 7.13). The loading is given by normal pressure of the top surface in two steps as given in Figure 7.15. Due to symmetry conditions, only one quarter part is modelled as shown in Figure 7.13 (dimensions are in [mm]).

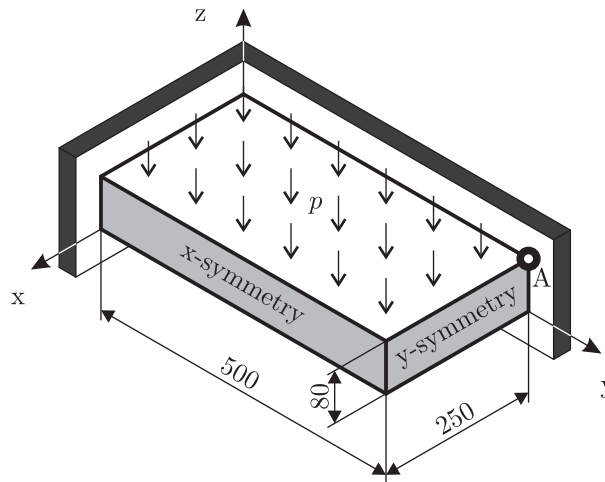


Figure 7.13: Quarter model of the plate analysed in Example 5.

Numerical calculations have been performed with 100 C3D8 elements (198 nodes) as illustrated in Figure 7.14. Material parameters are equivalent to those used in Example 4 except the mixed hardening parameter. In addition, here we analyze how the numerical results vary in terms of the parameter M .

As output, the von Mises equivalent stress (σ_{eqA}) is monitored at point A, where the material becomes plastic first. The reference solution σ_{eqA}^{ref} has been obtained with the UMAT code using 2048 load increments in each load step. The evolution of σ_{eqA}^{ref} through the loading is illustrated in Figure 7.15, where the reference solutions at the end of step 2 are also indicated.

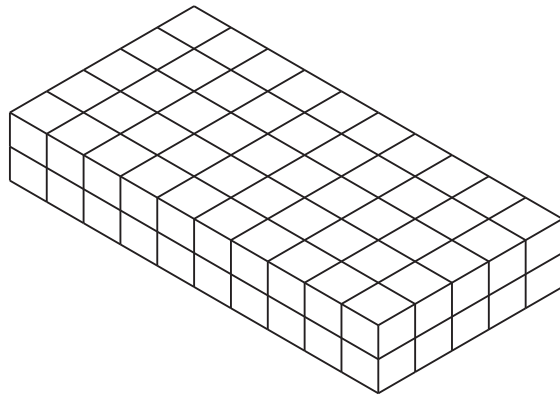


Figure 7.14: FE mesh in Example 5.

The errors of the ABAQUS internal scheme and the UMAT code are evaluated introducing the following relative norm

$$\mathcal{E}_\sigma = \left| \frac{\sigma_{eqA} - \sigma_{eqA}^{ref}}{\sigma_{eqA}^{ref}} \right| \cdot 100 \quad [\%]. \tag{7.9}$$

Observing Figure 7.16, the superior accuracy of the new UMAT code can also be recognized. For testing the speed of the algorithms the case of $M = 0.35$ has been analyzed and the total CPU time reported by the ABAQUS message file are compared in terms of the applied load increments (see Figure 7.17). In addition, the total number of iterations are collected in Table 7.9.

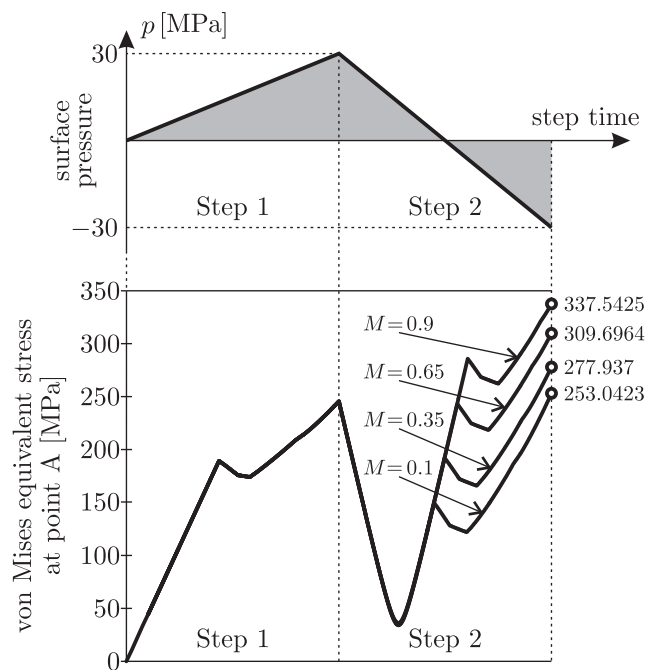


Figure 7.15: Loading history and the corresponding reference solution for various cases of the mixed hardening parameter M in Example 5.

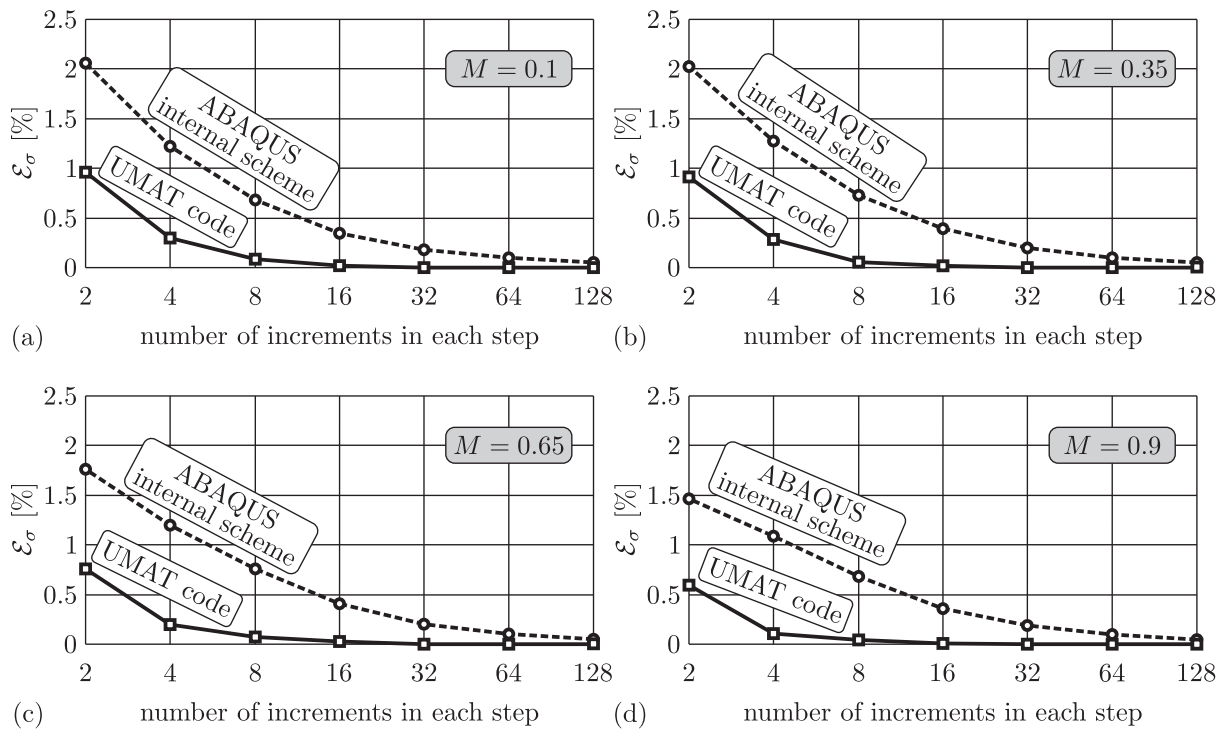


Figure 7.16: Comparisons of the ABAQUS internal scheme and the new method for various case of the mixed hardening parameter M in Example 3. (a) $M=0.1$. (b) $M=0.35$. (c) $M=0.65$. (d) $M=0.9$.

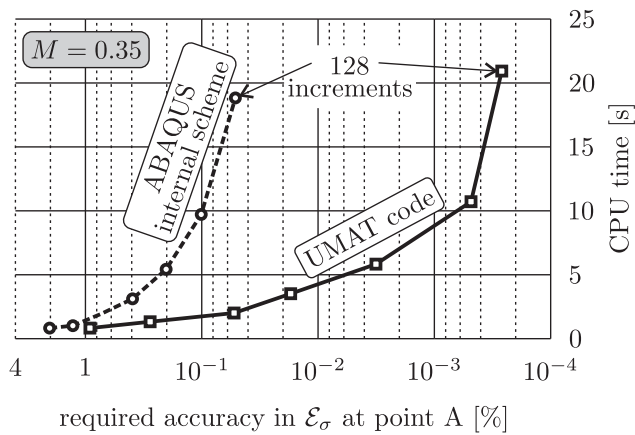


Figure 7.17: Total CPU time used by ABAQUS internal scheme and the UMAT code in terms of accuracy in Example 5.

Table 7.9: Total number of iterations in Example 5.

Applied increments in each step	Total number of iterations	
	ABAQUS	UMAT
2	10	9
4	16	16
8	27	26
16	47	47
32	76	75
64	132	133
128	256	256

7.3 Non-associative Drucker–Prager elastoplasticity model with linear isotropic hardening

7.3.1 Example 6: Strain increment needed to reach the apex

An initial stress state located on the smooth portion of the yield surface is considered. Depending on the input strain increment and the material parameters, the new stress state can arrive to the apex of the cone surface. Thus, it is obvious to examine this particular case substantially. In the following, the attention is focused on the situations, when the stress solution, corresponding to a given strain increment, can reach the apex.

Since the initial stress state at t_n corresponds to the elastic limit, the principal stress components can be written as

$$\sigma_{n1} = p_n + \sqrt{\frac{2}{3}} S_n \cos \theta, \quad (7.10)$$

$$\sigma_{2n} = p_n + \sqrt{\frac{2}{3}} S_n \cos \left(\theta - \frac{2\pi}{3} \right), \quad (7.11)$$

$$\sigma_{3n} = p_n + \sqrt{\frac{2}{3}} S_n \cos \left(\theta + \frac{2\pi}{3} \right), \quad (7.12)$$

where θ denotes the Lode's angle. The parameter S_n , using the yield condition, can be expressed as the function of the pressure as follows

$$S_n = \sqrt{2} (k_n - 3\alpha p_n). \quad (7.13)$$

In this case, the free parameters are the Lode's angle, θ and the pressure p_n . Note, that the initial stress state, given in an arbitrary coordinate system, can be related to the principal stresses defined above.

The strain and trial elastic stress increments during the time step Δt can be defined by

$$\Delta \boldsymbol{\varepsilon} = \Delta \mathbf{e} + \frac{1}{3} \text{tr} \Delta \boldsymbol{\varepsilon} \boldsymbol{\delta} \quad (7.14)$$

and

$$\Delta \boldsymbol{\sigma}_{trial} = \mathcal{D}^e : \Delta \boldsymbol{\varepsilon} = 2G \Delta \mathbf{e} + K \text{tr} \Delta \boldsymbol{\varepsilon} \boldsymbol{\delta} \quad (7.15)$$

while, their amplitudes can be expressed as

$$\|\Delta \boldsymbol{\varepsilon}\| = \sqrt{\|\Delta \mathbf{e}\|^2 + \frac{1}{3} (\text{tr} \Delta \boldsymbol{\varepsilon})^2}, \quad (7.16)$$

$$\|\Delta \boldsymbol{\sigma}_{trial}\| = \sqrt{4G^2 \|\Delta \mathbf{e}\|^2 + 3K^2 (\text{tr} \Delta \boldsymbol{\varepsilon})^2}. \quad (7.17)$$

Consider two orthogonal local coordinate systems $(\mathbf{t}, \mathbf{m}, \mathbf{n})$ and $(\mathbf{t}, \mathbf{h}, \mathbf{d})$ with common origin which is located at the initial stress point coordinate. The directions of unit vectors \mathbf{n} and \mathbf{d} correspond to the gradient of the yield and the plastic potential surfaces, respectively. The unit vector \mathbf{m} is located in the meridian of the cone, whereas, the direction of the unit vector \mathbf{h} is identical to the hydrostatic axis. Finally, the vector \mathbf{t} is orthogonal to the plane spanned by the unit vectors \mathbf{n} and \mathbf{m} (or \mathbf{d} and \mathbf{h}). These are illustrated in Figure 7.18.

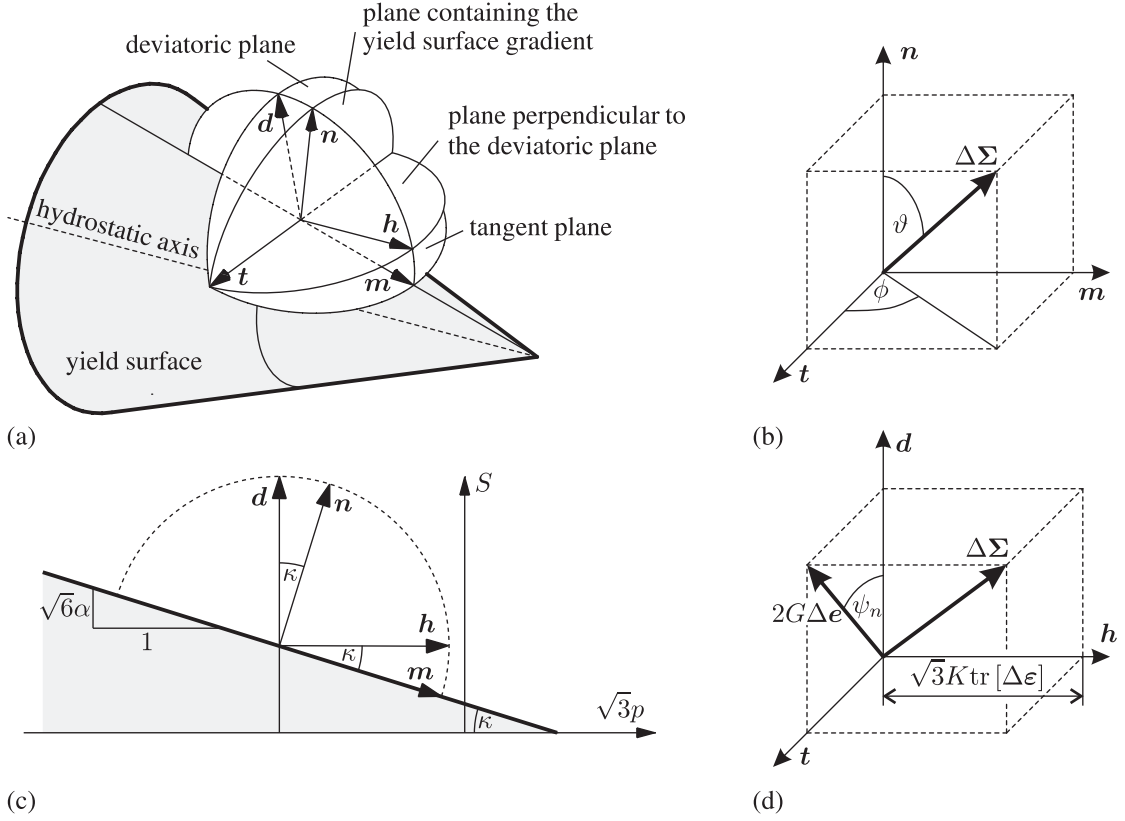


Figure 7.18: Illustration of the coordinate systems $(\mathbf{t}, \mathbf{m}, \mathbf{n})$ and $(\mathbf{t}, \mathbf{d}, \mathbf{h})$.

The basis vectors of these systems, using the parameters α and θ , are expressed by

$$\mathbf{t}^T = \frac{1}{\sqrt{6}} \left[-2\sin\theta, \sin\theta + \sqrt{3}\cos\theta, \sin\theta - \sqrt{3}\cos\theta \right], \quad (7.18)$$

$$\mathbf{m}^T = \frac{1}{\sqrt{3}\sqrt{1+6\alpha^2}} \left[1 - 2\sqrt{3}\alpha\cos\theta, 1 + \sqrt{3}\alpha\cos\theta - 3\alpha\sin\theta, 1 + \sqrt{3}\alpha\cos\theta + 3\alpha\sin\theta \right], \quad (7.19)$$

$$\mathbf{n}^T = \frac{\sqrt{2}}{\sqrt{1+6\alpha^2}} \left[\alpha + \frac{\cos\theta}{\sqrt{3}}, \alpha - \frac{\cos\theta}{2\sqrt{3}} + \frac{\sin\theta}{2}, \alpha - \frac{\cos\theta}{2\sqrt{3}} - \frac{\sin\theta}{2} \right]. \quad (7.20)$$

$$\mathbf{d}^T = \frac{1}{\sqrt{6}} \left[2\cos\theta, \sqrt{3}\sin\theta - \cos\theta, -\sqrt{3}\sin\theta - \cos\theta \right], \quad (7.21)$$

$$\mathbf{h}^T = \frac{1}{\sqrt{3}} [1, 1, 1]. \quad (7.22)$$

Now, define a vector, $\Delta\Sigma$, associated to the trial stress increment $\Delta\boldsymbol{\sigma}_{trial}$ in the coordinate system $(\mathbf{t}, \mathbf{m}, \mathbf{n})$:

$$\Delta\Sigma = \rho (\cos\vartheta \sin\phi \mathbf{t} + \sin\phi \sin\vartheta \mathbf{m} + \cos\vartheta \mathbf{n}), \quad (7.23)$$

where $\rho = \|\Delta\Sigma\| = \|\Delta\boldsymbol{\sigma}_{trial}\|$ is the magnitude of the trial stress increment. The limits for the angles are

$$0 \leq \vartheta < \frac{\pi}{2}, \quad -\frac{\pi}{2} \leq \phi \leq \frac{\pi}{2}. \quad (7.24)$$

Then, the same vector in the coordinate system $(\mathbf{t}, \mathbf{h}, \mathbf{d})$ can be expressed as

$$\Delta\Sigma = 2G \|\Delta\boldsymbol{\varepsilon}\| (\cos\psi_n \mathbf{d} + \sin\psi_n \mathbf{t}) + \sqrt{3}K \text{tr}\Delta\boldsymbol{\varepsilon} \mathbf{h}. \quad (7.25)$$

The parameters ρ , ϑ and ϕ can be related to the parameters $2G \|\Delta\boldsymbol{\varepsilon}\|$, $3K \text{tr}\Delta\boldsymbol{\varepsilon}$ and ψ_n by the following relationships:

$$2G \|\Delta\boldsymbol{\varepsilon}\| = \frac{\rho}{\sqrt{1+6\alpha^2}} \sqrt{\cos^2\phi + (\sqrt{6}\alpha \sin\vartheta - \cos\vartheta \sin\phi)^2}, \quad (7.26)$$

$$\sqrt{3}K \text{tr}\Delta\boldsymbol{\varepsilon} = \frac{\rho}{\sqrt{1+6\alpha^2}} (\sqrt{6}\alpha \cos\vartheta + \sin\vartheta \sin\phi), \quad (7.27)$$

$$\cos\psi_n = \frac{\cos\vartheta - \sqrt{6}\alpha \sin\vartheta \sin\phi}{\sqrt{\cos^2\phi + (\sqrt{6}\alpha \sin\vartheta - \cos\vartheta \sin\phi)^2}}. \quad (7.28)$$

Now, the new stress state at the end of the time interval $t \in [t_n, t_n + \Delta t]$ associated to the given strain increment can be evaluated. It is very important to emphasize that, the input set defined above can be used to describe the whole possible input strain increments. Namely, the parameter ranges of ϑ and ϕ defined in (7.24) cover the region (a half-sphere) for which the new stress state belongs to plastic state. Applying equations (7.26)-(7.28), the stress update can be evaluated using ϑ , ϕ and ρ as input parameters.

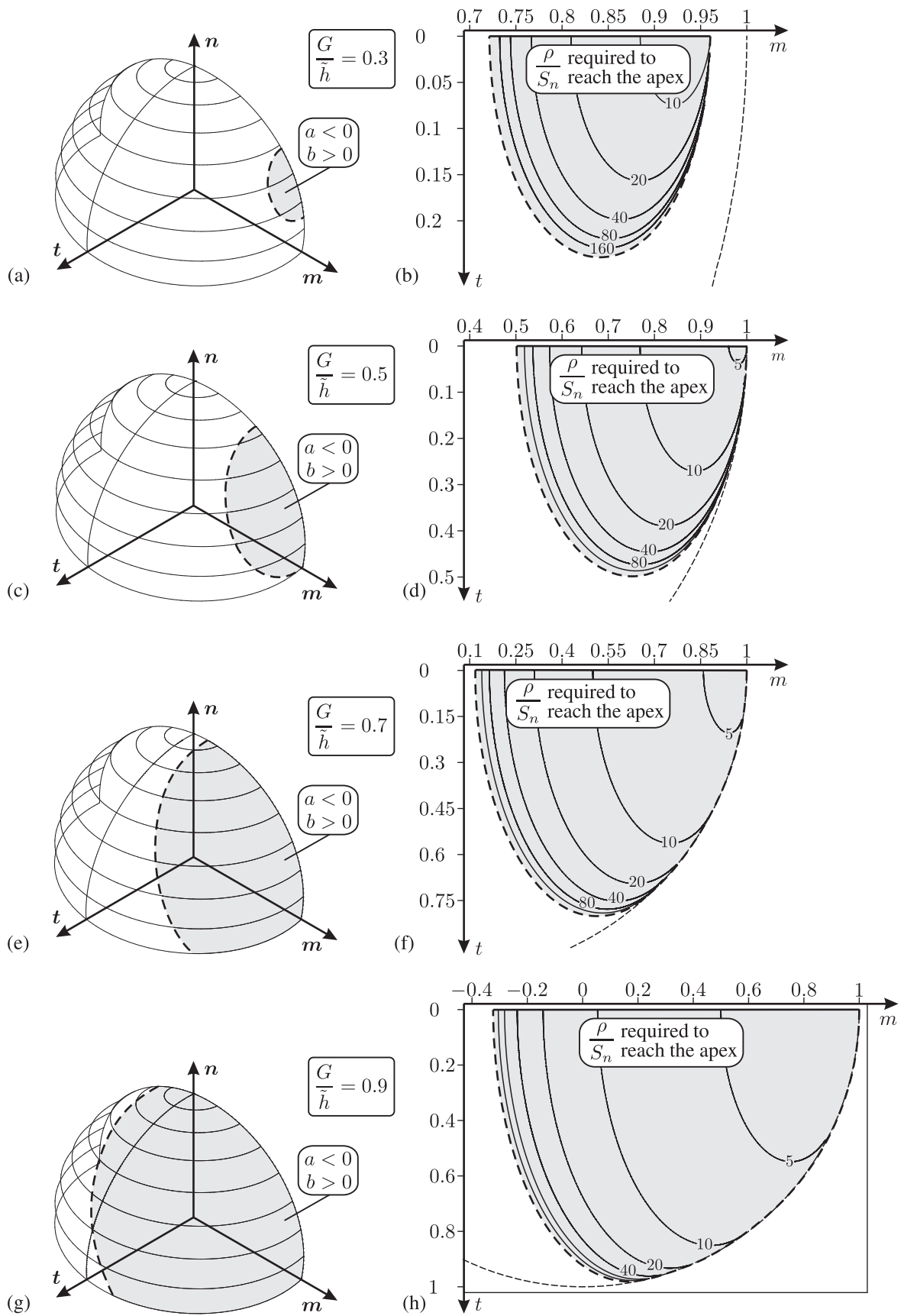


Figure 7.19: Values ρ/S_n required to reach the apex for given (t, m) pair.

Figure 7.19 illustrates the domain in the $(\mathbf{t}, \mathbf{m}, \mathbf{n})$ coordinate system, where the stress solution can reach the apex. The norm of the required strain increment is also demonstrated by plotting the contour lines of the ratio ρ/S_n over these domains. Four different G/\tilde{h} ratios are considered, while $\alpha = \frac{1}{\sqrt{6}}\tan 30^\circ$. By observing the results, it can be clearly concluded that the greater the value of G/\tilde{h} the larger the domain where the solution can reach the apex. At the boundaries of these regions, where $n \neq 0$, ρ must have infinite value to reach the apex, whereas at the boundaries where $n = 0$, the apex can be reached using finite values of ρ .

Another illustration can be seen in Figure 7.20, where the value of the ratio $2G \|\Delta \mathbf{e}\|/S_n$ needed to reach the apex, is presented for a given (ϕ, ϑ) pair. Each surfaces corresponds to a specific values of the ratio G/\tilde{h} . Here, the case, when $\kappa = 30^\circ$ is analyzed.

Finally, Figure 7.21 demonstrates the evaluation of the ratio S/S_n in terms of the input variable $2G \|\Delta \mathbf{e}\|/S_n$. Various direction of the input vector $\Delta \Sigma$ are considered in cases when $\kappa = 15^\circ$ and $\kappa = 45^\circ$, respectively. The particular value, where the ratio S/S_n becomes zero, denotes the special scenario when the stress solution has reached the apex.

It should be noted that the example presented here is a simple illustration of the proposed method. Several aspects of the Drucker–Prager model can be investigated using the technique applied in this example.

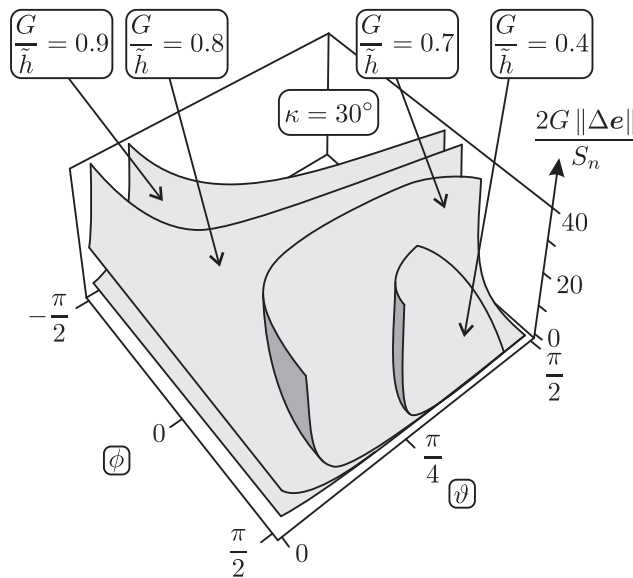


Figure 7.20: Values $2G \|\Delta \mathbf{e}\|/S_n$ required to reach the apex for given (ω, ϑ) pair.

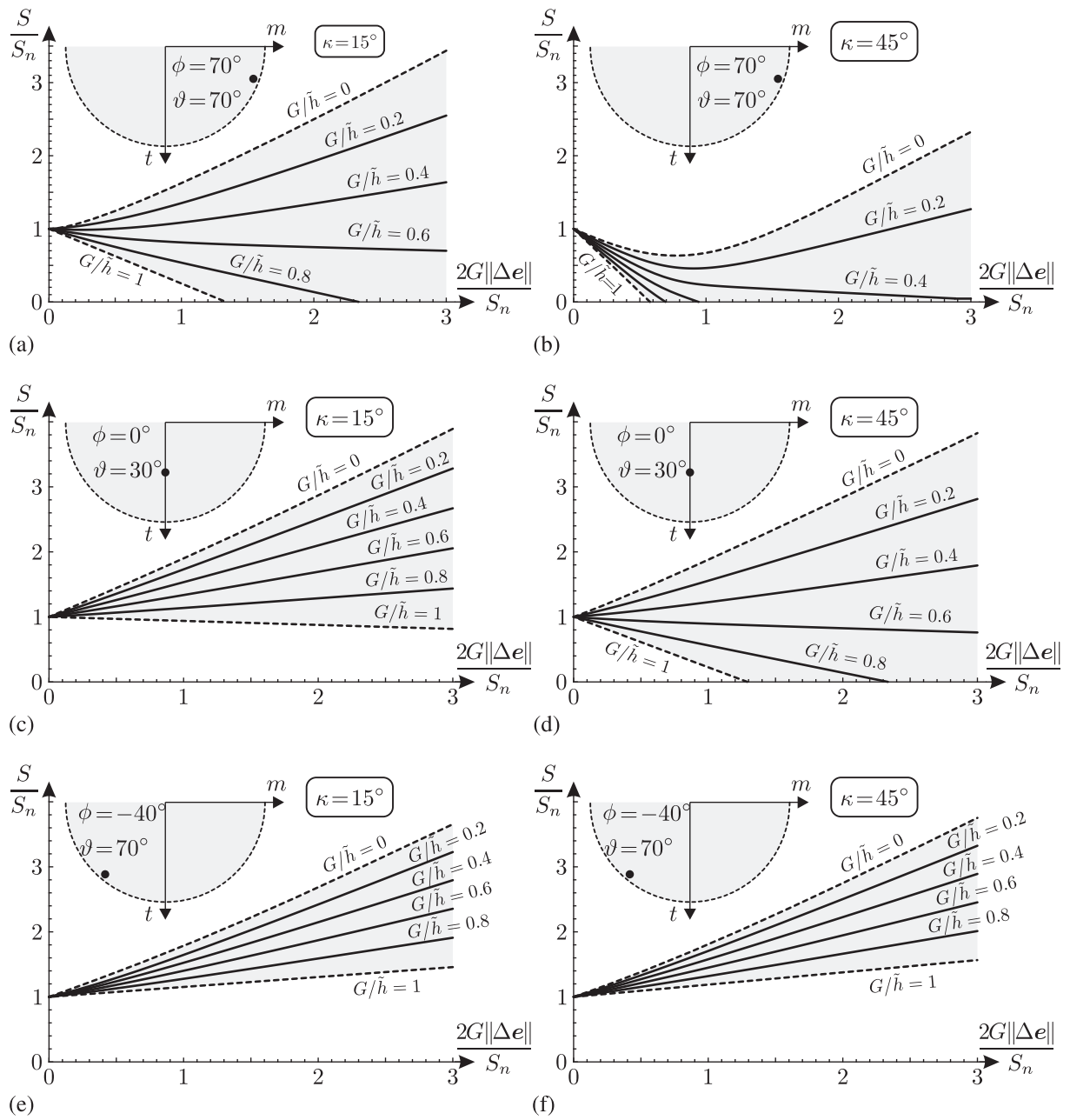


Figure 7.21: Variation of S/S_n in terms of the input parameter $2G\|\Delta e\|/S_n$ for particular orientation (ϕ, ϑ) .

7.3.2 Example 7: A non-proportional non-linear strain path

The second example demonstrates the accuracy of the proposed method for a non-linear strain input. In order to create an error analysis, it is necessary to know the exact stress solution for the given non-linear strain input. When the load is given by a linear (piecewise rectilinear) stress path in the stress space and linear hardening materials are considered, the corresponding strain solution $\boldsymbol{\varepsilon}(t)$ is generally non-linear. This $\boldsymbol{\varepsilon}(t)$ solution can be obtained analytically, since the inverse constitutive equation of the material model under consideration can be integrated analytically (see Section 4.3.2).

In this example, the stress as input parameter is controlled and the corresponding exact strain solution is computed first. Then, the strain increment, obtained previously, is considered as strain input for which the stress solution is computed with the method proposed for the constant strain input case. Therefore, we have an approximate stress solution for the strain increment, which is constructed from the non-linear strain solution obtained using constant stress input.

In the following, we consider a stress state $\boldsymbol{\sigma}_n$ located on the smooth portion of the yield surface. As input parameter a stress increment $\Delta\boldsymbol{\sigma}$ is given. Here we consider stress increments, which produce a new stress state located not in the apex. The exact strain solution $\Delta\boldsymbol{\varepsilon}$ is obtained using the analytical solutions proposed in see Section 4.3.2. It must be noted that the strain rate $\dot{\boldsymbol{\varepsilon}}$ is not constant over Δt in this case. Therefore, the following relative error $\mathcal{E}_{\Delta\boldsymbol{\sigma}}$ can be constructed:

$$\mathcal{E}_{\Delta\boldsymbol{\sigma}} = \frac{\|\Delta\boldsymbol{\sigma}^* - \Delta\boldsymbol{\sigma}\|}{\|\Delta\boldsymbol{\sigma}\|} \times 100 \text{ [\%]}, \quad (7.29)$$

where $\Delta\boldsymbol{\sigma}^*$ denotes the stress increment calculated for the input $\Delta\boldsymbol{\varepsilon}$ using the solution method proposed for linear strain path input. The error measure (7.29) can be represented efficiently in terms of the orientation and the norm of $\Delta\boldsymbol{\sigma}$ in the principal stress space. Let the material parameters be the following:

$$E = 60 \text{ MPa}, \quad \nu = 0.25, \quad H = 30 \text{ MPa}, \quad \alpha = 0.3, \quad \beta = 0.15 \quad (7.30)$$

and the norm of the deviatoric stress at the initial state is $R_n = 1 \text{ MPa}$. Figure 7.22 demonstrates the relative error measure (7.29) in terms of $\|\Delta\boldsymbol{s}\|$, ω_n and Δp .

These results give informative details about the accuracy of the proposed method if we approximate the nonlinear strain input with constant strain-rate.

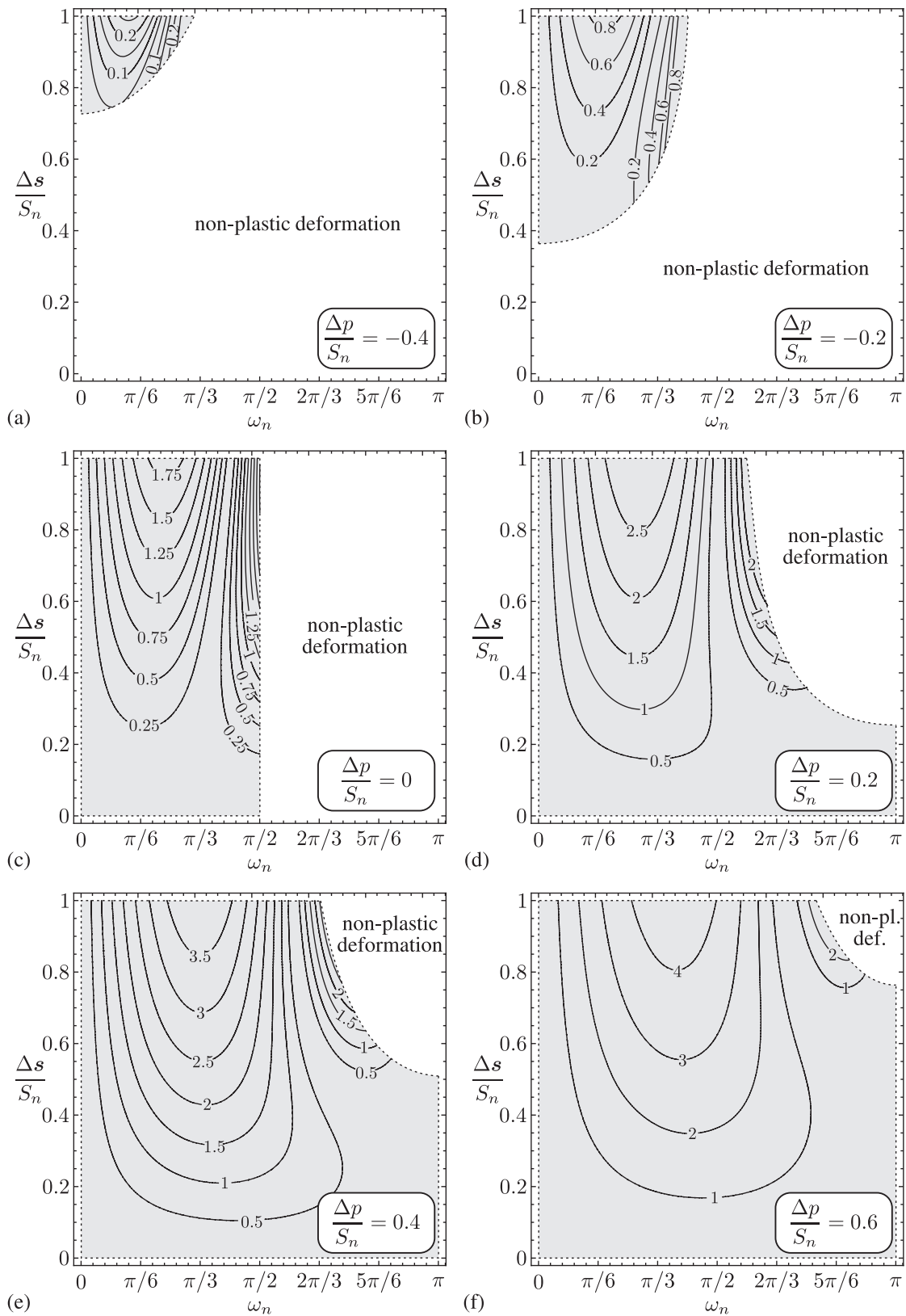


Figure 7.22: Relative error $\mathcal{E}_{\Delta\sigma}$ in terms of the angle ω_n and the parameter $\|\Delta s\|/R_n$.

8

Conclusions and Theses

Present dissertation was concerned with elastoplasticity theory, especially with the solution of constitutive equations. The main goal of this dissertation was to develop exact stress integration schemes for two commonly adopted elastoplastic constitutive models. One of them is the associative von Mises model governed by combined linear hardening, whereas the second one is the non-associative Drucker–Prager model with linear isotropic hardening. After a brief introduction of the necessary theoretical background, the well-known expression of the constitutive equations was formulated. Then, each model was considered in strain-driven and stress-driven case, respectively. The exact stress solution of the system of differential equations representing the constitutive equation was obtained for both models in case of strain-driven formulation. In addition, the exact strain solutions were also derived for the stress-driven case. The complete stress update procedures discussing all the special cases were also provided. Furthermore, the derivation of the algorithmically consistent tangent tensors made complete the numerical implementations. The accuracy and efficiency of the novel techniques were illustrated by performing a series of numerical test examples including finite element calculations as well.

The main advantage of the new stress update formulae is that they are based on the exact solutions of the corresponding constitutive equations. Consequently, their accuracies in numerical calculations are apparent. In addition, the simple structure of the stress update formulae provides their straightforward implementation in finite element codes. The new results may be usefully utilized in obtaining exact stress or strain solutions for particular elastoplastic problems where the exact solutions are needed to investigate the performance of other numerical schemes.

This work may provide a basis for other complicated models, where the exact solutions are still not clarified.

Thesis 1

I have derived the exact stress solution corresponding to the associative von Mises elastoplasticity model governed by the combined linear hardening rule.

I have obtained the exact solution of the differential equation describing the relationship between the stress rate and the strain rate tensors. The new stress solution is valid under the constant strain rate assumption and it take into account both the linear isotropic and linear kinematic hardening rules. The new solution method is based on the introduction of an angle-like parameter in the deviatoric planes. I have solved the differential equation defining the evaluation of this angle-like variable using an incomplete beta function.

Related publications: Kossa (2007, 2009); Kossa and Szabó (2007, 2009a,b)

Thesis 2

I have developed a complete stress update algorithm for the exact stress solution considered in Thesis 1. Furthermore, I have constructed the explicit expression of the corresponding consistent tangent tensor.

I have derived the discretized stress update formulae for the exact stress solution discussed in Thesis 1. Besides the general loading case, I have presented the stress update formulae for proportional loading. The new stress update algorithm is applicable to all possible loading scenarios that can occur during the loading. I have developed an efficient numerical technique to invert an incomplete beta function appearing in the stress update formulae. In addition, I have constructed the consistent tangent tensor, which is crucial for finite element implementation in order to have a quadratic rate of convergence. I have implemented the new stress update algorithm with the consistent tangent tensor into the commercial finite element software ABAQUS via its user material interface. The accuracy and efficiency of the new method has been proven by performing numerical test examples.

Related publications: Kossa (2009); Kossa and Szabó (2009b, 2010b)

Thesis 3

I have obtained the exact strain solution for the associative von Mises elastoplasticity model with combined linear hardening.

I have derived the exact solution of the differential equation corresponding to the inverse form of the constitutive equation discussed in Thesis 1. The new strain solution has been obtained assuming constant stress rate input and it takes into account the linear isotropic and the linear kinematic hardening rules. The solution method utilizes the introduction of an angle-like variable in the deviatoric planes. I have solved the evolutionary equation of this angle-like variable by utilizing an incomplete beta function.

Related publications: Kossa (2007); Kossa and Szabó (2007, 2009b)

Thesis 4

I have derived the exact stress solution for the non-associative Drucker–Prager elastoplastic model governed by linear isotropic hardening.

I have solved the differential equation describing the relation between the strain rate and the stress rate tensors. The new stress solution is valid under a constant strain rate assumption and it takes into account the linear isotropic hardening mechanism. The solution method utilizes an angle-like variable introduced in the deviatoric planes. I have obtained the solution of this angle-like parameter using an incomplete beta function. I have derived the analytical stress solution for deviatoric radial loading case. Furthermore, I have proposed an approach to solve the singularity problem appearing at the apex of the yield surface.

Related publications: Kossa (2011); Kossa and Szabó (2010a); Szabó and Kossa (2012)

Thesis 5

I have developed a complete stress update algorithm based on the exact stress solution discussed in Thesis 4. I have obtained the explicit expression of the corresponding consistent tangent tensor.

I have constructed the discretized stress update procedure based on the exact stress solution considered in Thesis 4. Besides the general loading case, I have presented the stress update formulae for the deviatoric radial loading case and for the special loading scenario, when the stress state is located at the apex of the yield surface. I have derived a condition to determine whether the updated stress will leave the apex or will remain at that point. By exact linearization of the stress update formulae, I have obtained the consistent tangent tensors for all loading cases.

Related publications: Kossa (2011); Kossa and Szabó (2010a); Szabó and Kossa (2012)

Thesis 6

I have obtained the analytical strain solution for the non-associative Drucker–Prager elastoplastic model governed by linear isotropic hardening.

I have derived the analytical solution of the differential equation corresponding to the inverse form of the constitutive equation considered in Thesis 4. The new solution is valid for linear isotropic hardening under constant stress rate assumption. The solution method is based on the introduction of an angle-like variable in the deviatoric planes. I have obtained the analytical solution for this angle-like variable providing the explicit expression.

Related publications: Kossa (2011); Kossa and Szabó (2010a); Szabó and Kossa (2012)



The incomplete beta function

A.1 Definition

According to Spanier and Oldham (1987), the incomplete beta function is defined by the indefinite integrals

$$B(x, a, b) = \int_0^x t^{a-1} (1-t)^{b-1} dt, \quad 0 \leq x < 1. \quad (\text{A.1})$$

An equivalent definition can be formulated as

$$B(x, a, b) = 2 \int_0^T (\sin t)^{2a-1} (\cos t)^{2b-1} dt, \quad 0 \leq T = \arcsin(\sqrt{x}) < \frac{\pi}{2}. \quad (\text{A.2})$$

For interchanging the parameters, the following intrarelation holds:

$$B(1-x, a, b) = \frac{\Gamma(a)\Gamma(b)}{\Gamma(a+b)} - B(x, b, a). \quad (\text{A.3})$$

Thus, by combining (A.2) and (A.3) we have the expression

$$B(1-x, a, b) = \frac{\Gamma(a)\Gamma(b)}{\Gamma(a+b)} - 2 \int_0^{\arcsin(\sqrt{x})} (\sin t)^{2b-1} (\cos t)^{2a-1} dt. \quad (\text{A.4})$$

Introducing $x = \sin^2 \theta$ we can reformulate the formula above as

$$B(\cos^2 \theta, a, b) = \frac{\Gamma(a)\Gamma(b)}{\Gamma(a+b)} - 2 \int_0^\theta (\sin t)^{2b-1} (\cos t)^{2a-1} dt. \quad (\text{A.5})$$

Consequently,

$$\int_0^\theta (\sin t)^{2b-1} (\cos t)^{2a-1} dt = \frac{1}{2} \frac{\Gamma(a) \Gamma(b)}{\Gamma(a+b)} - \frac{1}{2} B(\cos^2 \theta, a, b). \quad (\text{A.6})$$

Evaluating the integral on the left hand side between limits θ_1 and θ_2 :

$$\int_{\theta_1}^{\theta_2} (\sin t)^{2b-1} (\cos t)^{2a-1} dt = \int_0^{\theta_2} (\sin t)^{2b-1} (\cos t)^{2a-1} dt - \int_0^{\theta_1} (\sin t)^{2b-1} (\cos t)^{2a-1} dt, \quad (\text{A.7})$$

$$\boxed{\int_{\theta_1}^{\theta_2} (\sin t)^{2b-1} (\cos t)^{2a-1} dt = \frac{1}{2} B(\cos^2 \theta_1, a, b) - \frac{1}{2} B(\cos^2 \theta_2, a, b)}, \quad (\text{A.8})$$

where $0 \leq \theta_2 < \theta_1 < \frac{\pi}{2}$.

Remark: The incomplete beta function is defined for positive parameters $a, b > 0$. However, its definition can be extended, by regularization, to negative non-integer values of a and b (Gel'fand and Shilov, 1964). In addition, when the parameter a equals to zero or negative integer, the incomplete beta function has a singularity. The incomplete beta function, using the method proposed by Özçag et al. (2008), can also be extended for zero or negative integer values of a . The application of this method is presented in the paper of Szabó and Kossa (2012).

A.2 Differentiation rules

The derivative of the incomplete beta function $B(x, a, b)$ with respect to its argument x is (Wolfram Research, 2010d)

$$\frac{\partial}{\partial x} B(x, a, b) = x^{a-1} (1-x)^{b-1}, \quad (\text{A.9})$$

whereas with respect to a and b , respectively, are

$$\frac{\partial B(x, a, b)}{\partial a} = B(x, a, b) \ln x - x^a \Gamma(a)^2 {}_3\tilde{F}_2(a, a, 1-b; a+1, a+1; x), \quad (\text{A.10})$$

$$\begin{aligned} \frac{\partial B(x, a, b)}{\partial b} &= \Gamma(b)^2 (1-x)^b {}_3\tilde{F}_2(b, b, 1-a; b+1, b+1; 1-x) \\ &\quad - B(1-x, b, a) \ln(1-x) + B(a, b) (\Psi(b) - \Psi(a+b)), \end{aligned} \quad (\text{A.11})$$

where $\Gamma(\bullet)$ denotes the gamma function (Abramowitz and Stegun, 1968; Spanier and Oldham, 1987; Wolfram Research, 2010b), ${}_3\tilde{F}_2(\bullet, \bullet, \bullet; \bullet, \bullet; \bullet)$ stands for the regularized generalized hypergeometric function (Wolfram Research, 2010f), whereas $\Psi(\bullet)$ is the digamma function (Wolfram Research, 2010a). Expressions (A.10) and (A.11) can be simplified to the forms

$$\frac{\partial B(x, a, b)}{\partial a} = B(x, a, b) \ln x - \frac{x^a}{a^2} {}_3F_2(a, a, 1-b; a+1, a+1; x), \quad (\text{A.12})$$

$$\begin{aligned} \frac{\partial B(x, a, b)}{\partial b} &= \frac{(1-x)^b}{b^2} {}_3F_2(1-a, b, b; 1+b, 1+b; 1-x) \\ &\quad - B(1-x, b, a) \ln(1-x) + B(a, b) (\Psi(b) - \Psi(a+b)), \end{aligned} \quad (\text{A.13})$$

where ${}_3F_2(\bullet, \bullet, \bullet; \bullet, \bullet; \bullet)$ denotes the generalized hypergeometric function (Wolfram Research, 2010c). Inserting $x = \cos^2\theta$ into the formulas above, we arrive at

$$\frac{\partial B(\cos^2\theta, a, b)}{\partial \theta} = -\frac{4}{\sin 2\theta} \sin^{2b}\theta \cos^{2a}\theta = -2\sin^{2b-1}\theta \cos^{2a-1}\theta, \quad (\text{A.14})$$

$$\begin{aligned} \frac{\partial B(\cos^2\theta, a, b)}{\partial a} &= B(\cos^2\theta, a, b) \ln(\cos^2\theta) \\ &\quad - \frac{\cos^{2a}\theta}{a^2} {}_3F_2(a, a, 1-b; a+1, a+1; \cos^2\theta), \end{aligned} \quad (\text{A.15})$$

$$\begin{aligned} \frac{\partial B(\cos^2\theta, a, b)}{\partial b} &= \frac{\sin^{2b}\theta}{b^2} {}_3F_2(1-a, b, b; 1+b, 1+b; \sin^2\theta) \\ &\quad - B(\sin^2\theta, b, a) \ln(\sin^2\theta) \\ &\quad + B(a, b) (\Psi(b) - \Psi(a+b)). \end{aligned} \quad (\text{A.16})$$

A.3 Recursion formulae

Some useful recursion formulae are the followings (Spanier and Oldham, 1987):

$$B(x, a, b) = B(x, a+1, b) + B(x, a, b+1), \quad (\text{A.17})$$

$$B(x, a+1, b) = \frac{a}{b} B(x, a, b+1) - \frac{x^a(1-x)^b}{b}, \quad (\text{A.18})$$

$$B(x, a, b+1) = \frac{b}{a} B(x, a+1, b) + \frac{x^a(1-x)^b}{a}. \quad (\text{A.19})$$

These expressions can be reordered as follows

$$B(x, a, b) = \left(1 + \frac{b}{a}\right) B(x, a+1, b) + \frac{x^a(1-x)^b}{a}, \quad (\text{A.20})$$

$$B(x, a, b) = \left(1 + \frac{a}{b}\right) B(x, a, b+1) - \frac{x^a(1-x)^b}{b} \quad (\text{A.21})$$

and

$$B(x, a+1, b) = \frac{1}{a+b} \left(aB(x, a, b) - x^a(1-x)^b \right), \quad (\text{A.22})$$

$$B(x, a, b+1) = \frac{1}{a+b} \left(bB(x, a, b) + x^a(1-x)^b \right) \quad (\text{A.23})$$

and

$$B(x, a, b-1) = \frac{a-1}{b-1} B(x, a-1, b) - \frac{x^{a-1}(1-x)^{b-1}}{b-1}, \quad (\text{A.24})$$

$$B(x, a-1, b) = \frac{b-1}{a-1} B(x, a, b-1) + \frac{x^{a-1}(1-x)^{b-1}}{a-1}. \quad (\text{A.25})$$

B

Solution of linear non-homogeneous differential equations

A non-homogeneous linear differential equation is given in the form

$$\dot{x} = a(t)x + b(t), \quad (\text{B.1})$$

where $a, b : \mathbb{I} \rightarrow \mathbb{R}$ are continuous function on \mathbb{I} . The general solution for this type of equation can be written as a linear combination (Vrabie, 2004)

$$x(t) = A(t)x_n + B(t), \quad (\text{B.2})$$

where $x_n = x(t_n)$, $t > t_n$ and

$$A(t) = \exp\left(\int_{t_n}^t a(s) ds\right), \quad B(t) = \int_{t_n}^t \exp\left(\int_s^t a(\tau) d\tau\right) b(s) ds. \quad (\text{B.3})$$

This general solution can be easily extended to second-order tensorial form as

$$\dot{\mathbf{x}} = a(t)\mathbf{x} + b(t)\mathbf{C}, \quad (\text{B.4})$$

$$\mathbf{x}(t) = A(t)\mathbf{x}_n + B(t)\mathbf{C}, \quad (\text{B.5})$$

where \mathbf{C} is a constant.

C

Detailed derivation steps for the von Mises model

C.1 Solution for $\xi(t)$ in strain-driven case

From (4.11) it follows that

$$dt = Jd\psi, \quad J = -\frac{S_n (\sin\psi)^{2b-1}}{2G \|\dot{\mathbf{e}}\| \sin^{2b}\psi_n}. \quad (\text{C.1})$$

The rate-form expression (3.58) can be written as

$$\dot{\xi} = 2G\dot{\mathbf{e}} - 2G \|\dot{\mathbf{e}}\| (1 + 2b) \frac{\cos\psi}{S} \xi. \quad (\text{C.2})$$

Thus, the solution method described in Appendix B can be employed here. Applying (B.4) on (C.2) we have

$$a(\psi) = -\frac{2G \|\dot{\mathbf{e}}\|}{S_n} (1 + 2b) \cos\psi \left(\frac{\sin\psi_n}{\sin\psi} \right)^{2b}, \quad b(\psi) = 2G. \quad (\text{C.3})$$

Then, by knowing that $0 \leq \psi < \psi_n < \pi/2$ we can evaluate

$$A_\xi(\psi) = \exp \left(\int_{\psi_n}^{\psi} a(\tilde{\psi}) Jd\tilde{\psi} \right) = \left(\frac{\sin\psi}{\sin\psi_n} \right)^{2b+1}. \quad (\text{C.4})$$

Furthermore, using (B.3) we have

$$B_\xi(\psi) = \int_{\psi_n}^{\psi} \exp \left(\int_{\hat{\psi}}^{\psi} a(\tilde{\psi}) Jd\tilde{\psi} \right) b(\hat{\psi}) Jd\hat{\psi}, \quad (\text{C.5})$$

where

$$\exp \left(\int_{\hat{\psi}}^{\psi} a(\tilde{\psi}) J d\tilde{\psi} \right) = \left(\frac{\sin \psi}{\sin \hat{\psi}} \right)^{2b+1}. \quad (\text{C.6})$$

Therefore the parameter $B_{\xi}(\psi)$ becomes

$$B_{\xi}(\psi) = \int_{\psi_n}^{\psi} \left(\frac{\sin \psi}{\sin \hat{\psi}} \right)^{2b+1} b(\hat{\psi}) J d\hat{\psi} = \frac{S_n \sin(\psi_n - \psi)}{\|\dot{\mathbf{e}}\| \sin \psi_n} \left(\frac{\sin \psi}{\sin \psi_n} \right)^{2b}. \quad (\text{C.7})$$

Using the solution (4.10) we can simplify these parameters as

$$A_{\xi}(\psi) = \frac{S \sin \psi}{S_n \sin \psi_n}, \quad B_{\xi}(\psi) = \frac{S \sin(\psi_n - \psi)}{\|\dot{\mathbf{e}}\| \sin \psi_n}. \quad (\text{C.8})$$

Consequently $A_{\xi} = A_{\xi}(\psi)$ and $B_{\xi} = B_{\xi}(\psi)$ in (4.15).

C.2 Solution for $s(t)$ in strain-driven case

Integrating (4.17) yields

$$\int_{t_n}^t \dot{\mathbf{s}}(\tilde{t}) d\tilde{t} = \left(\int_{t_n}^t \dot{A}_s(\tilde{t}) d\tilde{t} \right) \boldsymbol{\xi}_n + \left(\int_{t_n}^t \dot{B}_s(\tilde{t}) d\tilde{t} \right) \dot{\mathbf{e}} \quad (\text{C.9})$$

$$= \left(\int_{\psi_n}^{\psi} \dot{A}_s(\tilde{\psi}) J d\tilde{\psi} \right) \boldsymbol{\xi}_n + \left(\int_{\psi_n}^{\psi} \dot{B}_s(\tilde{\psi}) J d\tilde{\psi} \right) \dot{\mathbf{e}}, \quad (\text{C.10})$$

where

$$A_s(\psi) = \int_{\psi_n}^{\psi} \dot{A}_s(\tilde{\psi}) J d\tilde{\psi} = \frac{2G}{(2G+h)(2b+1)} \left(\left(\frac{\sin \psi}{\sin \psi_n} \right)^{2b+1} - 1 \right), \quad (\text{C.11})$$

which can be simplified by inserting (C.8):

$$A_s(\psi) = \frac{2G(A_{\xi} - 1)}{(2G+h)(2b+1)}. \quad (\text{C.12})$$

Furthermore, the second coefficient in (C.10) has the form

$$B_s(\psi) = \int_{\psi_n}^{\psi} \dot{B}_s(\tilde{\psi}) J d\tilde{\psi} \quad (\text{C.13})$$

$$\begin{aligned} &= \frac{2GS_n}{(2G+h)\|\dot{\mathbf{e}}\|\sin^{2b+1}\psi_n} \int_{\psi_n}^{\psi} \cos\psi \sin(\psi_n - \psi) (\sin\psi)^{2b-1} d\tilde{\psi} \\ &\quad - \frac{S_n}{\|\dot{\mathbf{e}}\|\sin^{2b}\psi_n} \int_{\psi_n}^{\psi} (\sin\psi)^{2b-1} d\tilde{\psi}, \end{aligned} \quad (\text{C.14})$$

where the first integral on the right-hand side becomes

$$\begin{aligned} \int_{\psi_n}^{\psi} \cos\psi \sin(\psi_n - \psi) (\sin\psi)^{2b-1} d\tilde{\psi} &= \sin\psi_n \int_{\psi_n}^{\psi} \cos^2\psi (\sin\psi)^{2b-1} d\tilde{\psi} \\ &\quad - \cos\psi_n \int_{\psi_n}^{\psi} \cos\psi (\sin\psi)^{2b} d\tilde{\psi}. \end{aligned} \quad (\text{C.15})$$

Applying the formula (A.8) we can evaluate the expressions above:

$$\sin\psi_n \int_{\psi_n}^{\psi} \cos^2\psi (\sin\psi)^{2b-1} d\tilde{\psi} = \frac{\sin\psi_n}{2} \left(B\left(\cos^2\psi_n, \frac{3}{2}, b\right) - B\left(\cos^2\psi, \frac{3}{2}, b\right) \right), \quad (\text{C.16})$$

$$-\cos\psi_n \int_{\psi_n}^{\psi} \cos\psi (\sin\psi)^{2b} d\tilde{\psi} = -\cos\psi_n \left(\frac{(\sin\psi)^{2b+1}}{2b+1} - \frac{(\sin\psi_n)^{2b+1}}{2b+1} \right). \quad (\text{C.17})$$

Consequently, the first integral term in (C.14) reduces to

$$= \frac{B\left(\cos^2\psi_n, \frac{3}{2}, b\right) - B\left(\cos^2\psi, \frac{3}{2}, b\right)}{2} \sin\psi_n - \frac{(\sin\psi)^{2b+1} - (\sin\psi_n)^{2b+1}}{2b+1} \cos\psi_n, \quad (\text{C.18})$$

whereas the second integral in (C.14) can be expressed using (4.12) as

$$\int_{\psi_n}^{\psi} (\sin\psi)^{2b-1} d\psi = -\frac{2G\|\dot{\mathbf{e}}\|}{S_n} \sin^{2b}\psi_n (t - t_n). \quad (\text{C.19})$$

Finally, substituting (C.18) and (C.19) into (C.14) gives

$$\begin{aligned}
 B_s(\psi) &= \frac{2GS_n}{(2G+h)\|\dot{\epsilon}\|\sin^{2b+1}\psi_n} \frac{B\left(\cos^2\psi_n, \frac{3}{2}, b\right) - B\left(\cos^2\psi, \frac{3}{2}, b\right)}{2} \sin\psi_n \\
 &\quad - \frac{2GS_n}{(2G+h)\|\dot{\epsilon}\|\sin^{2b+1}\psi_n} \frac{(\sin\psi)^{2b+1} - (\sin\psi_n)^{2b+1}}{2b+1} \cos\psi_n \\
 &\quad - \frac{S_n}{\|\dot{\epsilon}\|\sin^{2b}\psi_n} \left(-\frac{2G\|\dot{\epsilon}\|}{S_n} \sin^{2b}\psi_n (t-t_n) \right), \tag{C.20}
 \end{aligned}$$

$$B_s(\psi) = \frac{GS_n \left(B\left(\cos^2\psi_n, \frac{3}{2}, b\right) - B\left(\cos^2\psi, \frac{3}{2}, b\right) \right)}{(2G+h)\|\dot{\epsilon}\|\sin^{2b}\psi_n} - \frac{S_n \cos\psi_n}{\|\dot{\epsilon}\|} A_s + 2G(t-t_n). \tag{C.21}$$

The expression above can be written in a much simpler form. Applying (A.22) we can reformulate the incomplete beta function terms as

$$B\left(\cos^2\psi_n, \frac{3}{2}, b\right) = \frac{2}{1+2b} \left(\frac{1}{2} B\left(\cos^2\psi_n, \frac{1}{2}, b\right) - \cos\psi_n (\sin\psi_n)^{2b} \right), \tag{C.22}$$

$$B\left(\cos^2\psi, \frac{3}{2}, b\right) = \frac{2}{1+2b} \left(\frac{1}{2} B\left(\cos^2\psi, \frac{1}{2}, b\right) - \cos\psi (\sin\psi)^{2b} \right). \tag{C.23}$$

Thus, it follows that

$$\begin{aligned}
 B\left(\cos^2\psi_n, \frac{3}{2}, b\right) - B\left(\cos^2\psi, \frac{3}{2}, b\right) &= \frac{1}{1+2b} \left(B\left(\cos^2\psi_n, \frac{1}{2}, b\right) - B\left(\cos^2\psi, \frac{1}{2}, b\right) \right) \\
 &\quad - \frac{2\cos\psi_n (\sin\psi_n)^{2b}}{1+2b} + \frac{2\cos\psi (\sin\psi)^{2b}}{1+2b} \tag{C.24}
 \end{aligned}$$

$$= \frac{1}{1+2b} \left(-\frac{4G\|\dot{\epsilon}\|}{S_n} \sin^{2b}\psi_n (t-t_n) \right) - \frac{2\cos\psi_n (\sin\psi_n)^{2b}}{1+2b} + \frac{2\cos\psi (\sin\psi)^{2b}}{1+2b}. \tag{C.25}$$

Therefore, the following relation holds:

$$\frac{GS_n \left(B\left(\cos^2\psi_n, \frac{3}{2}, b\right) - B\left(\cos^2\psi, \frac{3}{2}, b\right) \right)}{(2G+h)\|\dot{\epsilon}\|\sin^{2b}\psi_n} = \tag{C.26}$$

$$\frac{-4G^2(t-t_n)}{(2G+h)(1+2b)} - \frac{2GS_n \cos\psi_n}{(2G+h)(1+2b)\|\dot{\epsilon}\|} + \frac{2GS_n \cos\psi}{(2G+h)(1+2b)\|\dot{\epsilon}\|} \left(\frac{\sin\psi}{\sin\psi_n} \right)^{2b}. \tag{C.27}$$

Substituting back into (C.21) gives

$$B_s(\psi) = 2G(t-t_n) + \frac{2G(S\cos\psi - S_n A_\xi \cos\psi_n - 2G\|\dot{\epsilon}\|(t-t_n))}{(2G+h)(1+2b)\|\dot{\epsilon}\|}. \tag{C.28}$$

Further simplification can be made by inserting (4.10) and (4.16)₁ into the expression above:

$$B_s(\psi) = 2G(t-t_n) - \frac{2GS\sin(\psi-\psi_n)}{(2G+h)(1+2b)\|\dot{\epsilon}\|\sin\psi_n} - \frac{4G^2(t-t_n)}{(2G+h)(1+2b)}, \tag{C.29}$$

then using (4.16)₂ gives

$$B_s(\psi) = 2G(t - t_n) + \frac{2G(B_\xi - 2G(t - t_n))}{(2G + h)(1 + 2b)}. \quad (\text{C.30})$$

Consequently $A_s = A_s(\psi)$ and $B_s = B_s(\psi)$ in (4.19).

Remark: the expression of the parameter B_s published in the paper of Kossa and Szabó (2009b) has a much more complicated form. However that result is identical to (C.30). It can be simply proved, if we rewrite the term

$$B\left(\cos^2\psi_n, \frac{3}{2}, b\right) - B\left(\cos^2\psi, \frac{3}{2}, b\right) = 2 \int_{\psi_n}^{\psi} \cos^2\psi (\sin\psi)^{2b-1} \quad (\text{C.31})$$

in (C.20). Therefore, in view of (4.12), the following simplification holds:

$$2 \int_{\psi_n}^{\psi} \cos^2\psi (\sin\psi)^{2b-1} = 2 \int_{\psi_n}^{\psi} (1 - \sin^2\psi) (\sin\psi)^{2b-1} d\tilde{\psi} \quad (\text{C.32})$$

$$= 2 \int_{\psi_n}^{\psi} (\sin\psi)^{2b-1} d\tilde{\psi} - 2 \int_{\psi_n}^{\psi} (\sin\psi)^{2b+1} d\tilde{\psi} \quad (\text{C.33})$$

$$= -\frac{4G \|\dot{\mathbf{e}}\|}{S_n} \sin^{2b}\psi_n (t - t_n) - \left(B\left(\cos^2\psi_n, \frac{1}{2}, b + 1\right) - B\left(\cos^2\psi, \frac{1}{2}, b + 1\right) \right). \quad (\text{C.34})$$

If we substitute back (C.34) into (C.20), then we arrive at the formula, which was published in the paper of Kossa and Szabó (2009b).

C.3 Solution for $\xi(t)$ in stress-driven case

From (4.89) it follows that

$$dt = Jd\psi, \quad J = -\frac{S_n \sin^M \omega_n}{\|\dot{\mathbf{s}}\|} (\sin\omega)^{-M-1}. \quad (\text{C.35})$$

The evolutionary equation (3.63)₃ can be written as

$$\dot{\xi} = \dot{\mathbf{s}} - \frac{1 - M}{S} \|\dot{\mathbf{s}}\| \cos\omega \xi. \quad (\text{C.36})$$

Thus, the solution method described in Appendix B can be used. Applying (B.4) in (C.36) we have

$$a(\omega) = \frac{M - 1}{S_n} \|\dot{\mathbf{s}}\| \cos\omega \left(\frac{\sin\omega}{\sin\omega_n} \right)^M, \quad b(\omega) = 1. \quad (\text{C.37})$$

It follows from (B.5) that

$$A(\omega) = \exp\left(\int_{\omega_n}^{\omega} a(\tilde{\omega}) J d\tilde{\omega}\right) = \frac{S \sin\omega}{S_n \sin\omega_n} \quad (\text{C.38})$$

and

$$B(\omega) = \int_{\omega_n}^{\omega} \exp\left(\int_{\hat{\omega}}^{\omega} a(\tilde{\omega}) J d\tilde{\omega}\right) b(\hat{\omega}) J d\hat{\omega} = \frac{S \sin(\omega_n - \omega)}{\|\dot{\mathbf{s}}\| \sin\omega_n}. \quad (\text{C.39})$$

Thus, it follows that $A_\xi = A_\xi(\omega)$ and $B_\xi = B_\xi(\omega)$ in (4.92).

C.4 Solution for $e(t)$ in stress-driven case

Integrating (4.94) gives

$$\int_{t_n}^t \dot{e}(\tilde{t}) d\tilde{t} = \left(\int_{\omega_n}^{\omega} \dot{A}_e(\tilde{\omega}) J d\tilde{\omega}\right) \boldsymbol{\xi}_n + \left(\int_{\omega_n}^{\omega} \dot{B}_e(\tilde{\omega}) J d\tilde{\omega}\right) \dot{\mathbf{s}}. \quad (\text{C.40})$$

Parameter $A_e(\omega)$ is expressed as

$$A_e(\omega) = \int_{\omega_n}^{\omega} \dot{A}_e(\tilde{\omega}) J d\tilde{\omega} = \frac{1 - A_\xi}{h(1 - M)}, \quad (\text{C.41})$$

whereas parameter $B_e(\omega)$ is defined by

$$B_e(\omega) = \int_{\omega_n}^{\omega} \dot{B}_e(\tilde{\omega}) J d\tilde{\omega} \quad (\text{C.42})$$

$$= -\frac{S_n \sin^{M-1} \omega_n}{h \|\dot{\mathbf{s}}\|} \int_{\omega_n}^{\omega} (\sin\omega)^{-M-1} \cos\omega \sin(\omega_n - \omega) d\tilde{\omega} \\ - \frac{S_n \sin^M \omega_n}{2G \|\dot{\mathbf{s}}\|} \int_{\omega_n}^{\omega} (\sin\omega)^{-M-1} d\tilde{\omega}, \quad (\text{C.43})$$

where

$$\int_{\omega_n}^{\omega} (\sin\omega)^{-M-1} d\tilde{\omega} = -\frac{\|\dot{\mathbf{s}}\| (t - t_n)}{S_n \sin^M \omega_n} \quad (\text{C.44})$$

and

$$\int_{\omega_n}^{\omega} (\sin\omega)^{-M-1} \cos\omega \sin(\omega_n - \omega) d\tilde{\omega} = \quad (\text{C.45})$$

$$= \sin\omega_n \int_{\omega_n}^{\omega} (\cos\omega)^2 (\sin\omega)^{-M-1} d\tilde{\omega} - \cos\omega_n \int_{\omega_n}^{\omega} \cos\omega (\sin\omega)^{-M} d\tilde{\omega} \quad (\text{C.46})$$

$$= \frac{\sin\omega_n}{2} \left(B \left(\cos^2\omega_n, \frac{3}{2}, -\frac{M}{2} \right) - B \left(\cos^2\omega, \frac{3}{2}, -\frac{M}{2} \right) \right) - \frac{\cos\omega_n}{1-M} \left((\sin\omega)^{1-M} - (\sin\omega_n)^{1-M} \right). \quad (\text{C.47})$$

Substituting (C.44) and (C.47) back into (C.43) gives

$$B_e(\omega) = \frac{(t-t_n)}{2G} - \frac{S_n \cos\omega_n}{\|\dot{\mathbf{s}}\|} A_e - \frac{S_n \sin^M \omega_n}{2h \|\dot{\mathbf{s}}\|} \left(B \left(\cos^2\omega_n, \frac{3}{2}, -\frac{M}{2} \right) - B \left(\cos^2\omega, \frac{3}{2}, -\frac{M}{2} \right) \right). \quad (\text{C.48})$$

Using the formula (A.22), we can write the followings:

$$B \left(\cos^2\omega_n, \frac{3}{2}, -\frac{M}{2} \right) = \frac{2}{1-M} \left(\frac{1}{2} B \left(\cos^2\omega_n, \frac{1}{2}, -\frac{M}{2} \right) - \cos\omega_n (\sin\omega_n)^{-M} \right) \quad (\text{C.49})$$

$$= \frac{1}{1-M} B \left(\cos^2\omega_n, \frac{1}{2}, -\frac{M}{2} \right) - \frac{2\cos\omega_n (\sin\omega_n)^{-M}}{1-M}, \quad (\text{C.50})$$

$$B \left(\cos^2\omega, \frac{3}{2}, -\frac{M}{2} \right) = \frac{2}{1-M} \left(\frac{1}{2} B \left(\cos^2\omega, \frac{1}{2}, -\frac{M}{2} \right) - \cos\omega (\sin\omega)^{-M} \right) \quad (\text{C.51})$$

$$= \frac{1}{1-M} B \left(\cos^2\omega, \frac{1}{2}, -\frac{M}{2} \right) - \frac{2\cos\omega (\sin\omega)^{-M}}{1-M}. \quad (\text{C.52})$$

Consequently

$$\begin{aligned} & B \left(\cos^2\omega_n, \frac{3}{2}, -\frac{M}{2} \right) - B \left(\cos^2\omega, \frac{3}{2}, -\frac{M}{2} \right) = \\ &= \frac{1}{1-M} \left(B \left(\cos^2\omega_n, \frac{1}{2}, -\frac{M}{2} \right) - B \left(\cos^2\omega, \frac{1}{2}, -\frac{M}{2} \right) \right) \\ & \quad - \frac{2}{1-M} \left(\cos\omega_n (\sin\omega_n)^{-M} - \cos\omega (\sin\omega)^{-M} \right). \end{aligned} \quad (\text{C.53})$$

In view of (4.91) and substituting (C.53) into (C.48) yields

$$B_e(\omega) = \frac{(t-t_n)}{2G} + \frac{S_n \cos\omega_n}{\|\dot{\mathbf{s}}\| h (1-M)} A_\xi + \frac{(t-t_n)}{h (1-M)} - \frac{S \cos\omega}{h \|\dot{\mathbf{s}}\| (1-M)}, \quad (\text{C.54})$$

$$B_e(\omega) = \frac{(t-t_n)}{2G} + \frac{S_n \cos\omega_n A_\xi - S \cos\omega + \|\dot{\mathbf{s}}\| (t-t_n)}{h \|\dot{\mathbf{s}}\| (1-M)}. \quad (\text{C.55})$$

By inserting (4.93) we have

$$B_e(\omega) = \frac{(t-t_n)}{2G} + \frac{(t-t_n)}{h (1-M)} + \frac{S \sin(\omega - \omega_n)}{h (1-M) \|\dot{\mathbf{s}}\| \sin\omega_n}, \quad (\text{C.56})$$

$$B_e(\omega) = \frac{(t-t_n)}{2G} + \frac{(t-t_n) - B_\xi}{h (1-M)} \quad (\text{C.57})$$

Remark: the expression of the parameter B_e published in the paper of Kossa and Szabó (2009b) has different form than (C.57). However that result is identical to (C.57). It can be simply proved, if we rewrite the term

$$B\left(\cos^2\omega_n, \frac{3}{2}, -\frac{M}{2}\right) - B\left(\cos^2\omega, \frac{3}{2}, -\frac{M}{2}\right) = 2 \int_{\omega_n}^{\omega} (\cos\omega)^2 (\sin\omega)^{-M-1} d\tilde{\omega} \quad (\text{C.58})$$

$$= 2 \int_{\omega_n}^{\omega} (\sin\omega)^{-M-1} - 2 \int_{\omega_n}^{\omega} (\sin\omega)^{1-M} \quad (\text{C.59})$$

in (C.48). Therefore, in view of (4.12), the following simplification holds:

$$\begin{aligned} 2 \int_{\omega_n}^{\omega} (\sin\omega)^{-M-1} - 2 \int_{\omega_n}^{\omega} (\sin\omega)^{1-M} &= -\frac{2 \|\dot{\mathbf{s}}\|}{S_n \sin^M \omega_n} (t - t_n) \\ &\quad - B\left(\cos^2\omega, \frac{1}{2}, -\frac{M}{2}\right) + B\left(\cos^2\omega_n, \frac{1}{2}, -\frac{M}{2}\right). \end{aligned} \quad (\text{C.60})$$

If we substitute back (C.60) into (C.48), then we arrive at the formula, which was published in the paper of Kossa and Szabó (2009b).

C.5 Consistent elastoplastic tangent tensor

C.5.1 General loading case

In order to obtain the expression of the consistent tangent tensor, it is required to compute the derivatives of all the variables appearing in the stress update formulae. These derivatives are summarized in the following.

$\partial c / \partial \Delta \mathbf{e}$: The derivative of the yield function (5.15) written at the contact point yields

$$\frac{\partial}{\partial \Delta \mathbf{e}} (\|\boldsymbol{\xi}_c\| - R_n) = 0, \quad (\text{C.61})$$

$$\frac{\partial \|\boldsymbol{\xi}_c\|}{\partial \Delta \mathbf{e}} = \frac{\boldsymbol{\xi}_c}{\|\boldsymbol{\xi}_c\|} : \frac{\partial \boldsymbol{\xi}_c}{\partial \Delta \mathbf{e}} = \frac{\boldsymbol{\xi}_c}{\|\boldsymbol{\xi}_c\|} : \left(2Gc\mathbf{I} + 2G\Delta \mathbf{e} \otimes \frac{\partial c}{\partial \Delta \mathbf{e}} \right) = 0, \quad (\text{C.62})$$

$$\boxed{\frac{\partial c}{\partial \Delta \mathbf{e}} = -\frac{c}{S_c \|\Delta \mathbf{e}\| \cos \psi_c} \boldsymbol{\xi}_c} \quad (\text{C.63})$$

$\partial \boldsymbol{\xi}_c / \partial \Delta \mathbf{e}$: Combining (C.63) with (C.62) gives

$$\boxed{\frac{\partial \boldsymbol{\xi}_c}{\partial \Delta \mathbf{e}} = 2Gc\mathbf{I} - \frac{2Gc}{S_c \|\Delta \mathbf{e}\| \cos \psi_c} \Delta \mathbf{e} \otimes \boldsymbol{\xi}_c} \quad (\text{C.64})$$

$\partial \psi_c / \partial \Delta \mathbf{e}$: The derivative of the angle ψ_c defined at the contact point can be obtained as

$$\frac{\partial \psi_c}{\partial \Delta \mathbf{e}} = \left(\frac{\partial \cos \psi_c}{\partial \psi_c} \right)^{-1} \frac{\partial \cos \psi_c}{\partial \Delta \mathbf{e}} = \frac{-1}{\sin \psi_c} \frac{\partial}{\partial \Delta \mathbf{e}} \left(\frac{\boldsymbol{\xi}_c : \Delta \mathbf{e}}{S_c \|\Delta \mathbf{e}\|} \right). \quad (\text{C.65})$$

After simplification, we arrive at the linear combination

$$\boxed{\frac{\partial \psi_c}{\partial \Delta \mathbf{e}} = C_1 \boldsymbol{\xi}_c + C_2 \Delta \mathbf{e}}, \quad (\text{C.66})$$

where

$$C_1 = \frac{2Gc \|\Delta \mathbf{e}\| - S_c \cos \psi_c}{S_c^2 \|\Delta \mathbf{e}\| \cos \psi_c \sin \psi_c}, \quad C_2 = \frac{1}{\sin \psi_c} \left(\frac{\cos \psi_c}{\|\Delta \mathbf{e}\|^2} - \frac{2Gc}{S_c \|\Delta \mathbf{e}\|} \right). \quad (\text{C.67})$$

$\partial \psi_{n+1} / \partial \Delta \mathbf{e}$: Rewriting equation (5.11) for the case when elastic-plastic transition occurs yields the expression

$$B \left(\cos^2 \psi_{n+1}, \frac{1}{2}, b \right) - B \left(\cos^2 \psi_c, \frac{1}{2}, b \right) = \frac{4G(1-c) \|\Delta \mathbf{e}\|}{S_c} \sin^{2b} \psi_c. \quad (\text{C.68})$$

The derivative of all the variables appearing in the expression above have been already obtained, except the derivative of the final angle. Taking the derivatives of both sides, the expression for $\partial \psi_{n+1} / \partial \Delta \mathbf{e}$ can be obtained as

$$\boxed{\frac{\partial \psi_{n+1}}{\partial \Delta \mathbf{e}} = D_1 \boldsymbol{\xi}_c + D_2 \Delta \mathbf{e}}, \quad (\text{C.69})$$

where

$$D_1 = \frac{A_\xi}{S_{n+1}^2} \left(C_1 S_c^2 - 4Gb C_1 S_c \|\Delta \mathbf{e}\| (1-c) \cos \psi_c - 2Gc \tan \psi_c \right) \quad (\text{C.70})$$

$$D_2 = \frac{A_\xi}{S_{n+1}^2} \left(C_2 S_c^2 - 4Gb C_2 S_c \|\Delta \mathbf{e}\| (1-c) \cos \psi_c - \frac{2GS_c(1-c)}{\|\Delta \mathbf{e}\|} \sin \psi_c \right) \quad (\text{C.71})$$

$\partial S_{n+1} / \partial \Delta \mathbf{e}$: The derivative of the radius of the updated yield surface is computed using the chain rule:

$$\frac{\partial S_{n+1}}{\partial \Delta \mathbf{e}} = \frac{\partial S_{n+1}}{\partial \psi_c} \frac{\partial \psi_c}{\partial \Delta \mathbf{e}} + \frac{\partial S_{n+1}}{\partial \psi_{n+1}} \frac{\partial \psi_{n+1}}{\partial \Delta \mathbf{e}}. \quad (\text{C.72})$$

After simplification, it reduces to

$$\boxed{\frac{\partial S_{n+1}}{\partial \Delta \mathbf{e}} = 2b S_{n+1} \left(\frac{D_1}{\tan \psi_{n+1}} - \frac{C_1}{\tan \psi_c} \right) \boldsymbol{\xi}_c + 2b S_{n+1} \left(\frac{D_2}{\tan \psi_{n+1}} - \frac{C_2}{\tan \psi_c} \right) \Delta \mathbf{e}}. \quad (\text{C.73})$$

$\partial A_s / \partial \Delta \mathbf{e}$: By combining (5.8) and (5.12), parameter A_ξ can be written as

$$A_\xi = \left(\frac{\sin \psi_{n+1}}{\sin \psi_c} \right)^{2b+1}. \quad (\text{C.74})$$

Thus it follows that

$$A_s = \frac{2G}{(2G+h)(2b+1)} \left(\left(\frac{\sin \psi_{n+1}}{\sin \psi_c} \right)^{2b+1} - 1 \right), \quad (\text{C.75})$$

$$\frac{\partial A_s}{\partial \Delta \mathbf{e}} = \frac{\partial A_s}{\partial \psi_{n+1}} \frac{\partial \psi_{n+1}}{\partial \Delta \mathbf{e}} + \frac{\partial A_s}{\partial \psi_c} \frac{\partial \psi_c}{\partial \Delta \mathbf{e}}. \quad (\text{C.76})$$

Evaluating the derivative above leads the linear combination

$$\boxed{\frac{\partial A_s}{\partial \Delta \mathbf{e}} = A_1 \boldsymbol{\xi}_c + A_2 \Delta \mathbf{e}}, \quad (\text{C.77})$$

where

$$A_1 = \frac{2GA_\xi}{(2G+h)} \left(\frac{D_1}{\tan \psi_{n+1}} - \frac{C_1}{\tan \psi_c} \right), \quad A_2 = \frac{2GA_\xi}{(2G+h)} \left(\frac{D_2}{\tan \psi_{n+1}} - \frac{C_2}{\tan \psi_c} \right). \quad (\text{C.78})$$

$\partial B_s / \partial \Delta \mathbf{e}$: The derivative of parameter B_s is obtained as

$$\frac{\partial B_s}{\partial \Delta \mathbf{e}} = \frac{\partial B_s}{\partial B_\xi} \frac{\partial B_\xi}{\partial \Delta \mathbf{e}} = \frac{2G}{(2G+h)(1+2b)} \frac{\partial B_\xi}{\partial \Delta \mathbf{e}}, \quad (\text{C.79})$$

$$\frac{\partial B_s}{\partial \Delta \mathbf{e}} = \frac{2G}{(2G+h)(1+2b)} \frac{\partial}{\partial \Delta \mathbf{e}} \left(\frac{S}{(1-c)\|\Delta \mathbf{e}\|} \frac{\sin(\psi_c - \psi_{n+1})}{\sin \psi_c} \right), \quad (\text{C.80})$$

$$\frac{\partial B_s}{\partial \Delta \mathbf{e}} = \frac{\partial B_s}{\partial \psi_{n+1}} \frac{\partial \psi_{n+1}}{\partial \Delta \mathbf{e}} + \frac{\partial B_s}{\partial \psi_c} \frac{\partial \psi_c}{\partial \Delta \mathbf{e}} + \frac{\partial B_s}{\partial c} \frac{\partial c}{\partial \Delta \mathbf{e}} + \frac{\partial B_s}{\partial \|\Delta \mathbf{e}\|} \frac{\partial \|\Delta \mathbf{e}\|}{\partial \Delta \mathbf{e}} + \frac{\partial B_s}{\partial S} \frac{\partial S}{\partial \Delta \mathbf{e}}. \quad (\text{C.81})$$

The expression above reduces to

$$\boxed{\frac{\partial B_s}{\partial \Delta \mathbf{e}} = B_1 \boldsymbol{\xi}_c + B_2 \Delta \mathbf{e}}, \quad (\text{C.82})$$

where

$$B_1 = \frac{2GB_\xi}{(2G+h)(2b+1)(1-c)} \times \left(\frac{2bD_1}{\tan \psi_{n+1}} - \frac{D_1 - C_1}{\tan(\psi_c - \psi_{n+1})} - \frac{(2b+1)C_1}{\tan \psi_c} - \frac{c}{(1-c)\|\Delta \mathbf{e}\|S_c \cos \psi_c} \right), \quad (\text{C.83})$$

$$B_2 = \frac{2GB_\xi}{(2G+h)(2b+1)(1-c)} \times \left(\frac{2bD_2}{\tan \psi_{n+1}} - \frac{D_2 - C_2}{\tan(\psi_c - \psi_{n+1})} - \frac{(2b+1)C_2}{\tan \psi_c} - \frac{1}{\|\Delta \mathbf{e}\|^2} \right). \quad (\text{C.84})$$

$\partial \mathbf{s}_{n+1} / \partial \Delta \mathbf{e}$: In case of elastic-plastic transition, the stress update formula for the deviatoric stress is given by

$$\mathbf{s}_{n+1} = \mathbf{s}_c + A_s \boldsymbol{\xi}_c + B_s (1-c) \Delta \mathbf{e}. \quad (\text{C.85})$$

Consequently, the derivative of \mathbf{s}_{n+1} is calculated as

$$\begin{aligned} \frac{\partial \mathbf{s}_{n+1}}{\partial \Delta \mathbf{e}} &= \frac{\partial \mathbf{s}_{n+1}}{\partial \mathbf{s}_c} \frac{\partial \mathbf{s}_c}{\partial \Delta \mathbf{e}} + \frac{\partial \mathbf{s}_{n+1}}{\partial A_s} \otimes \frac{\partial A_s}{\partial \Delta \mathbf{e}} + \frac{\partial \mathbf{s}_{n+1}}{\partial \boldsymbol{\xi}_c} \frac{\partial \boldsymbol{\xi}_c}{\partial \Delta \mathbf{e}} + \frac{\partial \mathbf{s}_{n+1}}{\partial B_s} \otimes \frac{\partial B_s}{\partial \Delta \mathbf{e}} \\ &\quad + \frac{\partial \mathbf{s}_{n+1}}{\partial c} \otimes \frac{\partial c}{\partial \Delta \mathbf{e}} + \frac{\partial \mathbf{s}_{n+1}}{\partial \Delta \mathbf{e}} \frac{\partial \Delta \mathbf{e}}{\partial \Delta \mathbf{e}}, \end{aligned} \quad (\text{C.86})$$

where the identity $\partial \mathbf{s}_c / \partial \Delta \mathbf{e} = \partial \boldsymbol{\xi}_c / \partial \Delta \mathbf{e}$ can be applied, resulting the expression

$$\begin{aligned} \frac{\partial \mathbf{s}_{n+1}}{\partial \Delta \mathbf{e}} &= \boldsymbol{\xi}_c \otimes \frac{\partial A_s}{\partial \Delta \mathbf{e}} + (A_s + 1) \frac{\partial \boldsymbol{\xi}_c}{\partial \Delta \mathbf{e}} + (1 - c) \Delta \mathbf{e} \otimes \frac{\partial B_s}{\partial \Delta \mathbf{e}} \\ &\quad - B_s \Delta \mathbf{e} \otimes \frac{\partial c}{\partial \Delta \mathbf{e}} + B_s (1 - c) \mathcal{I}, \end{aligned} \quad (\text{C.87})$$

which can be simplified to

$$\boxed{\frac{\partial \mathbf{s}_{n+1}}{\partial \Delta \mathbf{e}} = a_1 \boldsymbol{\xi}_c \otimes \boldsymbol{\xi}_c + a_2 \boldsymbol{\xi}_c \otimes \Delta \mathbf{e} + a_3 \Delta \mathbf{e} \otimes \boldsymbol{\xi}_c + a_4 \Delta \mathbf{e} \otimes \Delta \mathbf{e} + a_5 \mathcal{I}}, \quad (\text{C.88})$$

where

$$a_1 = A_1, \quad a_2 = A_2, \quad a_3 = B_1 (1 - c) + c \frac{B_s - 2G(1 + A_s)}{S_c \|\Delta \mathbf{e}\| \cos \psi_c}, \quad (\text{C.89})$$

$$a_4 = B_2 (1 - c), \quad a_5 = B_s (1 - c) + 2Gc(1 + A_s). \quad (\text{C.90})$$

$\partial \mathbf{p}_{n+1} / \partial \Delta \boldsymbol{\varepsilon}$: Since the solution for the hydrostatic stress is obtained using elastic law, it is clearly follows that

$$\boxed{\frac{\partial \mathbf{p}_{n+1}}{\partial \Delta \boldsymbol{\varepsilon}} = K \boldsymbol{\delta} \otimes \boldsymbol{\delta}}. \quad (\text{C.91})$$

$\partial \boldsymbol{\sigma}_{n+1} / \partial \Delta \boldsymbol{\varepsilon}$: Combining (C.88) and (C.91), the consistent tensor can be obtained as

$$\mathcal{D}^{\text{cons}} = \frac{\partial \boldsymbol{\sigma}_{n+1}}{\partial \Delta \boldsymbol{\varepsilon}} = \frac{\partial \mathbf{s}_{n+1}}{\partial \Delta \boldsymbol{\varepsilon}} + \frac{\partial \mathbf{p}_{n+1}}{\partial \Delta \boldsymbol{\varepsilon}}, \quad (\text{C.92})$$

$$\boxed{\mathcal{D}^{\text{cons}} = a_1 \boldsymbol{\xi}_c \otimes \boldsymbol{\xi}_c + a_2 \boldsymbol{\xi}_c \otimes \Delta \mathbf{e} + a_3 \Delta \mathbf{e} \otimes \boldsymbol{\xi}_c + a_4 \Delta \mathbf{e} \otimes \Delta \mathbf{e} + a_5 \mathcal{T} + K \boldsymbol{\delta} \otimes \boldsymbol{\delta}}. \quad (\text{C.93})$$

C.5.2 Radial loading

When the increment produces radial loading, then the stress solution for the elastic-plastic transition case takes the form

$$\mathbf{s}_{n+1} = \mathbf{s}_c + \frac{2Gh(1-c)}{(2G+h)} \Delta \mathbf{e}. \quad (\text{C.94})$$

Using the identity $\partial \mathbf{s}_c / \partial \Delta \mathbf{e} = \partial \boldsymbol{\xi}_c / \partial \Delta \mathbf{e}$, the derivative of the updated deviatoric stress is obtained as

$$\frac{\partial \mathbf{s}_{n+1}}{\partial \Delta \boldsymbol{\varepsilon}} = \frac{\partial \mathbf{s}_{n+1}}{\partial \Delta \mathbf{e}} : \mathcal{T} = \frac{\partial \mathbf{s}_{n+1}}{\partial \mathbf{s}_c} \frac{\partial \mathbf{s}_c}{\partial \Delta \mathbf{e}} + \frac{\partial \mathbf{s}_{n+1}}{\partial c} \otimes \frac{\partial c}{\partial \Delta \mathbf{e}} + \frac{\partial \mathbf{s}_{n+1}}{\partial \Delta \mathbf{e}} \frac{\partial \Delta \mathbf{e}}{\partial \Delta \mathbf{e}}, \quad (\text{C.95})$$

$$\boxed{\frac{\partial \mathbf{s}_{n+1}}{\partial \Delta \boldsymbol{\varepsilon}} = \frac{2G(2Gc+h)}{2G+h} \mathcal{T} - \frac{4G^2c}{S_c \|\Delta \mathbf{e}\| (2G+h) \cos \psi_c} \Delta \mathbf{e} \otimes \boldsymbol{\xi}_c}. \quad (\text{C.96})$$

Then, by combining it with (C.91) we arrive at

$$\boxed{\mathcal{D}^{\text{cons}} = \frac{2G(2Gc+h)}{2G+h} \mathcal{T} - \frac{4G^2c}{S_c \|\Delta \mathbf{e}\| (2G+h) \cos \psi_c} \Delta \mathbf{e} \otimes \boldsymbol{\xi}_c + K \boldsymbol{\delta} \otimes \boldsymbol{\delta}. \quad (\text{C.97})$$

D

Detailed derivation steps for the Drucker–Prager model

D.1 Solution for $s(t)$ in strain-driven case

From (4.43) it follows that

$$dt = Jd\psi, \quad J = -\frac{S_n \cos^{2a-1} \left(\frac{\psi}{2} \right) \sin^{2b-1} \left(\frac{\psi}{2} \right)}{4G \|\dot{\mathbf{e}}\| \cos^{2a} \left(\frac{\psi_n}{2} \right) \sin^{2b} \left(\frac{\psi_n}{2} \right)}. \quad (\text{D.1})$$

The deviatoric strain rate (3.79) can be reformulated as

$$\dot{\mathbf{s}} = 2G\dot{\mathbf{e}} - \frac{2G^2 \|\dot{\mathbf{e}}\|}{\tilde{h}S} (\cos\psi + V) \mathbf{s}. \quad (\text{D.2})$$

According to (B.4) we can introduce that

$$a(\psi) = -\frac{2G^2 \|\dot{\mathbf{e}}\|}{\tilde{h}S} (\cos\psi + V), \quad b(\psi) = 2G. \quad (\text{D.3})$$

Consequently, parameter $A_s(\psi)$ is computed as

$$A_s(\psi) = \exp \left(\int_{\psi_n}^{\psi} a(\tilde{\psi}) J d\tilde{\psi} \right) = \exp \left(\frac{G}{\tilde{h}} \int_{\psi_n}^{\psi} \left(\frac{1}{\tan\tilde{\psi}} + V \frac{1}{\sin\tilde{\psi}} \right) d\tilde{\psi} \right) \quad (\text{D.4})$$

$$= \left(\frac{\cos \frac{\psi}{2}}{\cos \frac{\psi_n}{2}} \right)^{2a+1} \left(\frac{\sin \frac{\psi}{2}}{\sin \frac{\psi_n}{2}} \right)^{2b+1} = \frac{S}{S_n} \frac{\cos \frac{\psi}{2}}{\cos \frac{\psi_n}{2}} \frac{\sin \frac{\psi}{2}}{\sin \frac{\psi_n}{2}}, \quad (\text{D.5})$$

APPENDIX D. DETAILED DERIVATION STEPS FOR THE DRUCKER–PRAGER MODEL

$$A_s(\psi) = \frac{S \sin\psi}{S_n \sin\psi_n}. \quad (\text{D.6})$$

Similarly, parameter $B_s(\psi)$ is obtained as

$$B_s(\psi) = \int_{\psi_n}^{\psi} \exp\left(\int_{\hat{\psi}}^{\psi} a(\tilde{\psi}) J d\tilde{\psi}\right) b(\hat{\psi}) J d\hat{\psi}, \quad (\text{D.7})$$

$$B_s(\psi) = -\frac{S_n}{2\|\dot{\mathbf{e}}\|} \frac{\left(\cos\frac{\psi}{2}\right)^{2a+1} \left(\sin\frac{\psi}{2}\right)^{2b+1}}{\cos^{2a}\frac{\psi_n}{2} \sin^{2b}\frac{\psi_n}{2}} \int_{\psi_n}^{\psi} \frac{1}{\cos^2\frac{\hat{\psi}}{2} \sin^2\frac{\hat{\psi}}{2}} d\hat{\psi}, \quad (\text{D.8})$$

$$B_s(\psi) = \frac{S \sin(\psi_n - \psi)}{\|\dot{\mathbf{e}}\| \sin\psi_n}. \quad (\text{D.9})$$

Thus, it follows that $A_s = A_s(\psi)$ and $B_s = B_s(\psi)$ in (4.46).

D.2 Solution for $\mathbf{e}(t)$ in stress-driven case

From (4.111) it follows that

$$dt = J d\omega, \quad J = -\frac{S_n \sin\omega_n}{\|\dot{\mathbf{s}}\|} \frac{1}{\sin^2\omega}. \quad (\text{D.10})$$

Combining (4.79), (4.112) and (3.85) we can express \mathbf{s} in terms of the angle ω as

$$\mathbf{s} = \mathbf{s}_n + \frac{S_n \sin(\omega_n - \omega)}{\|\dot{\mathbf{s}}\| \sin\omega} \dot{\mathbf{s}}. \quad (\text{D.11})$$

Inserting (D.11) and (4.110) into (3.85), the deviatoric strain rate can be written in the form

$$\begin{aligned} \dot{\mathbf{e}} &= \frac{1}{2G} \dot{\mathbf{s}} + \frac{\|\dot{\mathbf{s}}\| \cos\omega \sin\omega}{2S_n j \sin\omega_n} \mathbf{s}_n + \frac{1}{2j} \frac{\sin(\omega_n - \omega) \cos\omega}{\sin\omega_n} \dot{\mathbf{s}} \\ &+ \frac{\alpha \text{tr} \dot{\boldsymbol{\sigma}} \sin\omega}{\sqrt{2} j S_n \sin\omega_n} \mathbf{s}_n + \frac{\alpha \text{tr} \dot{\boldsymbol{\sigma}}}{\sqrt{2} j \|\dot{\mathbf{s}}\|} \frac{\sin(\omega_n - \omega)}{\sin\omega_n} \dot{\mathbf{s}}. \end{aligned} \quad (\text{D.12})$$

Integrating both sides, using (D.10), yields

$$\mathbf{e} - \mathbf{e}_n = A_e \mathbf{s}_n + B_e \dot{\mathbf{s}}, \quad (\text{D.13})$$

where the parameters A_e and B_e , after simplification, become

$$A_e = \frac{1}{2j} \ln\left(\frac{S}{S_n}\right) + \frac{\alpha \text{tr} \dot{\boldsymbol{\sigma}}}{\sqrt{2} j \|\dot{\mathbf{s}}\|} \ln\left(\frac{\tan\frac{\omega_n}{2}}{\tan\frac{\omega}{2}}\right), \quad (\text{D.14})$$

$$B_e = \frac{(t - t_n)}{2} \left(\frac{1}{G} + \frac{1}{j}\right) + \frac{\alpha \text{tr} \dot{\boldsymbol{\sigma}} (S - S_n)}{\sqrt{2} j \|\dot{\mathbf{s}}\|^2} - \frac{S_n \sin\omega_n}{\|\dot{\mathbf{s}}\|} \left(\frac{A_e}{\tan\omega_n} + \frac{\omega_n - \omega}{2j}\right). \quad (\text{D.15})$$

Thus, it follows that $A_e = A_e(\omega)$ and $B_e = B_e(\omega)$ in (4.113).

D.3 Solution for $\text{tr}\boldsymbol{\varepsilon}(t)$ in stress-driven case

Inserting (4.104) and (4.107) into expression (3.86) results in the differential equation

$$\frac{1}{3}\text{tr}\dot{\boldsymbol{\varepsilon}} = \left(\frac{1}{9K} + \frac{\alpha\beta}{j} \right) \text{tr}\dot{\boldsymbol{\sigma}} + \frac{\beta}{\sqrt{2}j}\dot{S}, \quad (\text{D.16})$$

which can be simply integrated yielding the solution

$$\frac{1}{3}\text{tr}\boldsymbol{\varepsilon} - \frac{1}{3}\text{tr}\boldsymbol{\varepsilon}_n = \left(\frac{1}{9K} + \frac{\alpha\beta}{j} \right) \text{tr}\boldsymbol{\sigma} (t - t_n) + \frac{\beta(S - S_n)}{\sqrt{2}j}. \quad (\text{D.17})$$

D.4 Consistent elastoplastic tangent tensor

D.4.1 General case

This appendix presents the main derivation steps of the construction of the consistent tangent tensor for general loading case, when the apex has not been reached. For this reason, the derivatives of all parameters appearing in the stress update formulae have to be evaluated with respect to the strain increment. These are presented in the following.

$\partial V/\partial\Delta\boldsymbol{\varepsilon}$: The derivative of the parameter V with respect to $\Delta\boldsymbol{\varepsilon}$ is computed as

$$\frac{\partial V}{\partial\Delta\boldsymbol{\varepsilon}} = \frac{\partial V}{\partial(\text{tr}\Delta\boldsymbol{\varepsilon})}\boldsymbol{\delta} + \frac{\partial V}{\partial\|\Delta\boldsymbol{e}\|}\frac{\Delta\boldsymbol{e}}{\|\Delta\boldsymbol{e}\|} = \frac{3K\alpha}{\sqrt{2}G\|\Delta\boldsymbol{e}\|}\boldsymbol{\delta} - \frac{3K\alpha\text{tr}\Delta\boldsymbol{\varepsilon}}{\sqrt{2}G\|\Delta\boldsymbol{e}\|^3}\Delta\boldsymbol{e}, \quad (\text{D.18})$$

which can be simplified by substituting V back into the expression above:

$$\boxed{\frac{\partial V}{\partial\Delta\boldsymbol{\varepsilon}} = \frac{V}{\text{tr}\Delta\boldsymbol{\varepsilon}}\boldsymbol{\delta} - \frac{V}{\|\Delta\boldsymbol{e}\|^2}\Delta\boldsymbol{e}}. \quad (\text{D.19})$$

$\partial a/\partial\Delta\boldsymbol{\varepsilon}$ and $\partial b/\partial\Delta\boldsymbol{\varepsilon}$: The derivatives of parameter a and b with respect to $\Delta\boldsymbol{\varepsilon}$ are given by

$$\frac{\partial a}{\partial\Delta\boldsymbol{\varepsilon}} = \frac{\partial a}{\partial V}\frac{\partial V}{\partial\Delta\boldsymbol{\varepsilon}} = -\frac{G}{2\tilde{h}}V\left(\frac{1}{\text{tr}\Delta\boldsymbol{\varepsilon}}\boldsymbol{\delta} - \frac{1}{\|\Delta\boldsymbol{e}\|^2}\Delta\boldsymbol{e}\right), \quad (\text{D.20})$$

$$\boxed{\frac{\partial a}{\partial\Delta\boldsymbol{\varepsilon}} = \frac{a-b}{2}\left(\frac{1}{\text{tr}\Delta\boldsymbol{\varepsilon}}\boldsymbol{\delta} - \frac{1}{\|\Delta\boldsymbol{e}\|^2}\Delta\boldsymbol{e}\right)}, \quad (\text{D.21})$$

$$\frac{\partial b}{\partial\Delta\boldsymbol{\varepsilon}} = \frac{\partial b}{\partial V}\frac{\partial V}{\partial\Delta\boldsymbol{\varepsilon}} = \frac{G}{2\tilde{h}}V\left(\frac{1}{\text{tr}\Delta\boldsymbol{\varepsilon}}\boldsymbol{\delta} - \frac{1}{\|\Delta\boldsymbol{e}\|^2}\Delta\boldsymbol{e}\right), \quad (\text{D.22})$$

$$\boxed{\frac{\partial b}{\partial\Delta\boldsymbol{\varepsilon}} = \frac{b-a}{2}\left(\frac{1}{\text{tr}\Delta\boldsymbol{\varepsilon}}\boldsymbol{\delta} - \frac{1}{\|\Delta\boldsymbol{e}\|^2}\Delta\boldsymbol{e}\right)}. \quad (\text{D.23})$$

$\partial c/\partial\Delta\boldsymbol{\varepsilon}$: The yield function written at the contact point is given by

$$F_c = \frac{1}{\sqrt{2}}S_c + 3\alpha p_c - k_n = 0 \quad (\text{D.24})$$

APPENDIX D. DETAILED DERIVATION STEPS FOR THE DRUCKER–PRAGER MODEL

with

$$\mathbf{s}_c = \mathbf{s}_n + 2Gc\Delta\mathbf{e} \quad \text{and} \quad p_c = p_n + K\text{ctr}\Delta\boldsymbol{\varepsilon}. \quad (\text{D.25})$$

The derivatives of \mathbf{s}_c and p_c with respect to $\Delta\boldsymbol{\varepsilon}$ is calculated as

$$\frac{\partial \mathbf{s}_c}{\partial \Delta\boldsymbol{\varepsilon}} = \frac{\partial \mathbf{s}_c}{\partial \Delta\mathbf{e}} \frac{\partial \Delta\mathbf{e}}{\partial \Delta\boldsymbol{\varepsilon}} + \frac{\partial \mathbf{s}_c}{\partial c} \otimes \frac{\partial c}{\partial \Delta\boldsymbol{\varepsilon}} = 2Gc\boldsymbol{\mathcal{T}} + 2G\Delta\mathbf{e} \otimes \frac{\partial c}{\partial \Delta\boldsymbol{\varepsilon}} \quad (\text{D.26})$$

and

$$\frac{\partial p_c}{\partial \Delta\boldsymbol{\varepsilon}} = \frac{\partial p_c}{\partial (\text{tr}\Delta\boldsymbol{\varepsilon})} \frac{\partial (\text{tr}\Delta\boldsymbol{\varepsilon})}{\partial \Delta\boldsymbol{\varepsilon}} + \frac{\partial p_c}{\partial c} \frac{\partial c}{\partial \Delta\boldsymbol{\varepsilon}} = Kc\boldsymbol{\delta} + K\text{tr}\Delta\boldsymbol{\varepsilon} \frac{\partial c}{\partial \Delta\boldsymbol{\varepsilon}}. \quad (\text{D.27})$$

The derivative $\partial c/\partial \Delta\boldsymbol{\varepsilon}$ can be obtained if we rewrite the yield function in the form

$$\frac{1}{\sqrt{2}}S_c + 3\alpha p_c = k_n. \quad (\text{D.28})$$

Then, taking the derivatives of both sides with respect to $\Delta\boldsymbol{\varepsilon}$ gives

$$\frac{\partial}{\partial \Delta\boldsymbol{\varepsilon}} \left(\frac{1}{\sqrt{2}}S_c + 3\alpha p_c \right) = \frac{\partial k_n}{\partial \Delta\boldsymbol{\varepsilon}}, \quad (\text{D.29})$$

$$\frac{1}{\sqrt{2}} \frac{\partial S_c}{\partial \Delta\boldsymbol{\varepsilon}} + 3\alpha \frac{\partial p_c}{\partial \Delta\boldsymbol{\varepsilon}} = \mathbf{0}, \quad \implies \quad \frac{\partial p_c}{\partial \Delta\boldsymbol{\varepsilon}} = -\frac{1}{3\sqrt{2}\alpha} \frac{\partial S_c}{\partial \Delta\boldsymbol{\varepsilon}}. \quad (\text{D.30})$$

Extracting (D.29) gives

$$\frac{1}{\sqrt{2}} \frac{\partial S_c}{\partial \mathbf{s}_c} : \frac{\partial \mathbf{s}_c}{\partial \Delta\boldsymbol{\varepsilon}} + 3\alpha \frac{\partial p_c}{\partial \Delta\boldsymbol{\varepsilon}} = \mathbf{0}, \quad (\text{D.31})$$

$$\frac{1}{\sqrt{2}} \frac{\mathbf{s}_c}{S_c} : \left(2Gc\boldsymbol{\mathcal{T}} + 2G\Delta\mathbf{e} \otimes \frac{\partial c}{\partial \Delta\boldsymbol{\varepsilon}} \right) + 3\alpha \left(Kc\boldsymbol{\delta} + K\text{tr}\Delta\boldsymbol{\varepsilon} \frac{\partial c}{\partial \Delta\boldsymbol{\varepsilon}} \right) = \mathbf{0}, \quad (\text{D.32})$$

$$\left(\frac{\mathbf{s}_c : \Delta\mathbf{e}}{S_c} + V \|\Delta\mathbf{e}\| \right) \frac{\partial c}{\partial \Delta\boldsymbol{\varepsilon}} = -c \left(\frac{1}{S_c} \mathbf{s}_c + \frac{V \|\Delta\mathbf{e}\|}{\text{tr}\Delta\boldsymbol{\varepsilon}} \boldsymbol{\delta} \right). \quad (\text{D.33})$$

Therefore, we arrive at the expression

$$\frac{\partial c}{\partial \Delta\boldsymbol{\varepsilon}} = -\frac{c}{S_c \|\Delta\mathbf{e}\| (\cos\psi_c + V)} \mathbf{s}_c - \frac{cV}{\text{tr}\Delta\boldsymbol{\varepsilon} (\cos\psi_c + V)} \boldsymbol{\delta}, \quad (\text{D.34})$$

$$\boxed{\frac{\partial c}{\partial \Delta\boldsymbol{\varepsilon}} = -\frac{c}{(\cos\psi_c + V)} \left(\frac{1}{S_c \|\Delta\mathbf{e}\|} \mathbf{s}_c + \frac{V}{\text{tr}\Delta\boldsymbol{\varepsilon}} \boldsymbol{\delta} \right)}. \quad (\text{D.35})$$

$\partial S_c/\partial \Delta\boldsymbol{\varepsilon}$: Using (D.26) and (D.34) we can write that

$$\frac{\partial \mathbf{s}_c}{\partial \Delta\boldsymbol{\varepsilon}} = 2Gc\boldsymbol{\mathcal{T}} - \frac{2Gc}{S_c \|\Delta\mathbf{e}\| (\cos\psi_c + V)} \Delta\mathbf{e} \otimes \mathbf{s}_c - \frac{2GcV}{\text{tr}\Delta\boldsymbol{\varepsilon} (\cos\psi_c + V)} \Delta\mathbf{e} \otimes \boldsymbol{\delta} \quad (\text{D.36})$$

and

$$\frac{\partial S_c}{\partial \Delta\boldsymbol{\varepsilon}} = \frac{\partial S_c}{\partial \mathbf{s}_c} : \frac{\partial \mathbf{s}_c}{\partial \Delta\boldsymbol{\varepsilon}} = \frac{\mathbf{s}_c}{S_c} : \frac{\partial \mathbf{s}_c}{\partial \Delta\boldsymbol{\varepsilon}}. \quad (\text{D.37})$$

Combining the two equations above, the derivative of S_c can be expressed as

$$\boxed{\frac{\partial S_c}{\partial \Delta \boldsymbol{\varepsilon}} = \frac{2GcV}{(\cos\psi_c + V)} \left(\frac{1}{S_c} \mathbf{s}_c - \frac{\|\Delta \mathbf{e}\| \cos\psi_c}{\text{tr}\Delta \boldsymbol{\varepsilon}} \boldsymbol{\delta} \right)}. \quad (\text{D.38})$$

$\partial p_c / \partial \Delta \boldsymbol{\varepsilon}$: Combining (D.30)₂ and (D.38) we arrive at the expression

$$\boxed{\frac{\partial p_c}{\partial \Delta \boldsymbol{\varepsilon}} = -\frac{Kc}{\cos\psi_c + V} \left(\frac{\text{tr}\Delta \boldsymbol{\varepsilon}}{S_c \|\Delta \mathbf{e}\|} \mathbf{s}_c - \cos\psi_c \boldsymbol{\delta} \right)}. \quad (\text{D.39})$$

$\partial \psi_c / \partial \Delta \boldsymbol{\varepsilon}$: The derivative of $\cos\psi_c$ with respect to $\Delta \boldsymbol{\varepsilon}$ is computed by

$$\begin{aligned} \frac{\partial \cos\psi_c}{\partial \Delta \boldsymbol{\varepsilon}} &= \frac{\partial \left(\frac{\mathbf{s}_c : \Delta \mathbf{e}}{S_c \|\Delta \mathbf{e}\|} \right)}{\partial \mathbf{s}_c} : \frac{\partial \mathbf{s}_c}{\partial \Delta \boldsymbol{\varepsilon}} + \frac{\partial \left(\frac{\mathbf{s}_c : \Delta \mathbf{e}}{S_c \|\Delta \mathbf{e}\|} \right)}{\partial S_c} \frac{\partial S_c}{\partial \Delta \boldsymbol{\varepsilon}} \\ &\quad + \frac{\partial \left(\frac{\mathbf{s}_c : \Delta \mathbf{e}}{S_c \|\Delta \mathbf{e}\|} \right)}{\partial \Delta \mathbf{e}} : \frac{\partial \Delta \mathbf{e}}{\partial \Delta \boldsymbol{\varepsilon}} + \frac{\partial \left(\frac{\mathbf{s}_c : \Delta \mathbf{e}}{S_c \|\Delta \mathbf{e}\|} \right)}{\partial \|\Delta \mathbf{e}\|} \frac{\partial \|\Delta \mathbf{e}\|}{\partial \Delta \boldsymbol{\varepsilon}}. \end{aligned} \quad (\text{D.40})$$

Using this result, the quantity $\partial \psi_c / \partial \Delta \boldsymbol{\varepsilon}$ can be expressed with the linear combination

$$\boxed{\frac{\partial \psi_c}{\partial \Delta \boldsymbol{\varepsilon}} = C_1 \mathbf{s}_c + C_2 \Delta \mathbf{e} + C_3 \boldsymbol{\delta}}, \quad (\text{D.41})$$

where the following parameters are introduced:

$$C_1 = \frac{2Gc(1 + V \cos\psi_c)}{S_c^2 \sin\psi_c (\cos\psi_c + V)} - \frac{1}{S_c \sin\psi_c \|\Delta \mathbf{e}\|}, \quad (\text{D.42})$$

$$C_2 = \frac{S_c \cos\psi_c - 2Gc \|\Delta \mathbf{e}\|}{S_c \sin\psi_c \|\Delta \mathbf{e}\|^2}, \quad (\text{D.43})$$

$$C_3 = \frac{2GcV \|\Delta \mathbf{e}\| \sin^2\psi_c}{S_c \text{tr}\Delta \boldsymbol{\varepsilon} \sin\psi_c (\cos\psi_c + V)}. \quad (\text{D.44})$$

$\partial \psi_{n+1} / \partial \Delta \boldsymbol{\varepsilon}$: For simplifying the presentation, the following parameters are introduced:

$$\tilde{\alpha}_c = \frac{\partial B \left(\cos^2 \frac{\psi_c}{2}, a, b \right)}{\partial a}, \quad \tilde{\alpha}_{n+1} = \frac{\partial B \left(\cos^2 \frac{\psi_{n+1}}{2}, a, b \right)}{\partial a}, \quad (\text{D.45})$$

$$\tilde{\beta}_c = \frac{\partial B \left(\cos^2 \frac{\psi_c}{2}, a, b \right)}{\partial b}, \quad \tilde{\beta}_{n+1} = \frac{\partial B \left(\cos^2 \frac{\psi_{n+1}}{2}, a, b \right)}{\partial b}. \quad (\text{D.46})$$

They can be computed according to the formulae (A.15) and (A.16), respectively. Therefore, these parameters are calculated as

$$\begin{aligned}\tilde{\alpha}_c &= B\left(\cos^2\frac{\psi_c}{2}, a, b\right) \ln\left(\cos^2\frac{\psi_c}{2}\right) \\ &\quad - \frac{\cos^{2a}\frac{\psi_c}{2}}{a^2} {}_3F_2\left(a, a, 1-b; a+1, a+1; \cos^2\frac{\psi_c}{2}\right),\end{aligned}\tag{D.47}$$

$$\begin{aligned}\tilde{\alpha}_{n+1} &= B\left(\cos^2\frac{\psi_{n+1}}{2}, a, b\right) \ln\left(\cos^2\frac{\psi_{n+1}}{2}\right) \\ &\quad - \frac{\cos^{2a}\frac{\psi_{n+1}}{2}}{a^2} {}_3F_2\left(a, a, 1-b; a+1, a+1; \cos^2\frac{\psi_{n+1}}{2}\right),\end{aligned}\tag{D.48}$$

$$\begin{aligned}\tilde{\beta}_c &= \frac{\sin^{2b}\frac{\psi_c}{2}}{b^2} {}_3F_2\left(1-a, b, b; 1+b, 1+b; \sin^2\frac{\psi_c}{2}\right) \\ &\quad - B\left(\sin^2\frac{\psi_c}{2}, b, a\right) \ln\left(\sin^2\frac{\psi_c}{2}\right) + B(a, b) (\Psi(b) - \Psi(a+b)),\end{aligned}\tag{D.49}$$

$$\begin{aligned}\tilde{\beta}_{n+1} &= \frac{\sin^{2b}\frac{\psi_{n+1}}{2}}{b^2} {}_3F_2\left(1-a, b, b; 1+b, 1+b; \sin^2\frac{\psi_{n+1}}{2}\right) \\ &\quad - B\left(\sin^2\frac{\psi_{n+1}}{2}, b, a\right) \ln\left(\sin^2\frac{\psi_{n+1}}{2}\right) + B(a, b) (\Psi(b) - \Psi(a+b)).\end{aligned}\tag{D.50}$$

The discretized form of the expression defining the final angle ψ_{n+1} , when elastic-plastic transition occurs, is given by

$$B\left(\cos^2\frac{\psi_{n+1}}{2}, a, b\right) - B\left(\cos^2\frac{\psi_c}{2}, a, b\right) = \frac{4G(1-c)\|\Delta\mathbf{e}\|}{S_c \cos^{-2a}\left(\frac{\psi_c}{2}\right) \sin^{-2b}\left(\frac{\psi_c}{2}\right)}.\tag{D.51}$$

The derivatives of all the parameters appearing in this equation have been already obtained, except the derivative of the final angle ψ_{n+1} . Consequently, by taking the derivative of both sides, the derivative $\partial\psi_{n+1}/\partial\Delta\boldsymbol{\varepsilon}$ can be expressed. After simplification it reduces to the form

$$\boxed{\frac{\partial\psi_{n+1}}{\partial\Delta\boldsymbol{\varepsilon}} = D_1\mathbf{s}_c + D_2\Delta\mathbf{e} + D_3\boldsymbol{\delta}},\tag{D.52}$$

where

$$D_1 = \frac{C_1}{k_1} + \frac{k_4}{S_c} - \frac{k_5}{S_c},\tag{D.53}$$

$$D_2 = \frac{C_2}{k_1} - \frac{k_2}{\|\Delta\mathbf{e}\|} + \frac{k_3}{\|\Delta\mathbf{e}\|} - \frac{2G(1-c)\sin\psi_{n+1}}{S_{n+1}\|\Delta\mathbf{e}\|},\tag{D.54}$$

$$D_3 = \frac{C_3}{k_1} + \frac{k_2\|\Delta\mathbf{e}\|}{\text{tr}\Delta\boldsymbol{\varepsilon}} - \frac{k_3\|\Delta\mathbf{e}\|}{\text{tr}\Delta\boldsymbol{\varepsilon}} - \frac{k_4\|\Delta\mathbf{e}\|\cos\psi_c}{\text{tr}\Delta\boldsymbol{\varepsilon}} - \frac{k_5\|\Delta\mathbf{e}\|V}{\text{tr}\Delta\boldsymbol{\varepsilon}}\tag{D.55}$$

and

$$k_1 = \frac{S_{n+1} \sin \psi_c}{\sin \psi_{n+1} (2G \|\Delta \mathbf{e}\| (1-c) (a-b - (a+b) \cos \psi_c) + S_c)}, \quad (\text{D.56})$$

$$k_2 = \frac{2G (1-c) \sin \psi_{n+1}}{S_{n+1}} (a-b) \ln \left(\tan \frac{\psi_c}{2} \right), \quad (\text{D.57})$$

$$k_3 = \frac{\sin \psi_{n+1} (b-a) (\tilde{\alpha}_{n+1} - \tilde{\alpha}_c - \tilde{\beta}_{n+1} + \tilde{\beta}_c)}{4 \|\Delta \mathbf{e}\| \cos^2 a \left(\frac{\psi_{n+1}}{2} \right) \sin^{2b} \left(\frac{\psi_{n+1}}{2} \right)}, \quad (\text{D.58})$$

$$k_4 = \frac{4G^2 c (1-c) V \|\Delta \mathbf{e}\| \sin \psi_{n+1}}{S_{n+1} S_c (V + \cos \psi_c)}, \quad (\text{D.59})$$

$$k_5 = \frac{2G c \sin \psi_{n+1}}{S_{n+1} (V + \cos \psi_c)}. \quad (\text{D.60})$$

$\partial S_{n+1} / \partial \Delta \boldsymbol{\varepsilon}$: The derivative of the norm of the deviatoric stress at the end of the increment is obtained, using (5.22), as

$$\boxed{\frac{\partial S_{n+1}}{\partial \Delta \boldsymbol{\varepsilon}} = R_1 \mathbf{s}_c + R_2 \Delta \mathbf{e} + R_3 \boldsymbol{\delta}}, \quad (\text{D.61})$$

where

$$R_1 = D_1 n_1 + C_1 n_2 + \frac{2GcV S_{n+1}}{S_c^2 (V + \cos \psi_c)}, \quad (\text{D.62})$$

$$R_2 = D_2 n_1 + C_2 n_2 - \frac{n_3}{\|\Delta \mathbf{e}\|^2}, \quad (\text{D.63})$$

$$R_3 = D_3 n_1 + C_3 n_2 + \frac{n_3}{\text{tr} \Delta \boldsymbol{\varepsilon}} - \frac{2G \|\Delta \mathbf{e}\| c V S_{n+1} \cos \psi_c}{S_c \text{tr} \Delta \boldsymbol{\varepsilon} (V + \cos \psi_c)} \quad (\text{D.64})$$

and

$$n_1 = S_{n+1} \frac{b-a + (a+b) \cos \psi_{n+1}}{\sin \psi_{n+1}}, \quad (\text{D.65})$$

$$n_2 = S_{n+1} \left(a \tan \frac{\psi_c}{2} - \frac{b}{\tan \frac{\psi_c}{2}} \right), \quad (\text{D.66})$$

$$n_3 = S_{n+1} (a-b) \ln \left(\frac{\tan \frac{\psi_c}{2}}{\tan \frac{\psi_{n+1}}{2}} \right). \quad (\text{D.67})$$

$\partial A_s / \partial \Delta \boldsymbol{\varepsilon}$: The parameter A_s for the case, when elastic-plastic transition occurs is calculated by

$$A_s = \frac{S_{n+1} \sin \psi_{n+1}}{S_c \sin \psi_c}. \quad (\text{D.68})$$

APPENDIX D. DETAILED DERIVATION STEPS FOR THE DRUCKER–PRAGER MODEL

Its derivative is obtained using the chain rule:

$$\frac{\partial A_s}{\partial \Delta \boldsymbol{\varepsilon}} = \frac{\partial A_s}{\partial \psi_{n+1}} \frac{\partial \psi_{n+1}}{\partial \Delta \boldsymbol{\varepsilon}} + \frac{\partial A_s}{\partial \psi_c} \frac{\partial \psi_c}{\partial \Delta \boldsymbol{\varepsilon}} + \frac{\partial A_s}{\partial S_{n+1}} \frac{\partial S_{n+1}}{\partial \Delta \boldsymbol{\varepsilon}} + \frac{\partial A_s}{\partial S_c} \frac{\partial S_c}{\partial \Delta \boldsymbol{\varepsilon}}. \quad (\text{D.69})$$

After some straightforward manipulation, we arrive at the expression

$$\boxed{\frac{\partial A_s}{\partial \Delta \boldsymbol{\varepsilon}} = A_1 \mathbf{s}_c + A_2 \Delta \mathbf{e} + A_3 \boldsymbol{\delta}}, \quad (\text{D.70})$$

where

$$A_1 = \frac{R_1}{m_1} - \frac{C_1}{m_2} + \frac{D_1}{m_3} - \frac{m_4}{S_c}, \quad (\text{D.71})$$

$$A_2 = \frac{R_2}{m_1} - \frac{C_2}{m_2} + \frac{D_2}{m_3}, \quad (\text{D.72})$$

$$A_3 = \frac{R_3}{m_1} - \frac{C_3}{m_2} + \frac{D_3}{m_3} - \frac{m_4 \|\Delta \mathbf{e}\| \cos \psi_c}{\text{tr} \Delta \boldsymbol{\varepsilon}} \quad (\text{D.73})$$

and

$$m_1 = \frac{S_{n+1}}{A_s}, \quad m_2 = \frac{\tan \psi_c}{A_s}, \quad m_3 = \frac{S_c \sin \psi_c}{S_{n+1} \cos \psi_{n+1}}, \quad m_4 = \frac{2GcVA_s}{S_c(V + \cos \psi_c)}. \quad (\text{D.74})$$

$\partial B_s / \partial \Delta \boldsymbol{\varepsilon}$: The parameter B_s is computed as

$$B_s = \frac{S_{n+1}}{(1-c)\|\Delta \mathbf{e}\|} \frac{\sin(\psi_c - \psi_{n+1})}{\sin \psi_c}. \quad (\text{D.75})$$

Its derivative can be obtained using the chain rule:

$$\frac{\partial B_s}{\partial \Delta \boldsymbol{\varepsilon}} = \frac{\partial B_s}{\partial \psi_{n+1}} \frac{\partial \psi_{n+1}}{\partial \Delta \boldsymbol{\varepsilon}} + \frac{\partial B_s}{\partial \psi_c} \frac{\partial \psi_c}{\partial \Delta \boldsymbol{\varepsilon}} + \frac{\partial B_s}{\partial S_{n+1}} \frac{\partial S_{n+1}}{\partial \Delta \boldsymbol{\varepsilon}} + \frac{\partial B_s}{\partial \|\Delta \mathbf{e}\|} \frac{\partial \|\Delta \mathbf{e}\|}{\partial \Delta \boldsymbol{\varepsilon}} + \frac{\partial B_s}{\partial c} \frac{\partial c}{\partial \Delta \boldsymbol{\varepsilon}}. \quad (\text{D.76})$$

After simplification, the derivative of parameter B_s with respect to the strain increment is written as

$$\boxed{\frac{\partial B_s}{\partial \Delta \boldsymbol{\varepsilon}} = B_1 \mathbf{s}_c + B_2 \Delta \mathbf{e} + B_3 \boldsymbol{\delta}}, \quad (\text{D.77})$$

where

$$B_1 = \frac{R_1}{m_5} + \frac{D_1}{m_6} + \frac{C_1}{m_7}, \quad (\text{D.78})$$

$$B_2 = \frac{R_2}{m_5} + \frac{D_2}{m_6} + \frac{C_2}{m_7} - \frac{B_s}{\|\Delta \mathbf{e}\|^2}, \quad (\text{D.79})$$

$$B_3 = \frac{R_3}{m_5} + \frac{D_3}{m_6} + \frac{C_3}{m_7} \quad (\text{D.80})$$

and

$$m_5 = \frac{S_{n+1}}{B_s}, \quad m_6 = \frac{\tan(\psi_{n+1} - \psi_c)}{B_s}, \quad m_7 = \frac{(1-c)\|\Delta \mathbf{e}\| \sin^2 \psi_c}{S_{n+1} \sin \psi_{n+1}}. \quad (\text{D.81})$$

$\partial \mathbf{s}_{n+1} / \partial \Delta \boldsymbol{\varepsilon}$: The stress update formula for the deviatoric stress is given by

$$\mathbf{s}_{n+1} = A_s \mathbf{s}_c + B_s (1 - c) \Delta \mathbf{e}. \quad (\text{D.82})$$

Applying the chain rule, its derivative can be obtained:

$$\frac{\partial \mathbf{s}_{n+1}}{\partial \Delta \boldsymbol{\varepsilon}} = \frac{\partial \mathbf{s}_{n+1}}{\partial A_s} \otimes \frac{\partial A_s}{\partial \Delta \boldsymbol{\varepsilon}} + \frac{\partial \mathbf{s}_{n+1}}{\partial \mathbf{s}_c} \frac{\partial \mathbf{s}_c}{\partial \Delta \boldsymbol{\varepsilon}} + \frac{\partial \mathbf{s}_{n+1}}{\partial B_s} \otimes \frac{\partial B_s}{\partial \Delta \boldsymbol{\varepsilon}} + \frac{\partial \mathbf{s}_{n+1}}{\partial c} \otimes \frac{\partial c}{\partial \Delta \boldsymbol{\varepsilon}} + \frac{\partial \mathbf{s}_{n+1}}{\partial \Delta \mathbf{e}} \frac{\partial \Delta \mathbf{e}}{\partial \Delta \boldsymbol{\varepsilon}}, \quad (\text{D.83})$$

$$\begin{aligned} \frac{\partial \mathbf{s}_{n+1}}{\partial \Delta \boldsymbol{\varepsilon}} &= \mathbf{s}_c \otimes (A_1 \mathbf{s}_c + A_2 \Delta \mathbf{e} + A_3 \boldsymbol{\delta}) \\ &+ A_s \left(2Gc \mathcal{T} - \frac{2Gc \Delta \mathbf{e} \otimes \mathbf{s}_c}{S_c \|\Delta \mathbf{e}\| (\cos \psi_c + V)} - \frac{2GcV \Delta \mathbf{e} \otimes \boldsymbol{\delta}}{\text{tr} \Delta \boldsymbol{\varepsilon} (\cos \psi_c + V)} \right) \\ &+ (1 - c) \Delta \mathbf{e} \otimes (B_1 \mathbf{s}_c + B_2 \Delta \mathbf{e} + B_3 \boldsymbol{\delta}) \\ &+ B_s \Delta \mathbf{e} \otimes \left(\frac{c}{S_c \|\Delta \mathbf{e}\| (\cos \psi_c + V)} \mathbf{s}_c + \frac{cV}{\text{tr} \Delta \boldsymbol{\varepsilon} (\cos \psi_c + V)} \boldsymbol{\delta} \right) \\ &+ B_s (1 - c) \mathcal{T}. \end{aligned} \quad (\text{D.84})$$

$\partial p_{n+1} / \partial \Delta \boldsymbol{\varepsilon}$: The hydrostatic stress at the end of the increment is calculated as

$$p_{n+1} = p_c + (1 - c) K \left(1 - \frac{9K\alpha\beta}{\tilde{h} - G} \right) \text{tr} \Delta \boldsymbol{\varepsilon} - \frac{3\sqrt{2}\beta K}{2(\tilde{h} - G)} (S_{n+1} - S_c). \quad (\text{D.85})$$

Its derivative can be evaluated using the chain rule:

$$\begin{aligned} \frac{\partial p_{n+1}}{\partial \Delta \boldsymbol{\varepsilon}} &= \frac{\partial p_{n+1}}{\partial p_c} \frac{\partial p_c}{\partial \Delta \boldsymbol{\varepsilon}} + \frac{\partial p_{n+1}}{\partial c} \frac{\partial c}{\partial \Delta \boldsymbol{\varepsilon}} + \frac{\partial p_{n+1}}{\partial \text{tr} \Delta \boldsymbol{\varepsilon}} \frac{\partial \text{tr} \Delta \boldsymbol{\varepsilon}}{\partial \Delta \boldsymbol{\varepsilon}} \\ &+ \frac{\partial p_{n+1}}{\partial S_{n+1}} \frac{\partial S_{n+1}}{\partial \Delta \boldsymbol{\varepsilon}} + \frac{\partial p_{n+1}}{\partial S_c} \frac{\partial S_c}{\partial \Delta \boldsymbol{\varepsilon}}. \end{aligned} \quad (\text{D.86})$$

Finally, we arrive at the expression

$$\boxed{\frac{\partial p_{n+1}}{\partial \Delta \boldsymbol{\varepsilon}} = Q_1 \mathbf{s}_c + Q_2 \Delta \mathbf{e} + Q_3 \boldsymbol{\delta}}, \quad (\text{D.87})$$

where

$$Q_1 = \frac{R_1}{m_8}, \quad Q_2 = \frac{R_2}{m_8}, \quad Q_3 = \frac{R_3}{m_8} + K \left(1 - \frac{9K\alpha\beta}{\tilde{h} - G} \right), \quad m_8 = \frac{\sqrt{2}(G - \tilde{h})}{3K\beta}. \quad (\text{D.88})$$

Consequently, the derivative of the updated hydrostatic stress tensor is computed as

$$\frac{\partial \mathbf{p}_{n+1}}{\partial \Delta \boldsymbol{\varepsilon}} = \frac{\partial \mathbf{p}_{n+1}}{\partial p_{n+1}} \otimes \frac{\partial p_{n+1}}{\partial \Delta \boldsymbol{\varepsilon}} = \boldsymbol{\delta} \otimes (Q_1 \mathbf{s}_c + Q_2 \Delta \mathbf{e} + Q_3 \boldsymbol{\delta}). \quad (\text{D.89})$$

$\partial \boldsymbol{\sigma}_{n+1} / \partial \Delta \boldsymbol{\varepsilon}$: Combining (D.84) and (D.84), the explicit expression of the consistent tangent

APPENDIX D. DETAILED DERIVATION STEPS FOR THE DRUCKER–PRAGER MODEL

tensor can be obtained:

$$\mathcal{D}^{\text{cons}} = \frac{\partial \boldsymbol{\sigma}_{n+1}}{\partial \Delta \boldsymbol{\varepsilon}} = \frac{\partial \mathbf{s}_{n+1}}{\partial \Delta \boldsymbol{\varepsilon}} + \frac{\partial p_{n+1}}{\partial \Delta \boldsymbol{\varepsilon}}, \quad (\text{D.90})$$

$$\begin{aligned} \mathcal{D}^{\text{cons}} = & a_1 \mathbf{s}_c \otimes \mathbf{s}_c + a_2 \mathbf{s}_c \otimes \Delta \mathbf{e} + a_3 \mathbf{s}_c \otimes \boldsymbol{\delta} + a_4 \Delta \mathbf{e} \otimes \mathbf{s}_c + a_5 \Delta \mathbf{e} \otimes \Delta \mathbf{e} \\ & + a_6 \Delta \mathbf{e} \otimes \boldsymbol{\delta} + a_7 \boldsymbol{\delta} \otimes \mathbf{s}_c + a_8 \boldsymbol{\delta} \otimes \Delta \mathbf{e} + a_9 \boldsymbol{\delta} \otimes \boldsymbol{\delta} + a_{10} \mathcal{T}, \end{aligned} \quad (\text{D.91})$$

where

$$a_1 = A_1, \quad a_2 = A_2, \quad a_3 = A_3, \quad a_4 = (1 - c) B_1 + \frac{c(B_s - 2GA_s)}{S_c \|\Delta \mathbf{e}\| (\cos \psi_c + V)}, \quad (\text{D.92})$$

$$a_5 = (1 - c) B_2, \quad a_6 = (1 - c) B_3 + \frac{cV(B_s - 2GA_s)}{\text{tr} \Delta \boldsymbol{\varepsilon} (\cos \psi_c + V)}, \quad a_7 = Q_1, \quad (\text{D.93})$$

$$a_8 = Q_2, \quad a_9 = Q_3, \quad a_{10} = (1 - c) B_s + 2cGA_s. \quad (\text{D.94})$$

D.4.2 Deviatoric radial loading

The stress update formulae for the case, when elastic-plastic transition occurs become

$$S_{n+1} = \left(S_c - \frac{3\sqrt{2}K\alpha G}{\tilde{h}} (1 - c) \text{tr} \Delta \boldsymbol{\varepsilon} + q \cdot 2G \|\Delta \mathbf{e}\| (1 - c) \left(1 - \frac{G}{\tilde{h}} \right) \right), \quad (\text{D.95})$$

$$\mathbf{s}_{n+1} = \left(1 - \frac{3\sqrt{2}K\alpha G}{\tilde{h}S_c} (1 - c) \text{tr} \Delta \boldsymbol{\varepsilon} + q \cdot \frac{2G \|\Delta \mathbf{e}\| (1 - c)}{S_c} \left(1 - \frac{G}{\tilde{h}} \right) \right) \mathbf{s}_c, \quad (\text{D.96})$$

$$p_{n+1} = p_c + K \left(1 - \frac{9K\alpha\beta}{\tilde{h}} \right) (1 - c) \text{tr} \Delta \boldsymbol{\varepsilon} - q \frac{3\sqrt{2}KG\beta}{\tilde{h}} (1 - c) \|\Delta \mathbf{e}\|. \quad (\text{D.97})$$

$\partial c / \partial \Delta \boldsymbol{\varepsilon}$: Using (D.34) and the definition of parameter q , we can write that

$$\boxed{\frac{\partial c}{\partial \Delta \boldsymbol{\varepsilon}} = -\frac{c}{S_c \|\Delta \mathbf{e}\| (q + V)} \mathbf{s}_c - \frac{cV}{\text{tr} \Delta \boldsymbol{\varepsilon} (q + V)} \boldsymbol{\delta}}. \quad (\text{D.98})$$

$\partial S_c / \partial \Delta \boldsymbol{\varepsilon}$: In deviatoric radial loading case, the derivative (D.38) becomes

$$\boxed{\frac{\partial S_c}{\partial \Delta \boldsymbol{\varepsilon}} = \frac{2GcV}{q + V} \left(\frac{1}{S_c} \mathbf{s}_c - q \frac{\|\Delta \mathbf{e}\|}{\text{tr} \Delta \boldsymbol{\varepsilon}} \boldsymbol{\delta} \right)}. \quad (\text{D.99})$$

$\partial p_c / \partial \Delta \boldsymbol{\varepsilon}$: The derivative of the pressure at the contact point reduces to

$$\boxed{\frac{\partial p_c}{\partial \Delta \boldsymbol{\varepsilon}} = -\frac{Kc}{q + V} \left(\frac{\text{tr} \Delta \boldsymbol{\varepsilon}}{S_c \|\Delta \mathbf{e}\|} \mathbf{s}_c - q \boldsymbol{\delta} \right)}. \quad (\text{D.100})$$

$\partial \mathbf{s}_c / \partial \Delta \boldsymbol{\varepsilon}$: Expression (D.36) becomes

$$\frac{\partial \mathbf{s}_c}{\partial \Delta \boldsymbol{\varepsilon}} = 2Gc\boldsymbol{\mathcal{T}} - \frac{2Gc}{S_c \|\Delta \mathbf{e}\| (q+V)} \Delta \mathbf{e} \otimes \mathbf{s}_c - \frac{2GcV}{\text{tr} \Delta \boldsymbol{\varepsilon} (q+V)} \Delta \mathbf{e} \otimes \boldsymbol{\delta}. \quad (\text{D.101})$$

$\partial S_{n+1} / \partial \Delta \boldsymbol{\varepsilon}$: Using the stress update formula (D.95) and the chain rule:

$$\frac{\partial S_{n+1}}{\partial \Delta \boldsymbol{\varepsilon}} = \frac{\partial S_{n+1}}{\partial S_c} \frac{\partial S_c}{\partial \Delta \boldsymbol{\varepsilon}} + \frac{\partial S_{n+1}}{\partial c} \frac{\partial c}{\partial \Delta \boldsymbol{\varepsilon}} + \frac{\partial S_{n+1}}{\partial \text{tr} \Delta \boldsymbol{\varepsilon}} \frac{\partial \text{tr} \Delta \boldsymbol{\varepsilon}}{\partial \Delta \boldsymbol{\varepsilon}} + \frac{\partial S_{n+1}}{\partial \|\Delta \mathbf{e}\|} \frac{\partial \|\Delta \mathbf{e}\|}{\partial \Delta \boldsymbol{\varepsilon}}, \quad (\text{D.102})$$

$$\boxed{\frac{\partial S_{n+1}}{\partial \Delta \boldsymbol{\varepsilon}} = P_1 \mathbf{s}_c + P_2 \Delta \mathbf{e} + P_3 \boldsymbol{\delta}}, \quad (\text{D.103})$$

where

$$P_1 = \frac{2Gc(\tilde{h} - G)}{S_c \tilde{h}}, \quad P_2 = \frac{2G(1-c)(\tilde{h} - G)q}{\|\Delta \mathbf{e}\| \tilde{h}}, \quad P_3 = -\frac{3\sqrt{2}KG\alpha}{\tilde{h}}. \quad (\text{D.104})$$

$\partial \mathbf{s}_{n+1} / \partial \Delta \boldsymbol{\varepsilon}$: The derivative of the updated deviatoric stress is obtained using the chain rule as

$$\begin{aligned} \frac{\partial \mathbf{s}_{n+1}}{\partial \Delta \boldsymbol{\varepsilon}} &= \frac{\partial \mathbf{s}_{n+1}}{\partial S_c} \otimes \frac{\partial S_c}{\partial \Delta \boldsymbol{\varepsilon}} + \frac{\partial \mathbf{s}_{n+1}}{\partial c} \otimes \frac{\partial c}{\partial \Delta \boldsymbol{\varepsilon}} + \frac{\partial \mathbf{s}_{n+1}}{\partial \text{tr} \Delta \boldsymbol{\varepsilon}} \otimes \frac{\partial \text{tr} \Delta \boldsymbol{\varepsilon}}{\partial \Delta \boldsymbol{\varepsilon}} \\ &\quad + \frac{\partial \mathbf{s}_{n+1}}{\partial \|\Delta \mathbf{e}\|} \otimes \frac{\partial \|\Delta \mathbf{e}\|}{\partial \Delta \boldsymbol{\varepsilon}} + \frac{\partial \mathbf{s}_{n+1}}{\partial \mathbf{s}_c} \frac{\partial \mathbf{s}_c}{\partial \Delta \boldsymbol{\varepsilon}}. \end{aligned} \quad (\text{D.105})$$

After simplification, it can be written by

$$\boxed{\frac{\partial \mathbf{s}_{n+1}}{\partial \Delta \boldsymbol{\varepsilon}} = a_1 \mathbf{s}_c \otimes \mathbf{s}_c + a_2 \mathbf{s}_c \otimes \Delta \mathbf{e} + a_3 \mathbf{s}_c \otimes \boldsymbol{\delta} + a_4 \Delta \mathbf{e} \otimes \mathbf{s}_c + a_5 \Delta \mathbf{e} \otimes \boldsymbol{\delta} + a_{10} \boldsymbol{\mathcal{T}}}, \quad (\text{D.106})$$

where

$$a_1 = \frac{2Gc}{S_c^2} \left(1 - \frac{G}{\tilde{h}}\right) - \frac{2GcS_{n+1}V}{S_c^3(q+V)}, \quad a_2 = \frac{2Gq(1-c)(\tilde{h} - G)}{\tilde{h}S_c \|\Delta \mathbf{e}\|}, \quad (\text{D.107})$$

$$a_3 = \frac{3\sqrt{2}K\alpha}{S_c} \left(\frac{cq}{q+V} \frac{S_{n+1}}{S_c} - \frac{G}{\tilde{h}}\right), \quad a_4 = -\frac{2GcS_{n+1}}{S_c^2 \|\Delta \mathbf{e}\| (q+V)}, \quad (\text{D.108})$$

$$a_5 = -\frac{2GcV S_{n+1}}{S_c \text{tr} \Delta \boldsymbol{\varepsilon} (q+V)}, \quad a_{10} = \frac{2GcS_{n+1}}{S_c}. \quad (\text{D.109})$$

$\partial p_{n+1} / \partial \Delta \boldsymbol{\varepsilon}$: Applying the chain rule, the derivative of the pressure at the end of the increment can be calculated by

$$\frac{\partial p_{n+1}}{\partial \Delta \boldsymbol{\varepsilon}} = \frac{\partial p_{n+1}}{\partial p_c} \frac{\partial p_c}{\partial \Delta \boldsymbol{\varepsilon}} + \frac{\partial p_{n+1}}{\partial c} \frac{\partial c}{\partial \Delta \boldsymbol{\varepsilon}} + \frac{\partial p_{n+1}}{\partial \text{tr} \Delta \boldsymbol{\varepsilon}} \frac{\partial \text{tr} \Delta \boldsymbol{\varepsilon}}{\partial \Delta \boldsymbol{\varepsilon}} + \frac{\partial p_{n+1}}{\partial \|\Delta \mathbf{e}\|} \frac{\partial \|\Delta \mathbf{e}\|}{\partial \Delta \boldsymbol{\varepsilon}}, \quad (\text{D.110})$$

$$\boxed{\frac{\partial p_{n+1}}{\partial \Delta \boldsymbol{\varepsilon}} = a_7 \boldsymbol{\delta} \otimes \mathbf{s}_c + a_8 \boldsymbol{\delta} \otimes \Delta \mathbf{e} + a_9 \boldsymbol{\delta} \otimes \boldsymbol{\delta}}, \quad (\text{D.111})$$

APPENDIX D. DETAILED DERIVATION STEPS FOR THE DRUCKER–PRAGER MODEL

where

$$a_7 = \frac{-3\sqrt{2}KG\beta c}{\tilde{h}S_c}, \quad a_8 = \frac{-3\sqrt{2}GKq\beta(1-c)}{\|\Delta\mathbf{e}\|\tilde{h}}, \quad a_9 = \frac{K(h-9K\alpha\beta)}{\tilde{h}}. \quad (\text{D.112})$$

$\partial\boldsymbol{\sigma}_{n+1}/\partial\Delta\boldsymbol{\varepsilon}$: Combining (D.106) and (D.111), the consistent tangent tensor can be expressed as

$$\begin{aligned} \mathcal{D}^{\text{cons}} = & a_1\mathbf{s}_c \otimes \mathbf{s}_c + a_2\mathbf{s}_c \otimes \Delta\mathbf{e} + a_3\mathbf{s}_c \otimes \boldsymbol{\delta} + a_4\Delta\mathbf{e} \otimes \mathbf{s}_c + a_5\Delta\mathbf{e} \otimes \Delta\mathbf{e} \\ & + a_6\Delta\mathbf{e} \otimes \boldsymbol{\delta} + a_7\boldsymbol{\delta} \otimes \mathbf{s}_c + a_8\boldsymbol{\delta} \otimes \Delta\mathbf{e} + a_9\boldsymbol{\delta} \otimes \boldsymbol{\delta} + a_{10}\mathcal{T}. \end{aligned} \quad (\text{D.113})$$

D.4.3 Special cases when the apex can be reached

D.4.3.1 General loading case

It is a possible scenario, that the n th state is located in the elastic domain and the stress path reaches the apex. It clearly follows from the condition (5.30) that the new stress state in this particular case cannot leave the apex upon further loading. Thus, the stress update formulae become

$$\mathbf{s}_{n+1} = \mathbf{0}, \quad p_{n+1} = p_a + (1-c_a)(1-c)K\Delta\epsilon \left(3 - \frac{27K\alpha\beta}{\tilde{h}-G} \right), \quad (\text{D.114})$$

where p_a denotes the pressure at the apex. It is calculated as

$$p_a = p_c + c_a(1-c)K\Delta\epsilon \left(3 - \frac{27K\alpha\beta}{\tilde{h}-G} \right) + \frac{3\sqrt{2}\beta K}{2(\tilde{h}-G)}S_c, \quad (\text{D.115})$$

where $p_c = p_n + 3Kc\Delta\epsilon$ is the pressure at the contact point. Inserting p_a and p_c into (D.114) we arrive at the solution for the updated pressure:

$$p_{n+1} = p_c + (1-c)K\text{tr}\Delta\boldsymbol{\varepsilon} \left(1 - \frac{9K\alpha\beta}{\tilde{h}-G} \right) + \frac{3\sqrt{2}\beta K}{2(\tilde{h}-G)}S_c. \quad (\text{D.116})$$

The derivatives $\partial c/\partial\Delta\boldsymbol{\varepsilon}$, $\partial p_c/\partial\Delta\boldsymbol{\varepsilon}$ and $\partial S_c/\partial\Delta\boldsymbol{\varepsilon}$ have been already obtained by (D.35), (D.39) and (D.38), respectively. Using the chain rule, $\partial p_{n+1}/\partial\Delta\boldsymbol{\varepsilon}$ can be obtained as

$$\frac{\partial p_{n+1}}{\partial\Delta\boldsymbol{\varepsilon}} = \frac{\partial p_{n+1}}{\partial p_c} \frac{\partial p_c}{\partial\Delta\boldsymbol{\varepsilon}} + \frac{\partial p_{n+1}}{\partial c} \frac{\partial c}{\partial\Delta\boldsymbol{\varepsilon}} + \frac{\partial p_{n+1}}{\partial \text{tr}\Delta\boldsymbol{\varepsilon}} \frac{\partial \text{tr}\Delta\boldsymbol{\varepsilon}}{\partial\Delta\boldsymbol{\varepsilon}} + \frac{\partial p_{n+1}}{\partial S_c} \frac{\partial S_c}{\partial\Delta\boldsymbol{\varepsilon}}. \quad (\text{D.117})$$

After simplification it reduces to

$$\frac{\partial p_{n+1}}{\partial\Delta\boldsymbol{\varepsilon}} = \left(1 - \frac{9K\alpha\beta}{\tilde{h}-G} \right) \boldsymbol{\delta}. \quad (\text{D.118})$$

It follows that the consistent tangent tensor for this case is given by

$$\boxed{\mathcal{D}^{\text{cons}} = \frac{\partial\boldsymbol{\sigma}_{n+1}}{\partial\Delta\boldsymbol{\varepsilon}} = \frac{\partial p_{n+1}}{\partial\Delta\boldsymbol{\varepsilon}} = K \left(1 - \frac{9K\alpha\beta}{\tilde{h}-G} \right) \boldsymbol{\delta} \otimes \boldsymbol{\delta}}. \quad (\text{D.119})$$

D.4.3.2 Deviatoric radial loading case

The stress update formula for the pressure, when elastic-plastic transition occurs is

$$p_{n+1} = p_a + (1 - c_a)(1 - c)K\Delta\epsilon \left(3 - \frac{27K\alpha\beta}{\tilde{h} - G} \right), \quad (\text{D.120})$$

where

$$p_a = p_c + c_a(1 - c)K\Delta\epsilon \left(3 - \frac{27K\alpha\beta}{\tilde{h} - G} \right) + \frac{3K\beta}{\sqrt{2}(\tilde{h} - G)}S_c. \quad (\text{D.121})$$

Combining the two equations above, the solution for the updated pressure reduces to

$$p_{n+1} = p_c + (1 - c)K\text{tr}\Delta\epsilon \left(1 - \frac{9K\alpha\beta}{\tilde{h} - G} \right) + \frac{3\sqrt{2}\beta K}{2(\tilde{h} - G)}S_c. \quad (\text{D.122})$$

Since the stress update formula is the same as in case of general loading case, it can be clearly concluded, that the consistent tangent has exactly the same structure as given in (D.119).

D.4.3.3 n th state is located at the apex

When the initial state is located at the apex and the new stress state remains at the apex then the pressure, according to (5.29), is computed as

$$p_{n+1} = p_n + K\Delta\epsilon \left(3 - \frac{27K\alpha\beta}{\tilde{h} - G} \right). \quad (\text{D.123})$$

Consequently, the consistent tangent tensor is computed as

$$\boxed{\mathcal{D}^{\text{cons}} = \frac{\partial \boldsymbol{\sigma}_{n+1}}{\partial \Delta \boldsymbol{\epsilon}} = \frac{\partial p_{n+1}}{\partial \Delta \boldsymbol{\epsilon}} = K \left(1 - \frac{9K\alpha\beta}{\tilde{h} - G} \right) \boldsymbol{\delta} \otimes \boldsymbol{\delta}}. \quad (\text{D.124})$$

If the updated stress is located on the smooth portion of the yield surface then the stress update formulae, according to (5.31) and (5.32), become

$$\boldsymbol{s}_{n+1} = \left(2G \left(1 - \frac{G}{\tilde{h}} \right) - \frac{3\sqrt{2}KG\alpha\text{tr}\Delta\epsilon}{\tilde{h}\|\Delta\boldsymbol{e}\|} \right) \Delta\boldsymbol{e}, \quad (\text{D.125})$$

$$p_{n+1} = p_a + K \left(1 - \frac{9K\alpha\beta}{\tilde{h}} \right) \text{tr}\Delta\epsilon - \frac{3\sqrt{2}KG\beta}{\tilde{h}} \|\Delta\boldsymbol{e}\|. \quad (\text{D.126})$$

Consequently, it follows that the derivative of the updated deviatoric stress is computed as

$$\frac{\partial \boldsymbol{s}_{n+1}}{\partial \Delta \boldsymbol{\epsilon}} = \frac{\partial \boldsymbol{s}_{n+1}}{\partial \Delta \boldsymbol{e}} : \frac{\partial \Delta \boldsymbol{e}}{\partial \Delta \boldsymbol{\epsilon}} + \frac{\partial \boldsymbol{s}_{n+1}}{\partial \|\Delta \boldsymbol{e}\|} \otimes \frac{\partial \|\Delta \boldsymbol{e}\|}{\partial \Delta \boldsymbol{\epsilon}} + \frac{\partial \boldsymbol{s}_{n+1}}{\partial \text{tr}\Delta \boldsymbol{\epsilon}} \otimes \frac{\partial \text{tr}\Delta \boldsymbol{\epsilon}}{\partial \Delta \boldsymbol{\epsilon}}, \quad (\text{D.127})$$

$$\frac{\partial \boldsymbol{s}_{n+1}}{\partial \Delta \boldsymbol{\epsilon}} = 2G \left(1 - \frac{G}{\tilde{h}} (1 + V) \right) \boldsymbol{\mathcal{T}} + \frac{2G^2V}{\tilde{h}\|\Delta\boldsymbol{e}\|^2} \Delta\boldsymbol{e} \otimes \Delta\boldsymbol{e} - \frac{2G^2V}{\tilde{h}\text{tr}\Delta\boldsymbol{\epsilon}} \Delta\boldsymbol{e} \otimes \boldsymbol{\delta}, \quad (\text{D.128})$$

APPENDIX D. DETAILED DERIVATION STEPS FOR THE DRUCKER–PRAGER MODEL

whereas the the derivative of the pressure at the end of the increment is

$$\frac{\partial p_{n+1}}{\partial \Delta \boldsymbol{\varepsilon}} = K \left(1 - \frac{9K\alpha\beta}{\tilde{h} - G} \right) \boldsymbol{\delta} - \frac{3\sqrt{2}KG\beta}{\tilde{h} \|\Delta \boldsymbol{e}\|} \Delta \boldsymbol{e}, \quad (\text{D.129})$$

$$\frac{\partial \mathbf{p}_{n+1}}{\partial \Delta \boldsymbol{\varepsilon}} = K \left(1 - \frac{9K\alpha\beta}{\tilde{h} - G} \right) \boldsymbol{\delta} \otimes \boldsymbol{\delta} - \frac{3\sqrt{2}KG\beta}{\tilde{h} \|\Delta \boldsymbol{e}\|} \boldsymbol{\delta} \otimes \Delta \boldsymbol{e}. \quad (\text{D.130})$$

Combining (D.128) and (D.130), the consistent tangent tensor can be constructed as

$$\boxed{\mathcal{D}^{\text{cons}} = a_1 \Delta \boldsymbol{e} \otimes \Delta \boldsymbol{e} + a_2 \Delta \boldsymbol{e} \otimes \boldsymbol{\delta} + a_3 \boldsymbol{\delta} \otimes \Delta \boldsymbol{e} + a_4 \boldsymbol{\delta} \otimes \boldsymbol{\delta} + a_5 \mathcal{T}}, \quad (\text{D.131})$$

where

$$a_1 = \frac{3\sqrt{2}KG\alpha \text{tr} \Delta \boldsymbol{\varepsilon}}{\tilde{h} \|\Delta \boldsymbol{e}\|^3}, \quad a_2 = -\frac{3\sqrt{2}KG\alpha}{\tilde{h} \|\Delta \boldsymbol{e}\|}, \quad a_3 = -\frac{3\sqrt{2}KG\beta}{\tilde{h} \|\Delta \boldsymbol{e}\|}, \quad (\text{D.132})$$

$$a_4 = K \left(1 - \frac{9K\alpha\beta}{\tilde{h} - G} \right), \quad a_5 = 2G \left(1 - \frac{G}{\tilde{h}} \right) - \frac{3\sqrt{2}KG\alpha \text{tr} \Delta \boldsymbol{\varepsilon}}{\tilde{h} \|\Delta \boldsymbol{e}\|}. \quad (\text{D.133})$$



Nested derivatives

E.1 Definition

This section presents the method proposed by Dominici (2003) to compute the series expansion for the inverse of a given function.

Definition. The n th nested derivative $\mathcal{D}^n [f](x)$ of the function $f(x)$ is defined by the following recursion:

$$\mathcal{D}^0 [f](x) = 1, \tag{E.1}$$

$$\mathcal{D}^n [f](x) = \frac{d}{dx} [f(x) \cdot \mathcal{D}^{n-1} [f](x)], \quad n \geq 1. \tag{E.2}$$

Let

$$h(x) = \int_{x_0}^x \frac{1}{f(t)} dt, \quad \tilde{z} = h(\tilde{x}), \tag{E.3}$$

with $f(\tilde{x}) \neq 0, \pm\infty$ and its inverse $H(x) = h^{-1}(x)$. Then,

$$H(z) = \tilde{x} + f(\tilde{x}) \sum_{n \geq 1} \mathcal{D}^{n-1} [f](\tilde{x}) \frac{(z - \tilde{z})^n}{n!}, \tag{E.4}$$

where $|z - \tilde{z}| < \varepsilon$, for some $\varepsilon > 0$.

E.2 Application of nested derivatives in the stress update algorithm proposed for the von Mises model

The most computationally demanding task during the proposed integration scheme is to determine the value of the angle ψ at the end of the increment, i.e., Equation (5.11) has to be solved for ψ_{n+1} , when elastic-plastic transition occurs. This involves the inversion of an incomplete beta function. Closed-form expression for the inverse incomplete beta function does not exist, therefore, a numerical scheme is needed. Here, an accurate algorithm based on the theory of nested derivatives (see Appendix E.1) presented by Dominici (2003) is provided. Using this method, we have a series expansion for the inverse incomplete beta function. The main steps of the proposed technique are summarized in the following (Kossa and Szabó, 2010b).

Step 1: Input parameters are: $G, H, M, R_n, c, \|\Delta\mathbf{e}\|, \psi_c$. First, the following material parameters have to be calculated:

$$h = \frac{2}{3}H, \quad b = -\frac{Mh}{2(2G+h)}, \quad m = 1 - 2b. \quad (\text{E.5})$$

Step 2: Calculation of the l.h.s. of the equation (5.11) rewritten for the case, when elastic-plastic transition occurs:

$$z = -\frac{2G(1-c)\|\Delta\mathbf{e}\|}{R_n \sin^{-2b}\psi_c}. \quad (\text{E.6})$$

Step 3: Estimation of the final angle. A possible and efficient way to obtain this estimated value is the following: First, the final radius of the yield surface is determined by using the formula corresponding to the radial return method (Simo and Hughes, 1998):

$$\tilde{R}_{n+1} = R_n - 2b(\|\boldsymbol{\xi}_{trial}\| - R_n). \quad (\text{E.7})$$

Here, and in the following, overtilded characters mean estimated quantities. The solution of the radius of the updated yield surface is obtained using (5.12) with the substitution $\psi_n = \psi_c$. Inserting the estimated value (E.7) into this expression allows us to express the estimated value of ψ_{n+1} as

$$\tilde{\psi} = \arcsin \left(\left(\frac{R_n}{\tilde{R}_{n+1}} \right)^{-\frac{1}{2b}} \sin\psi_c \right). \quad (\text{E.8})$$

Step 4: Calculation of the r.h.s. using the estimated value (E.8) in expression (5.11) rewritten for the case, when elastic-plastic transition occurs:

$$\tilde{z} = \frac{1}{2}B \left(\cos^2\psi_c, \frac{1}{2}, b \right) - \frac{1}{2}B \left(\cos^2\tilde{\psi}, \frac{1}{2}, b \right). \quad (\text{E.9})$$

E.2. APPLICATION OF NESTED DERIVATIVES IN THE STRESS UPDATE ALGORITHM PROPOSED FOR THE VON MISES MODEL

Step 5: Thus, the series expansion of the angle ψ_{n+1} , using nested derivatives, can be written in the form (see Appendix E.1)

$$\psi_{n+1} = \tilde{\psi} + \sin^m \tilde{\psi} \sum_{n \geq 1} \mathcal{D}^{n-1} [f] (\tilde{\psi}) \frac{(z - \tilde{z})^n}{n!}, \quad (\text{E.10})$$

where $\mathcal{D}^{n-1} [f]$ denotes the $(n-1)$ th nested derivative corresponding to the function $f(t) = \sin^m t$. Expressions of the first six nested derivatives have been obtained by utilizing (E.2):

$$\mathcal{D}^0 [f] (t) = 1, \quad (\text{E.11})$$

$$\mathcal{D}^1 [f] (t) = \frac{m \cos t}{(\sin t)^{1-m}}, \quad (\text{E.12})$$

$$\mathcal{D}^2 [f] (t) = \frac{m}{(\sin t)^{2-2m}} [2m \cos^2 t - 1], \quad (\text{E.13})$$

$$\mathcal{D}^3 [f] (t) = \frac{m \cos t}{(\sin t)^{3-3m}} [2 - 7m + (3 + 3 \cos 2t)m^2], \quad (\text{E.14})$$

$$\mathcal{D}^4 [f] (t) = \frac{m}{(\sin t)^{4-4m}} [-4 - 2 \cos 2t + (18 + 11 \cos 2t)m - 46m^2 \cos^2 t + 24m^3 \cos^4 t], \quad (\text{E.15})$$

$$\begin{aligned} \mathcal{D}^5 [f] (t) = & \frac{m \cos t}{(\sin t)^{5-5m}} [20 + 4 \cos 2t - (114 + 32 \cos 2t)m \\ & + (228 + 101 \cos 2t)m^2 - 326m^3 \cos^2 t + 120m^4 \cos^4 t], \end{aligned} \quad (\text{E.16})$$

$$\begin{aligned} \mathcal{D}^6 [f] (t) = & \frac{m}{2 (\sin t)^{6-6m}} [-4(33 + 26 \cos 2t + \cos 4t) + (912 + 792 \cos 2t + 44 \cos 4t)m \\ & + (-57(43 + 42 \cos 2t) - 197 \cos 4t)m^2 + (8 \cos^2 t \cdot (668 + 233 \cos 2t))m^3 \\ & - 5112m^4 \cos^4 t + 1440m^5 \cos^6 t]. \end{aligned} \quad (\text{E.17})$$

Remark: In the numerical evaluation, such as in a Fortran77 code, of an incomplete beta function, the continued fraction representation is one of the most useful technique. The algorithm given by Press et al. (1992) accepts values of a and b only from the the positive range. During the proposed integration scheme, the argument b is negative in (E.9), therefore, the numerical algorithm presented by Press et al. (1992) cannot be applied directly. To overcome this problem, we can convert the incomplete beta functions in (E.9) to ones having positive b parameters, using the transformation rule (A.17) as

$$B \left(\cos^2 \psi, \frac{1}{2}, b \right) = \left(1 + \frac{1}{2b} \right) B \left(\cos^2 \psi, \frac{1}{2}, 1 + b \right) - \frac{\cos \psi}{b \sin^{-2b} \psi}. \quad (\text{E.18})$$

Therefore, the expression on the left-hand side in (E.18) is transformed to a formula, which contains an incomplete beta function, where the term $1 + b$ has a positive value. Thus, the numerical algorithm presented in Press et al. (1992) is now applicable for our problem.

Bibliography

- ABAQUS: 2007, *Version 6.7*, Dassault Systèmes.
- Abramowitz, M. and Stegun, I. A.: 1968, *Handbook of Mathematical Functions*, Vol. 55 of *Applied Mathematics Series*, Dover Publications, New York.
- Anandarajah, A.: 2010, *Computational methods in elasticity and plasticity*, Springer.
- Armstrong, P. J. and Frederick, C. O.: 1966, A mathematical representation of the multiaxial Bauschinger effect, *Technical Report RD/B/N731*, Central Electricity Generating Board, Berkeley.
- Artioli, E., Auricchio, F. and Beirão da Veiga, L.: 2006, A novel 'optimal' exponential-based integration algorithm for von-Mises plasticity with linear hardening: theoretical analysis on yield consistency, accuracy, convergence and numerical investigations, *International Journal for Numerical Methods in Engineering* **67**, 449–498.
- Artioli, E., Auricchio, F. and Beirão da Veiga, L.: 2007, Generalized midpoint integration algorithms for j_2 plasticity with linear hardening, *International Journal for Numerical Methods in Engineering* **72**, 422–463.
- Auricchio, F. and Beirão da Veiga, L.: 2003, On a new integration scheme for von-Mises plasticity with linear hardening, *International Journal for Numerical Methods in Engineering* **56**, 1375–1396.
- Auricchio, F. and Taylor, R. L.: 1995, Two material models for cyclic plasticity: Nonlinear kinematic hardening and generalized plasticity, *International Journal of Plasticity* **11**, 65–98.
- Axelsson, K. and Samuelsson, A.: 1979, Finite element analysis of elastic-plastic materials displaying mixed hardening, *International Journal for Numerical Methods in Engineering* **14**, 211–225.
- Bauschinger, J.: 1881, Über die Veränderung der Elastizitätsgrenze und des Elastizitätsmodulus verschiedener Metalle, *Civilingenieur* **1881**, 239–348.
- Caddemi, S.: 1994, Computational aspects of the integration of the von Mises linear hardening constitutive laws, *International Journal of Plasticity* **10**, 935–956.
- Chan, A. H. C.: 1996, Exact stress integration for von Mises elasto-plastic model with constant hardening modulus, *International Journal for Numerical and Analytical Methods in Geomechanics* **20**, 605–613.

- Chen, W. F.: 2007, *Plasticity in Reinforced Concrete*, J. Ross, New York.
- Chen, W. F. and Han, D. J.: 2007, *Plasticity for Structural Engineers*, J. Ross Publishing, New York.
- Chen, W. F. and Saleeb, A. F.: 1982, *Constitutive equations for engineering materials. Volume 1: Elasticity and Modeling*, Wiley.
- Cocchetti, G. and Perego, U.: 2003, A rigorous bound on error in backward-difference elastoplastic time-integration, *Computer Methods in Applied Mechanics and Engineering* **192**, 4909–4927.
- Cosserat, E. and Cosserat, F.: 1909, *Théorie des corps déformables*, Hermann and Sons, Paris.
- de Souza Neto, E. A., Perić, D. and Owen, D. R. J.: 2008, *Computational methods for plasticity*, Wiley.
- Doghri, I.: 2000, *Mechanics of deformable solids*, Springer.
- Dominici, D.: 2003, Nested derivatives: a simple method for computing series expansions of inverse functions, *International Journal of Mathematics and Mathematical Sciences* **2003**, 3699–3715.
- Drucker, D. C. and Prager, W.: 1952, Soil mechanics and plastic analysis or limit design, *Quarterly of Applied Mathematics* **10**, 157–162.
- Dunne, F. and Petrinic, N.: 2005, *Introduction to Computational Plasticity*, Oxford University Press, New York.
- Eringen, A. C.: 1999, *Microcontinuum field theories. I. Foundations and solids*, Springer, New York.
- Frederick, C. O. and Armstrong, P. J.: 2007, A mathematical representation of the multiaxial Bauschinger effect, *Materials at High Temperatures* **24**, 1–26.
- Gambin, W.: 2001, *Plasticity and textures*, Kluwer Academic Publishers.
- Gel'fand, I. M. and Shilov, G. E.: 1964, *Generalized Functions, Vol. 1: Properties and Operations*, Academic Press, New York.
- Genna, F. and Pandolfi, A.: 1994, Accurate numerical integration of Drucker–Prager's constitutive equations, *Meccanica* **29**, 239–260.
- Gratacos, P., Montmitonnet, P. and Chenot, J. L.: 1992, An integration scheme for Prandtl–Reuss elastoplastic constitutive equations, *International Journal for Numerical Methods in Engineering* **33**, 943–961.
- Haigh, B. F.: 1920, The strain-energy function and the elastic limit, *Engineering (London)* **109**, 158–160.
- Hiley, R. A. and Rouainia, M.: 2008, Explicit Runge–Kutta methods for the integration of rate-type constitutive equations, *Computational Mechanics* **42**, 53–66.

- Hjiaj, M., Fortin, J. and de Saxcé, G.: 2003, A complete stress update algorithm for non-associated Drucker–Prager model including treatment of apex, *International Journal of Engineering Science* **41**, 1109–1143.
- Hofstetter, G. and Taylor, R. L.: 1991, Treatment of the corner region for Drucker–Prager type plasticity, *Zeitschrift für angewandte Mathematik und Mechanik* **6**, 589–591.
- Hong, H. K. and Liu, C. S.: 1997, Prandtl–Reuss elastoplasticity: on–off switch and superposition formulae, *International Journal of Solids and Structures* **34**, 4281–4304.
- Ibrahimbegovic, A.: 2009, *Nonlinear solid mechanics*, Springer.
- Itskov, M.: 2009, *Tensor Algebra and Tensor Analysis for Engineers*, 2nd edn, Springer.
- Jirásek, M. and Bažant, Z. P.: 2002, *Inelastic analysis of structures*, Wiley, England.
- Jones, R. M.: 2009, *Deformation theory of plasticity*, Bull Ridge Publishing.
- Khan, A. S. and Huang, S.: 1995, *Continuum Theory of Plasticity*, Wiley, New York.
- Khoei, A. R. and Jamali, N.: 2005, On the implementation of a multi-surface kinematic hardening plasticity and its applications, *International Journal of Plasticity* **21**, 1741–1770.
- Koiter, W. T.: 1953, Stress strain relations, uniqueness and variational theorems for elastic-plastic materials with a singular yield surface, *Quarterly of Applied Mathematics* pp. 350–534.
- Kossa, A.: 2007, Integration method for constitutive equation of von Mises elastoplasticity with linear hardening, *Periodica Polytechnica* **51**, 71–75.
- Kossa, A.: 2009, Rugalmas-képlékeny testek anyagegyenleteinek egzakt integrálási módszerei., *Építés-Építészettudomány* **37**, 241–264.
- Kossa, A.: 2011, Egzakt feszültségszámító eljárás a Drucker–Prager-féle rugalmas-képlékeny anyagmodellre izotrop keményedés esetén, *XI. Magyar Mechanikai Konferencia*, Miskolc, Hungary.
- Kossa, A. and Szabó, L.: 2007, Rugalmas-képlékeny testek konstitutív egyenleteinek integrálása lineáris izotróp és kinematikai keményedés esetén, *X. Magyar Mechanikai Konferencia*, Miskolc, Hungary.
- Kossa, A. and Szabó, L.: 2009a, Computational aspects of the integration of von Mises elastoplasticity model with combined hardening, *Computational Plasticity X: Fundamentals and Applications*, Barcelona, Spain.
- Kossa, A. and Szabó, L.: 2009b, Exact integration of the von Mises elastoplasticity model with combined linear isotropic-kinematic hardening, *International Journal of Plasticity* **25**, 1083–1106.
- Kossa, A. and Szabó, L.: 2010a, Exact stress update procedure for the hardening Drucker–Prager material model, *Seminar at Department of Aerospace and Mechanical Engineering, University of Arizona*.

- Kossa, A. and Szabó, L.: 2010b, Numerical implementation of a novel accurate stress integration scheme of the von Mises elastoplasticity model with combined linear hardening, *Finite Elements in Analysis and Design* **46**, 391–400.
- Krieg, R. D. and Krieg, D. B.: 1977, Accuracies of numerical solution methods for the elastic-perfectly plastic model, *Journal of Pressure Vessel Technology* **99**, 510–515.
- Krieg, R. D. and Xu, S.: 1997, Plane stress linear hardening plasticity theory, *Finite Elements in Analysis and Design* **27**, 41–67.
- Lemaitre, J. and Chaboche, J. L.: 1990, *Mechanics of solid materials*, Cambridge University Press.
- Liu, C. S.: 2004a, A consistent numerical scheme for Mises mixed hardening constitutive equations, *International Journal of Plasticity* **20**, 663–704.
- Liu, C. S.: 2004b, Internal symmetry groups for the Drucker–Prager material model of plasticity and numerical integrating methods, *International Journal of Solids and Structures* **41**, 3771–3791.
- Loret, B. and Prevost, J. H.: 1986, Accurate numerical solutions for Drucker–Prager elastic-plastic models, *Computer Methods in Applied Mechanics and Engineering* **54**, 259–277.
- Luenberger, D. G. and Ye, Y.: 2008, *Linear and nonlinear programming*, 3rd edn, Springer.
- Mendelson, A.: 1968, *Plasticity: Theory and applications*, The Macmillan Company.
- Nemat-Nasser, S.: 2004, *Plasticity. A treatise on finite deformation of heterogeneous inelastic materials*, Cambridge University Press.
- Özçag, E., Ege, I. and Gürçay, H.: 2008, An extension of the incomplete beta function for negative integers, *Journal of Mathematical Analysis and Applications* **338**, 984–992.
- Ponthot, J. P.: 2002, Unified stress update algorithms for the numerical simulation of large deformation elasto-plastic and elasto-viscoplastic processes, *International Journal of Plasticity* **18**, 91–126.
- Prager, W.: 1955, The Theory of Plasticity: A Survey of Recent Achievements (James Clayton Lecture), *Proc. Institute of Mechanical Engineering* **169**, 41–57.
- Prager, W.: 1956, A new method of analyzing stress and strains in work-hardening solids, *Journal of Applied Mechanics* **23**, 493–496.
- Prandtl, L.: 1925, Spannungsverteilung in plastischen Körpern, *Proceedings of the 1st International Congress on Applied Mechanics* **1925**, 43–54.
- Press, W. H., Teukolsky, S. A., Vetterling, W. T. and Flannery, B. P.: 1992, *Numerical recipes in Fortran 77*, Cambridge University Press, Cambridge.
- Reuss, E.: 1930, Berücksichtigung der elastischen Formänderung in der Plastizitätstheorie, *Zeitschrift für angewandte Mathematik und Mechanik* **10**, 266–274.

- Rezaiee-Pajand, M. and Nasirai, C.: 2008, On the integration schemes for Drucker-Prager's elastoplastic models based on exponential maps, *International Journal for Numerical Methods in Engineering* **74**, 799–826.
- Rezaiee-Pajand, M. and Sharifian, M.: 2012, A novel formulation for integrating nonlinear kinematic hardening Drucker-Prager's yield condition, *European Journal of Mechanics - A/Solids* **31**, 163–178.
- Rezaiee-Pajand, M., Sharifian, M. and Sharifian, M.: 2011, Accurate and approximate integrations of Drucker-Prager plasticity with linear isotropic and kinematic hardening, *European Journal of Mechanics - A/Solids* **30**, 345–361.
- Ristinmaa, M. and Tryding, J.: 1993, Exact integration of constitutive equations in elastoplasticity, *International Journal for Numerical Methods in Engineering* **36**, 2525–2544.
- Romashchenko, V. A., Lepikhin, P. P. and Ivashchenko, K. B.: 1999, Exact solution of problems of flow theory with isotropic-kinematic hardening. part 1. setting the loading trajectory in the space of stress, *Strength of Materials* **31**, 582–591.
- Sadd, M. H.: 2009, *Elasticity: Theory, Applications, and Numerics*, Academic Press.
- Sherman, J. and Morrison, W. J.: 1949, Adjustment of an inverse matrix corresponding to a change in one element of a given matrix, *The Annals of Mathematical Statistics* **21**, 124–127.
- Simo, J. C. and Hughes, T. J. R.: 1998, *Computational Inelasticity*, Springer, New York.
- Skrzypek, J. J.: 1993, *Plasticity and creep*, CRC Press.
- Sloan, S. W. and Booker, J. R.: 1992, Integration of Tresca and Mohr-Coulomb constitutive relations in plane strain elastoplasticity, *International Journal for Numerical Methods in Engineering* **33**, 163–196.
- Spanier, J. and Oldham, K. B.: 1987, *An atlas of functions*, Springer.
- Stein, E., de Borst, R. and Hughes, T. J. R.: 2004, *Encyclopedia of computational mechanics. Volume 2*, John Wiley & Sons.
- Szabó, L.: 1985, Evaluation of elasto-viscoplastic tangent matrices without numerical inversion, *Computers and Structures* **21**, 1235–1236.
- Szabó, L.: 2009, A semi-analytical integration method for J2 flow theory of plasticity with linear isotropic hardening, *Computer Methods in Applied Mechanics and Engineering* **198**, 2151–2166.
- Szabó, L. and Kossa, A.: 2012, A new exact integration method for the Drucker-Prager elastoplastic model with linear isotropic hardening, *International Journal of Solids and Structures* **49**, 170–190.
- Szabó, L. and Kovács, Á.: 1987, Numerical implementation of Prager's kinematic hardening model in exactly integrated form for elastic-plastic analysis, *Computers and Structures* **26**, 815–822.

- von Mises, R.: 1913, Mechanik der festen Körper im plastisch deformablen Zustand, *Nachrichten von der Gesellschaft der Wissenschaften zu Göttingen, Mathematisch-Physikalische Klasse* **1913**, 582–592.
- Vrabie, I. I.: 2004, *Differential equations*, World Scientific Publishing, Singapore.
- Wallin, M. and Ristinmaa, M.: 2001, Accurate stress updating algorithm based on constant strain rate assumption, *Computer Methods in Applied Mechanics and Engineering* **190**, 5583–5601.
- Wang, X. and Chang, L.: 1985, Exact integration of constitutive equations of kinematic hardening material and its extended applications, *SMIRT-8, Brussels, Proc. Paper L2/3*.
- Wang, X. and Chang, L.: 1987, Exact integration of constitutive equations of kinematic hardening materials and its extended applications, *Acta Mechanica Sinica* **3**, 139–149.
- Wei, Z., Perić, D. and Owen, D. R. J.: 1996, Consistent linearization for the exact stress update of Prandtl–Reuss non-hardening elastoplastic models, *International Journal for Numerical Methods in Engineering* **39**, 1219–1235.
- Westergaard, H. M.: 1920, On the resistance of ductile materials to be combined stresses in two and three directions perpendicular to one another, *Journal of the Franklin Institute* **189**, 627–640.
- Westergaard, H. M.: 1952, *Theory of elasticity and plasticity*, Dover Publications.
- Wolfram Research: 2010a, Digamma function.
URL: <http://functions.wolfram.com/PDF/PolyGamma.pdf>
- Wolfram Research: 2010b, Gamma function.
URL: <http://functions.wolfram.com/PDF/Gamma.pdf>
- Wolfram Research: 2010c, Generalized hypergeometric function.
URL: <http://functions.wolfram.com/PDF/Hypergeometric0F0.pdf>
- Wolfram Research: 2010d, Incomplete beta function.
URL: <http://functions.wolfram.com/PDF/Beta3.pdf>
- Wolfram Research: 2010e, *Mathematica Edition: Version 8.0*, Wolfram Research.
- Wolfram Research: 2010f, Regularized generalized hypergeometric function.
URL: <http://functions.wolfram.com/PDF/HypergeometricPFQRegularized.pdf>
- Yang, Y., Muraleetharan, K. K. and Yu, H. S.: 2008, Generalized trapezoidal numerical integration of an advanced soil model, *International Journal for Numerical and Analytical Methods in Geomechanics* **32**, 43–64.
- Yoder, P. J. and Whirley, R. G.: 1984, On the numerical implementation of elastoplastic models, *Journal of Applied Mechanics* **51**, 283–288.